REPORT DOCUMENTATION PAGE

Form Approved OMB No. 0704-0188

1. REPORT DATE *(DD-MM-YYYY)*	2. REPORT TYPE	3. DATES COVERED *(From – To)*
31-03-2006	Final Report	1 August 2004 - 10-May-06

4. TITLE AND SUBTITLE

A Proposal to Develop and Test a Fibre-Optic Coupled Solar Thermal Propulsion System for Microsatellites

5a. CONTRACT NUMBER
FA8655-04-1-3030

5b. GRANT NUMBER

5c. PROGRAM ELEMENT NUMBER

6. AUTHOR(S)

Paul Henshall

5d. PROJECT NUMBER

5d. TASK NUMBER

5e. WORK UNIT NUMBER

7. PERFORMING ORGANIZATION NAME(S) AND ADDRESS(ES)

University of Surrey
Guildford GU2 7XH
United Kingdom

8. PERFORMING ORGANIZATION REPORT NUMBER

N/A

9. SPONSORING/MONITORING AGENCY NAME(S) AND ADDRESS(ES)

EOARD
PSC 821 BOX 14
FPO 09421-0014

10. SPONSOR/MONITOR'S ACRONYM(S)

11. SPONSOR/MONITOR'S REPORT NUMBER(S)
SPC 04-3030

12. DISTRIBUTION/AVAILABILITY STATEMENT

Approved for public release; distribution is unlimited.

13. SUPPLEMENTARY NOTES

14. ABSTRACT

This report results from a contract tasking University of Surrey. Solar Thermal Propulsion (STP) previously envisioned for large spacecraft and capable of high levels of propulsive performance (<1000s Isp) is currently being adapted for use on microsatellites at the University of Surrey. In utilising the high propulsive capability offered by STP, significant mass savings are possible. Conventional STP system concepts encounter difficulties in conforming to the low mass and volume requirements of a micro-satellite platform. The enabling technology for this concept is the advent of low attenuation high numerical aperture fibre optics. Applying fibre optics to STP allows the solar concentrator mirror to be mechanically decoupled from the solar heat exchanger as well as granting power input from multiple solar concentrators into a single heat exchanger. This ability allows STP systems with static concentrators to perform apogee raising and circularisation manoeuvres via a direct gain scheme, rather than being restricted to thrusting along the Sun vector. Thus the application of fibre optics accommodates a higher level of system flexibility and simplicity in comparison to conventional STP direct gain concepts for micro-satellites. This report presents a detailed analysis and design of a STP technology demonstration system incorporating fibre optics. Results are presented for solar concentrator surface quality measurements, fibre optic transmission testing and on the initial performance of a prototype pointing mechanism that utilizes a novel approach for Sun tracking and feedback.
.

15. SUBJECT TERMS

Solar, fiber optic, thermal propulsion, EOARD

16. SECURITY CLASSIFICATION OF:			17. LIMITATION OF ABSTRACT	18, NUMBER OF PAGES	19a. NAME OF RESPONSIBLE PERSON
a. REPORT	b. ABSTRACT	c. THIS PAGE			BARRETT A. FLAKE
UNCLAS	UNCLAS	UNCLAS	UL	93	19b. TELEPHONE NUMBER *(Include area code)* +44 (0)20 7514 4285

Fibre Optic Solar Thermal Propulsion Technology Demonstration

P.R. Henshall

Surrey Space Centre
School of Electronics and Physical Sciences
University of Surrey
Guildford, Surrey GU2 5XH, UK

March 2006

Abstract

Solar Thermal Propulsion (STP) previously envisioned for large spacecraft and capable of high levels of propulsive performance (<1000s I_{sp}) is currently being adapted for use on micro-satellites at the University of Surrey. In utilising the high propulsive capability offered by STP, significant mass savings are possible. Conventional STP system concepts encounter difficulties in conforming to the low mass and volume requirements of a micro-satellite platform. The enabling technology for this concept is the advent of low attenuation high numerical aperture fibre optics. Applying fibre optics to STP allows the solar concentrator mirror to be mechanically decoupled from the solar heat exchanger as well as granting power input from multiple solar concentrators into a single heat exchanger. This ability allows STP systems with static concentrators to perform apogee raising and circularisation manoeuvres via a direct gain scheme, rather than being restricted to thrusting along the Sun vector. Thus the application of fibre optics accommodates a higher level of system flexibility and simplicity in comparison to conventional STP direct gain concepts for micro-satellites. This report presents a detailed analysis and design of a STP technology demonstration system incorporating fibre optics. Results are presented for solar concentrator surface quality measurements, fibre optic transmission testing and on the initial performance of a prototype pointing mechanism that utilizes a novel approach for Sun tracking and feedback.

Contents

Nomenclature

A	Area
A_a	Aperture area
A_f	Focal spot area
A_e	Nozzle exit area
A^*	Nozzle throat area
b	Damping ratio
β_T	Isothermal compressibility of core
c	Speed of light (2.9979×10^8 m/s)
CR_g	Geometric concentration ratio
d	diameter
δ	Deflection
d_c	Concentrator diameter
d_f	Fibre diameter
den	Density
D	Tube diameter
ε	Emissivity
E	Young's modulus
f	Focal length
f_f	Darcy-Weisbach friction factor
F	Focus
g	Gravitational acceleration ($9.81 m/s^2$)
γ	Ratio of specific heats
h	Concentrator height
h_c	Heat transfer coefficient
η	Efficiency

I	Impulse
I	Armature current
I_{sp}	Specific Impulse
J	Inertia
k	Thermal conductivity
k_b	Boltzmann constant (1.38×10^{-23} $m^2kgs^{-2}K^{-1}$)
k_t	Armature constant
L	Inductance
λ	Wavelength
$\dot{m}$	Mass flow rate
M	Mass
M_b	Burnout mass
M_o	Starting mass
M_p	Propellant mass
M_r	Receiver mass
$\overline{M}$	Molecular mass
M_j	Molecular weight of the jth modifier
μ	Viscosity
n	Trailing-edge (TE) nondimensional angular deflection rate
n_e	External refractive index
n_{core}	Core refractive index
n_{clad}	Cladding refractive index
NA	Numerical aperture
N_A	Avogadro's number (6.022×10^{23})
N_u	Nusselt number
π	Pi (3.14159)
P	Power

P_a	Ambient Pressure
P_c	Chamber pressure
P_e	Exit pressure
P_r	Prandtl number
p	Photoelastic coefficient
$\dot{Q}$	Heat flux
θ_f	Angular form error
θ_s	Solar half angle
$\dot{\theta}$	Angular rate
ρ	Reflection angle
ρ	Core density
R	Resistance
$\overline{R}$	Universal gas constant (8.3144 $Jmol^{-1}K^{-1}$)
R_e	Reynolds number
σ	Stefan-Boltzmann constant (5.67×10^{23} $JK^{-4}m^{-2}s^{-1}$)
s	Complex frequency
S_λ	Energy per unit volume per unit wavelength
t	Time
T	Thrust
T	Torque
T_b	Blackbody temperature
T_c	Chamber temperature
T_f	Fictive temperature
T_r	Reciver temperature
T_s	Surface temperature
ΔT	Temperature difference
u_e	Exhaust velocity

V	Voltage
ΔV	Velocity change
ψ_a	Fibre acceptance angle
ψ_r	Concentrator rim angle
x	Coordinate
y	Coordinate

Section 1

1 Introduction

1.1 Solar Thermal Propulsion For Small Satellites

Solar thermal propulsion (STP) is the utilization of concentrated Sunlight for the purposes of heating a propellant to high temperatures via a heat exchanger. Sunlight concentration is achieved via an optical concentrating system, such as a series of lenses or mirrors. This concentrated sunlight impinges on a blackbody cavity receiver, which is subsequently heated to high temperatures. A propellant feed system causes a monopropellant to flow around the cavity receiver where heat is exchanged from the receiver to the propellant. The sunlight concentration system is orientated via a space mechanism or via the spacecraft attitude system to point at the Sun; control electronics and sensors are employed to actuate the mechanism and provide telemetry.

STP has been under development for over 40 years. The research originally undertaken was commonly a costly venture due to the requirement to attain a high system performance on the order of 1000s specific Impulse. This invariably required the use of very large inflatable/deployable solar concentrators that could collect a massive amount of solar power. This power was delivered to a cavity receiver heat exchanger capable of operating at temperatures as high as 3000 K. The propellant selected was hydrogen, which at such high temperatures would deliver the required performance. Subsequently this demanded the design of large-scale spacecraft, dominated by their propulsion systems.

(a) **(b)**

Figure 1.1: (a) Early AFRL STP concept [1]. (b) NASA Shooting Star Experiment [2]

An early STP concept formulated by AFRPL makes use of two large off-axis inflatable reflectors to collect the necessary energy; the scale of the system is depicted in figure (1.1a). A refractory metal cavity heat exchanger accepts the light from the reflectors and operates on a 'direct-gain' basis at temperatures up to 3,000K, with hydrogen as a propellant. This requires the large reflectors to tilt and rotate to track the sun [1]. Another more recent concept is the NASA Marshall Shooting Star Flight Experiment, depicted in figure (1.1b). This concept employs a thin film deployable Fresnel primary concentrator and a secondary refractive concentrator. This is the first example of a dielectric medium being employed to transmit light into a heat exchanger [2]. The designs of these systems harbored many technological unknowns at the time. Specifically: inflatable structures, high temperature materials and the storage of cryogenic hydrogen.

From 2000 to the present, research at the University of Surrey in the UK has concentrated on adapting STP to small satellites. Conventional small satellite propulsion systems are typically low performance systems, mainly due to the low resource capacity of a small satellite. For example the UK-DMC microsatellite, a product of SSTL, weighs only 88kg with dimensions of 640x640x680mm. Its propulsion system, a butane based monopropellant resistojet, produced a specific impulse of 85s and was capable of a 20m/s Delta-V [3]. The STP system designed at Surrey is significantly simpler than previous STP concepts, foregoing any mechanisms and making use of more storable propellants, such as ammonia. The system employs a 'thermal-storage' cavity heat exchanger and uses the spacecrafts attitude control system to point the concentrator. The concentrator itself is a small rigid concentrator encapsulating one facet of the spacecraft (Figure (1.2a)). This STP system design has constraints in terms of maneuvering and firing strategies, but the system is robust, cheap, reliable and very competitive in terms of performance and ΔV capability, with the possibility of achieving specific impulses between 200 and 400s. Such a technology could allow a microsatellite to perform a larger variety of space missions, thus reducing the cost of space access, which is the typical trend of small satellite budgets.

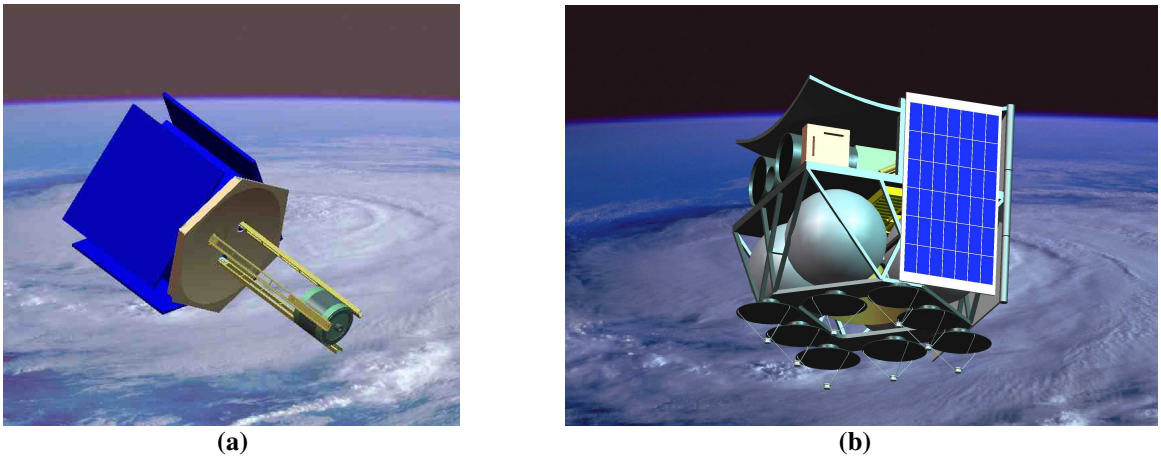

(a) **(b)**

Figure 1.2: (a) Surrey Space Centre STP concept. (b) Multiple small concentrator STP system

1.2 Fibre Optics for the Transmission of Concentrated Sunlight

Using fiber optics for the transmission of highly concentrated solar energy is a concept that has existed since the 1970s. Since then potential applications of the technology have been proposed that include: solar energy collection devices, solar surgery and nanomaterials manufacture. Developments in fibre optic manufacture have provided core glass materials of progressively better quality and therefore improved light transmission properties. Recent tests of light transmission through fibre optics, at the Ben-Gurion University of the Negrev, have shown potential for transmission efficiencies as high as 80% [4] (Figure (1.3a)).

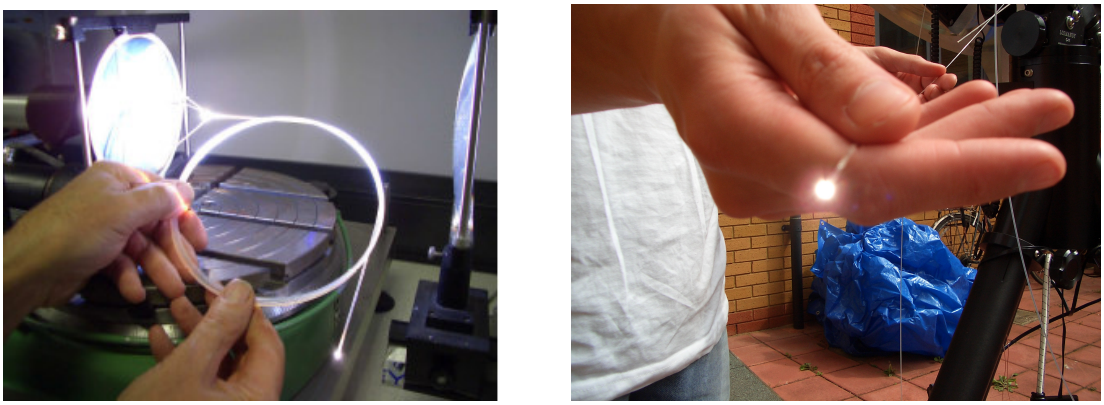

(a) **(b)**

Figure 1.3: (a) Fibre optic transmission test at SSTL's solar simulator facility. (b) Fibre optic on-Sun transmission test at the Surrey Space Centre

In 2004 the use of fiber optics in a small satellite STP system was proposed. With the application of fiber optics to a small satellite STP system, a degree of flexibility with regard to system design and thrusting can be realized. For example with fiber optics the cavity receiver can be mechanically decoupled from the concentrator and can be placed anywhere on the spacecraft. The system mass can also be significantly reduced as employing fiber optics allows multiple smaller concentrators, which can be independently pointed on-sun, to replace a single large fixed concentrator (Figure (1.2b)). Given that the mass of a (concentrator) mirror scales as the 4^{th} power of the diameter, smaller mirrors are favoured. This flexibility comes at a cost however; the energy traveling along the fiber is attenuated and reduces the end-to-end efficiency of the system. Also there is the added complexity of separately pointing each mirror in an array. This research has demonstrated the validity of applying a fibre augmented solar thermal propulsion system to a small satellite.

1.3 Scope of Research

The scope of this research is broad and incorporates a wide field of academic and industrial topics. The main theme of this research is the technological development of a fibre augmented solar thermal propulsion system for a small satellite for the purposes of a technology

demonstration. Firstly the main benefits of the introduction of fibre optics to a solar thermal propulsion system, suitable for a small satellite, are identified. Then a number of appropriate small satellite missions that could gain from this technology are investigated to determine mission specific requirements. These requirements are passed through to the preliminary design of the separate components that make up the propulsion system. Each component was designed to the Surrey Space Centres mantra of low cost access to space. This requires that the system and component features be kept small, simple and affordable. This reduces the number of technological unknowns and provides a more fully developed system.

These designs are then subjected to computational modelling through the use of standard and validated codes in the areas of ray tracing, thermal analysis and control analysis, to demonstrate expected performance. A number of computational modelling tools were created to this end and an existing integrated system model of a conventional solar thermal propulsion system for a micro satellite was adapted to incorporate fibre optics.

The practical element of this research focused on the technology requiring the most development, namely the fibre optics and the pointing control of the solar concentrators. A suitable fibre optic cable was identified and was subjected to transmission, thermal and stress tests. Suitable fibre optic connectors were fabricated and tolerance tested. A novel concept for pointing control of a solar concentrator was developed and tested using an Xpc-target system for pointing control and analysis. The development of a prototype miniature receiver/thruster assembly was limited to design work only. This is because it was considered a more difficult engineering task to develop a solar power collection and delivery system, which would fulfil the strict tolerances necessary to allow the system to function. However given the heritage of solar thermal propulsion work at the Surrey Space Centre it is considered an achievable task to rapidly manufacture a flight ready STP thruster.

Section 2

2 Literature Survey

2.1 Solar Thermal Propulsion Concepts and Heritage

Krafft Ehricke, a German-American space flight engineer, was the first to conceive the concept of solar thermal propulsion in 1956 [5]. By 1962 the first solar thermal rocket engine was successfully tested at the U.S Air Force Rocket Propulsion Laboratory (AFRPL) located at Edwards Air Force Base, California. This first test demonstrated the great potential of STP with an engine specific impulse of 680s using hydrogen as propellant [6]. This value of specific impulse is extremely competitive by current spacecraft bipropellant engine standards, which are capable of approximately 340s. Specific impulse (I_{sp}) rates the amount of propellant required to provide a certain change in velocity. It is defined as the thrust (T) divided by the weight of the mass flow rate ($\dot{m}$) [7]:

$$I_{sp} = \frac{T}{\dot{m}g} = \frac{I}{M_p g} = \frac{u_e}{g} \quad \ldots\ldots(2.1)$$

Where u_e is exhaust product velocity and g is gravitational acceleration. Thus this first test of STP demonstrates that to produce the same impulse (I) as a modern state-of-the-art bipropellant engine an STP engine could potentially only require approximately half the mass of propellant (M_p). This increase in propellant efficiency is advantageous in terms of cost and can enable a given satellite to have a greater portion of it's mass devoted to payload. Potential mass savings of propellant becomes more substantial for manoeuvres and space missions requiring larger changes in velocity increment (ΔV). This relation is visible from the so called "rocket equation" devised by Tsiolkovsky [7]:

$$\Delta V = u_e \ln \frac{M_o}{M_b} = I_{sp} g \ln \frac{M_o}{M_b} \quad \ldots\ldots(2.2)$$

Where M_0 is the starting mass of the rocket and M_b is the burnout mass of the rocket, generally a combination of structure mass and payload mass. For small ΔV requirements moderate differences in specific impulse are relatively unimportant as the mass saving in propellant is only marginal. To demonstrate this consider a 100kg satellite capable of 50 m/s ΔV for orbit maintenance

manoeuvres. A propellant mass saving of 0.85kg is incurred by employing a propulsion system capable of 680s instead of 340s. However, a 1,000kg satellite or upper-stage capable 0f 4,200 m/s ΔV (typical for LEO-GEO transfer) would incur a mass saving of over 1,600kg. This comparison does not take into account the complexities of the varying propulsion systems capable of these performances but serves to demonstrate that for larger ΔV requirements STP becomes increasingly more appealing.

From the 1960's through to the 1970's the development of STP was delayed by investigations into other forms of high performance propulsion, such as solar electric and nuclear thermal concepts. Interest in the STP concept was increased by a technical report written by Etheridge in 1979 [6], which concentrated on the value of STP for high ΔV space missions. Etheridge analysed a number of STP configurations and identified key technologies that would enable a performance of up to 1000s specific impulse. Technologies such as large, low mass, inflatable concentrators and refractory metal windowed solar cavity receivers were employed to heat a particle laden hydrogen flow up to temperatures of 2,800K. The report concluded that STP was a viable option for high ΔV missions and offered a good compromise between an ion bombardment type propulsion system (long trip time/high payload mass) and a LO_2-LH_2 stage (short trip time/low payload mass). Since the appearance of the Etheridge report much research has been conducted into the key technologies identified regarding STP system components. Consequently a number of varying STP configurations employing these technologies exist. A relatively recent concept is the Integrated Solar Upper Stage (ISUS) program developed at the US Air Force Phillips Laboratory and ground tested at the National Lewis Research Centre (NASA-LeRC) around 1997, figure-(2.1). This STP configuration employed deployable, faceted concentrator arrays to gather the necessary power to the solar cavity receiver [8]. However, despite recent advances in technology and substantial past research a, solar thermal propulsion system is yet to be launched.

(a)

(b)

Figure 2.1: (a) Integrated Solar Upper Stage. (b) NASA-LeRC tank six test facility [8]

2.1.1 Sunlight Concentration Techniques

The harnessing of concentrated sunlight is a very old concept and has been practiced for thousands of years; possibly as early as the clay-tablet era in Mesopotamia (~2000BC), when

(a) **(b)**

Figure 2.2: (a) Parabolic solar cooker. (b) Fresnel solar cooker

polished golden vessels were used to ignite alter fires [9]. Development of solar energy technology speeded up over the course of the 18th and 20th centuries. In 1747 astronomer Jacques Cassini constructed a lens 112cm in diameter that was capable of melting an iron rod, suggesting temperature of around 1000°C. A common use of simple sunlight concentrating technology is for cooking food in arid/desert environments. The two most common methods of sunlight concentration are parabolic and Fresnel lenses/mirrors figure (2.1). Solar furnaces in the 19th century would employ faceted flat mirrors arranged in a parabolic manner such that they had a common focus. Modern technology allows the construction of mirrors with parabolic surfaces of excellent surface quality. The geometric concentration ratio (CR_g) of a concentrating component is defined as [10]:

$$CR_g = \frac{A_a}{A_f} \quad \ldots\ldots(2.3)$$

Where A_a is the aperture area and A_f is the focal spot area. A large geometric concentration ratio indicates an ability to harness a large intensity of light. Thus the concentration ratio has a big impact on the final temperature of the solar energy receiver. If we consider a windowless cavity receiver, the size of the aperture in to the cavity is reduced for larger concentration ratios of the concentrating optics, thus reducing radiative heat loss. The Stefan-Boltzmann law of radiation, is given by:

$$P = \varepsilon\sigma A T_s^{\,4} \quad \ldots\ldots(2.4)$$

Where P is the power radiated from a body of surface temperature T_s, surface area A and emissivity ε. Equation (2.4) indicates that the smaller the area of a body being heated by an

external source, the higher the temperature of the body when a power balance is struck between incoming power and radiated power.

Past STP configurations rely on the collection of large amounts of solar power to heat a propellant, which is typically hydrogen. Grossman [1] of L'Garde Inc, discusses the design of an STP configuration employing twin off-axis inflatable parabolic concentrators, having an elliptical rim semi-major axis of 40m, figure (2.3). The intensity of solar energy at the Earth's orbital radius is 1,353 W/m^2, suggesting the power collected by these twin concentrators is on the order of 2 MW. This collected power heats the hydrogen propellant to a temperature of 2,500°C, which when exhausted through the thruster produces 196 N of thrust. Grossman states that a concentration ratio of 10,000:1 is required to achieve the necessary propellant temperature.

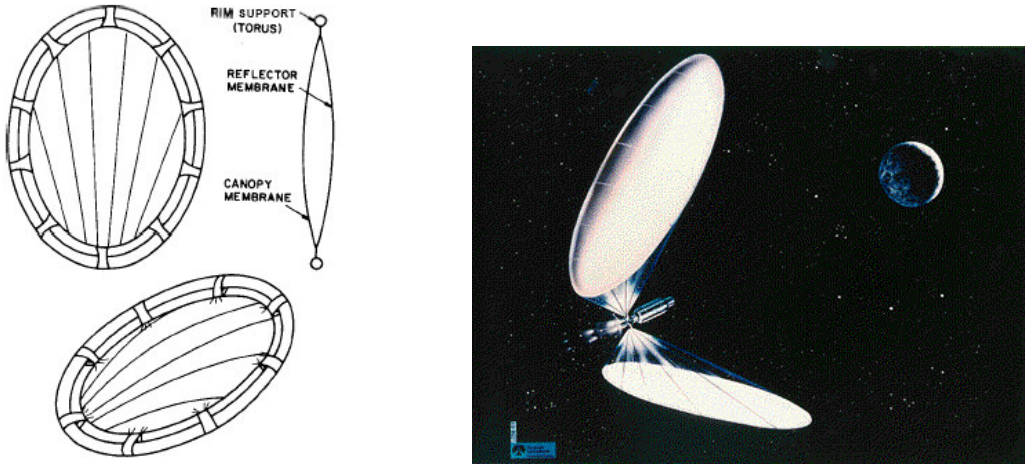

(a) **(b)**

Figure 2.3: (a) Inflatable parabolic concentrator design. (b) L'Garde Inc STP concept [1]

Thin film inflatable concentrators offer a specific weight of <1kg/m^2, which is promising considering the large collecting areas required [11]. What they lack is sufficient surface quality to attain a large enough concentration ratio. Pearson [12] of SRS Technologies reports a 1.14mm RMS (Root Mean Square) shape error, over a 2-year storage period, for a 5m inflatable

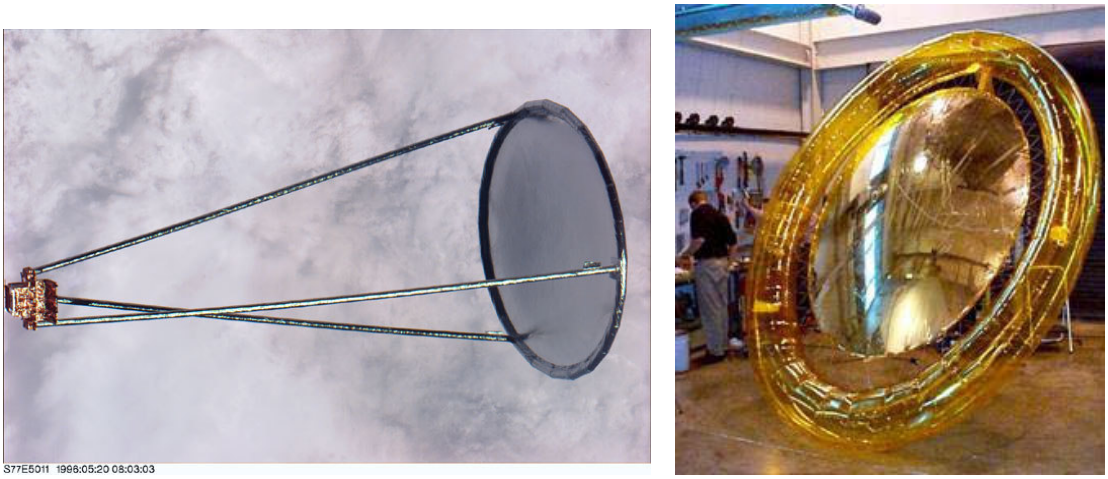

(a) **(b)**

Figure 2.4: (a) The L'Garde inflatable antenna experiment.
(b) Inflatable concentrator of SRS Technologies [13, 12].

concentrator. AFRL in conjunction with SRS and NASA have manufactured and tested inflatable concentrators of varying size. A number of inflatable structures have been manufactured and tested, including a flight test of an inflatable antenna. The Inflatable Antenna Experiment (IAE) was a joint venture between NASA and L'Garde Inc. A 14m diameter inflatable antenna, designed for millimetre-wavelength communications, was launch during a Space Shuttle mission in 1996. The experiment was intended to supply data on surface form errors and thermal stability over orbital periods. However the antenna failed to inflate to a functional pressure and was only able to deploy due to residual gas within the inflation system [13] (Figure (2.4a)).

An alternative concentrating system was investigated by NASA, in the form of the Shooting Star Experiment (SSE) (figure (1.1b)), and consisted of a thin film, deployable, Fresnel primary concentrator. Due to the poor concentration ratio of the primary concentrator a secondary concentrator was employed to gather the light in to the thruster and increase the over all concentration ratio, (figure (2.5)) [14].

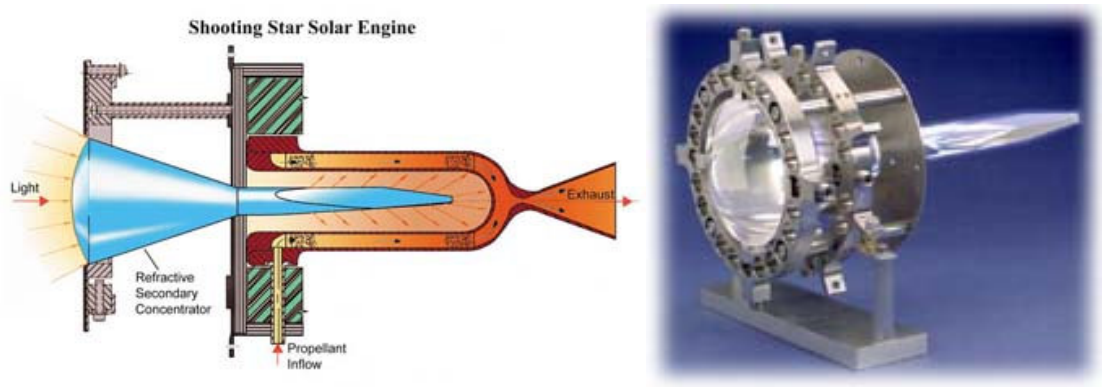

(a) **(b)**

Figure 2.5: (a) Refractive secondary concentrator design.
(b) Zirconium prototype refractive secondary concentrator [14]

Through refraction and total internal reflection light from the primary is channelled in to the thruster, which reaches temperature in excess of 2000K. The secondary concentrator is typically manufactured from sapphire or zirconium, materials which are capable of withstanding such high temperatures. The secondary is capable of augmenting the primary concentration by an additional 20:1 ratio. This innovative high efficiency concentrator offered significantly higher throughput efficiency over other secondary concentration schemes, such as a hollow reflective secondary only offering an additional 7:1 concentration. Other advantages included the ability to tailor the radiative energy distribution upon the cavity wall and no requirement for active cooling [15].

Alternative concentration system configurations have been considered over the years including solid precision surface concentrators, deployable petal structures and tensioned membranes. Although solid and deployable petal structures incur higher specific weights > 1 kg/m^2 this can be compensated by increased performance. The Integrated Solar Upper Stage (ISUS) program developed at the US Air Force Phillips Laboratory, see figure (2.1a), employed deployable,

faceted concentrator arrays to power a thermal-storage thruster[1]. The higher performance potential of thermal storage thrusters allowed the reduction in size of the concentrator array and compensated for the additional array mass [16].

2.1.2 Solar Thruster Heritage

Solar thermal propulsion is a monopropellant propulsion system and in order to provide a competitive performance must heat the propellant to high temperatures via an external means. Many of the concepts discussed in the previous section relied upon the collection of massive amounts of power to directly heat the propellant via the solar cavity receiver. Therefore the power available to heat the propellant is limited by the collection area of the solar concentrators. In other chemical bi-propellant propulsion systems the energy available to heat the propellant is obtained through the decomposition or combustion of the propellant and no external heating system is required. These systems are designed such that heat transfer between propellant and the engine wall is minimised, where as in a solar thermal propulsion system this heat transfer is maximised. Alternatively, for a STP system, the propellant can be heated directly from the concentrated solar radiation, this requires an enclosed cavity with a windowed aperture and "seedant" particles present within the propellant to increase absorption. Both the above concepts require the concentrating system to be pointed at the sun during the burn [17].

A report written by Shoji [17] for AFRL, trades a variety of solar heat exchanger concepts in terms of performance, life, reliability and cost. Five concepts were traded, including:

- Windowless heat exchanger cavity: Solar energy is received through the cavity aperture and hydrogen propellant flows through the walls of the cavity. Maximum propellant temperature is limited to the maximum allowable termperature of the cavity wall material. Performance estimated at 900s specific impulse.
- Windowed particulate absorption: A seed or molecular constituent is mixed in to the propellant to directly absorb the solar radiation. A transparent window is employed to contain the propellant flow and is cooled by pure hydrogen, which also prevents deposition of the seed on the window. The absorbing component of the propellant has a high molecular weight, which restricts performance to 1000s specific impulse.
- Windowed rotating bed: Similar to the particulate absorption concept. A rotating porous cylinder creates a centrifugal force to retain the seed component of the hydrogen

[1] Thermal storage solar thermal thrusters store energy from the incoming light in high heat capacity materials. Heat is then removed from the thruster by the propellant. This concept offers high performance as the power transferred to the propellant is not limited to just the power collected by the concentration system.

propellant. This concept requires high temperature bearings and seals and can provide a performance of 1100s specific impulse.

- Windowed alkali metal absorption: Easily ionised alkali metals such as lithium are introduced into the hydrogen propellant to create a radiation absorbing plasma. Again pure hydrogen is used to cool the window and prevent deposition of the alkali metal. The higher molecular weight of the alkali metals compared to hydrogen lowers the achievable specific impulse to 1000s. This concept was first introduced by Rault and Hertberg [18]
- Windowed graded porous material absorption: A series of porous refractory carbide disks within a regeneratively cooled cylindrical absorption chamber. These disks absorb solar radiation and transfer heat to the hydrogen propellant flowing through the pores of the disks. Porosity is optimised for propellant heat absorption with a reasonable pressure drop through the disks. A system performance of 1050s is estimated.

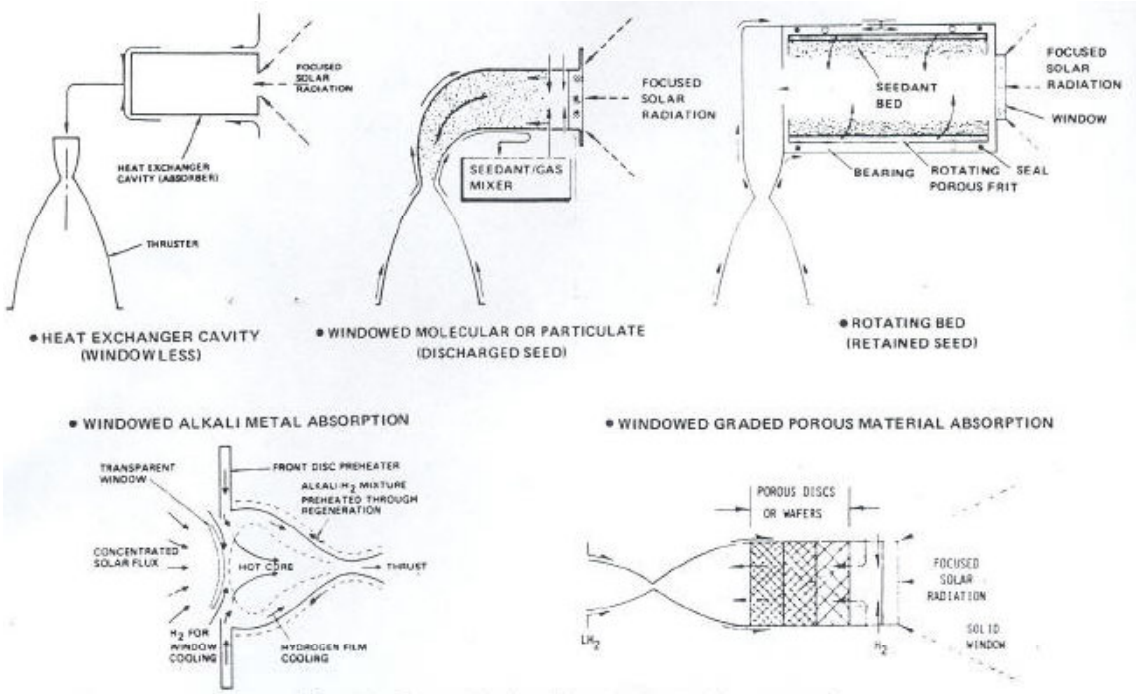

Figure 2.6: Various STP 'direct-gain' receiver concepts [17]

The windowless heat exchanger cavity had been previously identified as the most suitable for near-term proof-of-principle physical testing, owing to it's relatively low mass, high reliability and low cost. Shoji [19] discusses in-depth the design and manufacture of a high performance ground-test STP thruster. Rhenium was selected for the high temperature absorber thruster due to its ability to withstand high temperatures while at the same time remaining ductile and weldable, see figure (2.7a). The solar absorber is a coiled rhenium tube and the thruster is a rhenium converging/diverging nozzle. Performance calculations provide a relation between final hydrogen propellant temperatures and delivered specific impulse shown in figure (2.7b). Smaller

windowless STP thrusters were manufactured and tested at the National Aerospace Laboratory (NAL) of Japan [20]. These thrusters were designed for operation aboard 5–50kg nano/microsatellites and were designed with receiver cavity apertures of size 10, 20 and 50 mm. Single crystal tungsten and molybdenum were used to construct these thrusters. Patented by the National Research Institute of Metals (NRIM) these unique materials exhibited no high temperature recrystallisation embrittlement. The testing of these thrusters demonstrated a performance of 750s at temperatures as high as 2,000K with nitrogen and helium gas as propellant.

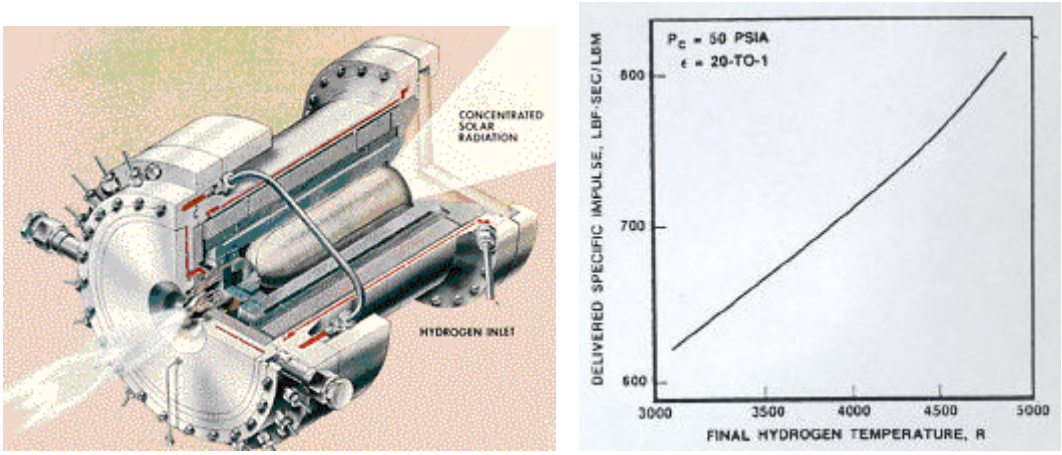

(a) **(b)**

Figure 2.7: (a) Ground test rhenium STP receiver.
(b) Hydrogen propellant temperature vs. performance [21]

An alternative approach to the direct heating of propellant via a heat exchanger or direct absorption was investigated for the Integrated Solar Upper Stage (ISUS). This alternative approach employed high heat capacity materials to absorb and store the energy from the incident concentrated sunlight. This approach permits the ability to thrust without the concentrator system targeting the sun and offers higher thrust firings or smaller concentrator systems, as the power to the propellant is now only limited to what can be stored by the high heat capacity materials. The ISUS cavity receiver, referred to as the Receiver-Absorber-Converter (RAC), consisted of a graphite black body cavity with high temperature insulation around its exterior. The graphite thermal storage cylinder was coated with rhenium, protecting it from hydrogen sublimating at high temperatures [21]. The ISUS RAC was ground tested at the National Lewis Research Centre (NASA-LeRC) in 1997. Figure (2.1b) shows the Tank 6 facility at NASA-LeRC, which is a high vacuum chamber with a 30 kW xenon arc lamp solar simulator capable of simulating the sunlight environment in space. The peak specific impulse achieved by the ISUS RAC on July 22, 1997 was estimated from test data to be 742s with hydrogen propellant [22].

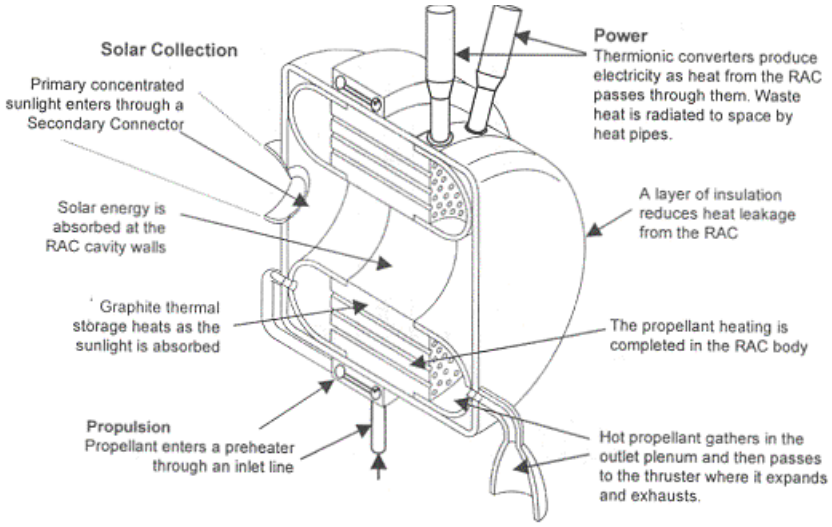

Figure 2.8: ISUS RAC design [22]

Recent research conducted at the University of Surrey looked in to the use of high heat capacity ceramics for thermal storage STP cavity receivers. TiB2/BN and zirconia-strengthened boron nitride (ZSBN) cavity receivers were successfully tested at a temperature of 2,000K and subjected to helium, nitrogen and ammonia propellant at temperatures as high as 1,700K [23].

2.1.3 Propellants for Solar Thermal Propulsion

For STP concepts from the 1960s through to the present, hydrogen has been the propellant of choice. The reason for this is due to hydrogen having the lowest molecular mass ($\overline{M}$) available, and for a given chamber temperature (T_c), provides the highest specific impulse in comparison to any other propellant. This is demonstrated in the following relation [7]:

$$u_e = \sqrt{\frac{2\gamma\overline{R}}{(\gamma-1)\overline{M}} T_c \left[1-\left(\frac{P_e}{P_c}\right)^{(\gamma-1)/\gamma}\right]} \quad \ldots\ldots(2.5)$$

Where γ is the ratio of specific heats, $\overline{R}$ is the universal gas constant, P_e is the propellant exit pressure and P_c is the propellant chamber pressure. Equation (2.5) demonstrates that for smaller molecular weights higher exhaust velocities are possible, granting greater performance, for a given temperature. Although hydrogen provides high performances difficulty is experienced in the storage of hydrogen. With a low storage density of 71 kg/m^3, hydrogen requires large storage tank volumes to provide enough volume for the required mass. Tank volume is typically minimised by storing liquid hydrogen in a cryogenic tank but this requires substantial power to maintain. Also any heat transfer to the liquid hydrogen could result in boil off and disastrous increases in tank pressure. This is more the case for the long-term storage of hydrogen envisioned by STP concepts. Subsequently hydrogen storage tanks tend to be large, heavy and power hungry.

Returning again to considering the ISUS, Cady [24] proposes a design for a Cryogenic Storage and Propellant Feed System (CSPFS) for use with the ISUS. The CSPFS is required to provide efficient storage and delivery of liquid hydrogen to the STP system for a 30-day mission duration. A multilayer-insulated tank is used to prevent liquid hydrogen boil-off. A zero-g Thermodynamic Vent System (TVS) subcools and collects counter flowing liquid hydrogen in a Liquid Acquisition Device (LAD), eliminating a need for a pressurisation system. Additional heat from the tank is removed by subcooled hydrogen passed through a heat exchanger. All the vent flow from the TVS is used in the STP engine and none is jettisoned. Chato [25] discusses the requirement for space testing of the TVS device despite extensive ground testing. Space testing was deemed necessary due to the TVS sensitivity to low gravity and the design of suitable equipment to test the storage concept was proposed in the form of the Hydrogen On-Orbit Storage And Supply Experiment (HOSS). This included the design of a 36 to 80 litre dewar, depicted in figure (2.9):

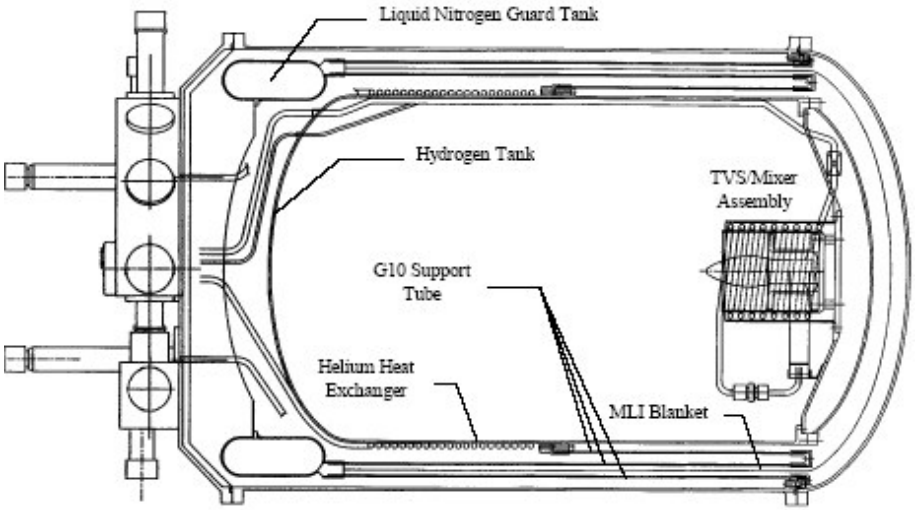

Figure 2.9: HOSS experiment dewar [25]

The study conducted by Chato demonstrated the availability of insulation and guard techniques for ground processing capable of storing liquid hydrogen in the dewars without venting in excess of 144 hours.

In this report more storable, conventional propellants are proposed for use with STP, such as hydrazine (N_2H_4) and ammonia (NH_3). Although suffering from higher molecular weight inefficiencies these propellants are much more storable (hydrazine: 1,004.5 kg/m^3, ammonia: 630 kg/m^3). Ammonia offers particularly simple storage options with its ability to self regulate under its own vapour pressure at 8bar while remaining relatively easy to handle. Both hydrazine and ammonia suffer from the endothermic reaction resulting from the ammonia's decomposition thus limiting performances to the 200s specific impulse range for non-STP augmented systems.

2.1.4 Pointing Control of Concentrator Assemblies

Limited information is available for concentrator pointing control concepts of past STP configurations, this is mainly due to research programs focussing more on concentrator and cavity receiver aspects of the STP systems. Past "direct-gain" concepts in which power is transferred directly from the concentrator array to the propellant via a heat exchanger often employed twin off axis inflatable parabolic concentrators as discussed by Grossman [1] of L'Garde Inc, see figure (2.3b). Grossman describes a pointing mechanism capable of two-degrees of freedom pointing of the twin concentrators coupled with the attitude system, enabling continuous sun tracking during a burn. A control system is described that is capable of sensing the location of the concentrated sun-spot with respect to the engine aperture via heat/temperature sensors located on a turntable around the absorber aperture. Grossman states that the concept was not final and other methods were being investigated.

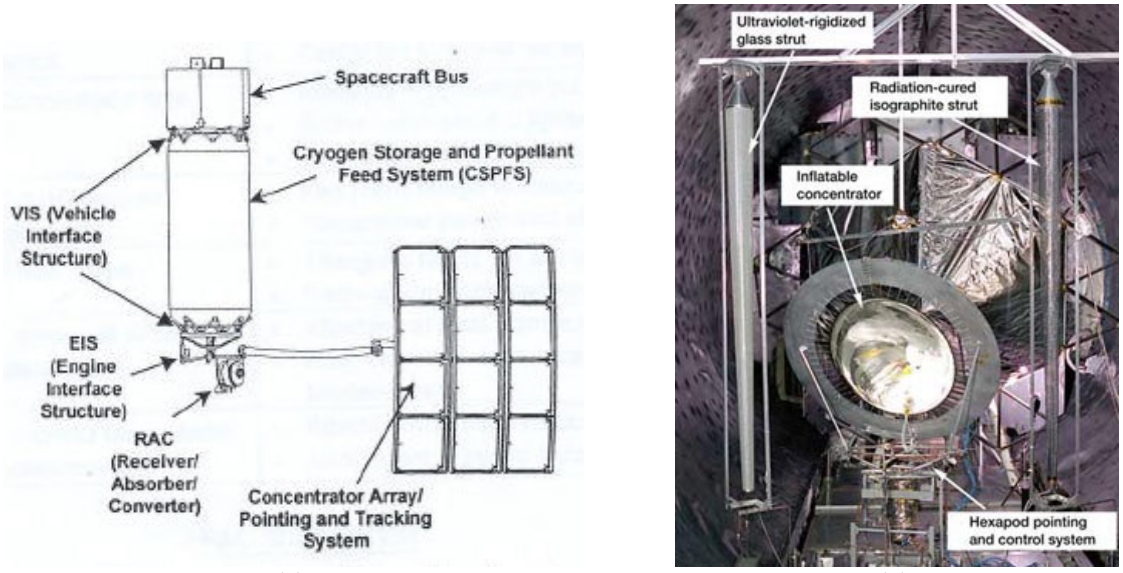

(a) **(b)**

Figure 2.10: (a) SOTV configuration. (b) ATK hexapod pointing system [21,8]

Partch [21] describes a two-axis gimbal mechanism for pointing motions, for the Solar Orbit Transfer Vehicle (SOTV) space experiment, a follow on concept to the ISUS, see figure (2.10a). Partch identifies a worst-case solar alignment error of 0.1°. AFRL research in to inflatable concentrators involved the use of the Tank 6 solar thermal vacuum facility at NASA's Glen Research Centre (GRC). The inflatable concentrator tested in this program exhibited excellent slope error of (~2mrad) and collection efficiency. The concentrator struts were mounted on a 6-degree-of freedom, electrical-actuator-driven, remote-controlled base. ATK Thiokol Propulsion developed this hexapod pointing system, see figure (2.10b).

2.2 Fibre Optics for the Transmission of High Intensity Sunlight

2.2.1 Previous Work

The concept of applying optical fibres to the transmission of solar radiation is relatively young. The earliest record found is a paper submitted by Kato and Nakamura to the Journal of Applied Physics [26] in 1976. In this paper they discuss the application of optical fibres to the transmission of broad-spectrum solar radiation. Kato identifies that the exploitation of pure fused silica and high silica content glass for optical fibres has led to remarkable reduction in light attenuation. Applications such as low cost earth based solar power plants, solar heating and cooling of buildings; under water energy transmission and high power-density spacecraft bound photovoltaic solar cells are suggested. Kato discusses the attenuation effects typical of low-loss silica fibre optics and describes the main intrinsic cause to be the presence of high O-H (Hydroxyl Ion)[2] concentrations and defects within the core material. Based on these intrinsic attenuation mechanisms Kato and Nakamura show that fused silica optical fibres can transmit concentrated solar radiation effectively over distances of 40m, see figure (2.11a).

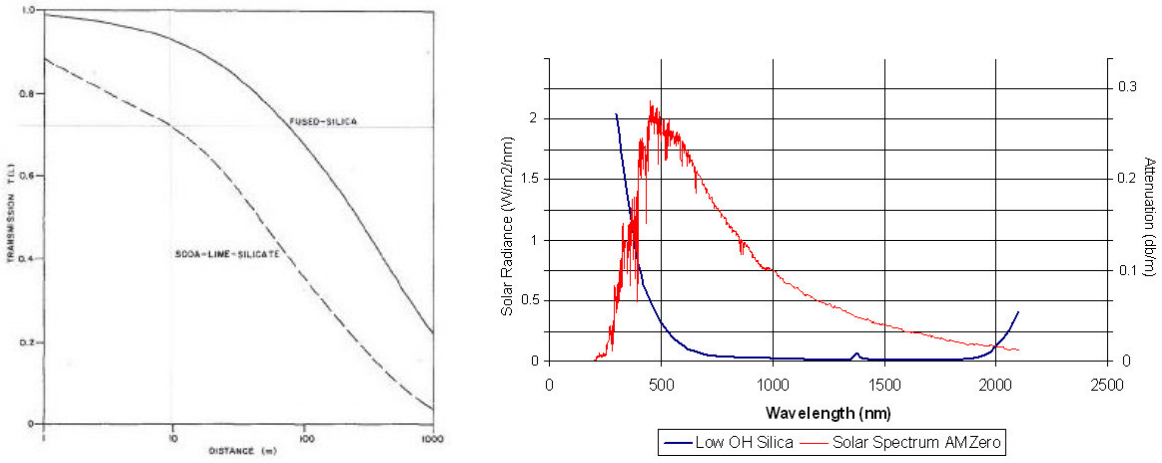

(a) **(b)**

Figure 2.11: (a) Transmission vs. distance graph for selected fibre optic materials (b) Solar spectrum superimposed on fused silica attenuation spectrum [26,27]

In figure (2.11b) we see the AM0[3] solar spectrum superimposed over the attenuation spectrum of a modern low-OH fused silica fibre optic cable [27], indicating fused silica's suitability for transmitting solar radiation. The small peak observed in figure (2.11b) at ~1400nm is an OH absorption peak. Planck's blackbody radiation law very well represents the AM0 solar spectrum:

[2] The Hydroxyl Ion (O-H) is representative of water being present in the atmosphere during the manufacture of the fibre optic.
[3] The AM0 spectrum is the solar spectrum experienced in space. Other spectrums, AM1, AM1.5 etc, are solar spectrums experienced through the Earth's atmosphere at varying angles.

$$S_\lambda = \frac{8\pi hc}{\lambda^5}\frac{1}{e^{hc/\lambda kT_b}-1} \quad \ldots\ldots(2.6)$$

Where S_λ is the energy per unit volume per unit wavelength (λ). Also h is Planck's constant, c is the speed of light, k is Boltzmann's constant, and T_b is the blackbody temperature in degrees Kelvin.

The earliest record of an effort to transmit high intensity solar energy through a fibre optic cable is reported by Cariou [28] in 1982. Cariou describes the use of a small parabolic concentrator to direct light in to a 10m fibre optic cable. A transmitted power of 2W at a concentration of 3000 is reported with a transmission efficiency of 70%. Further research conducted by Liang [29] in 1998 demonstrated transmission efficiencies of 60% when transmitting 60W of power over a 3m long anhydroguide[4] PCS low OH Vis-IR fibre. A parabolic primary concentrator was used to focus light, via a secondary mirror and an aspheric lens, into a fibre bundle made up of 19 1.5mm diameter fibre optics, see figure (2.12a).

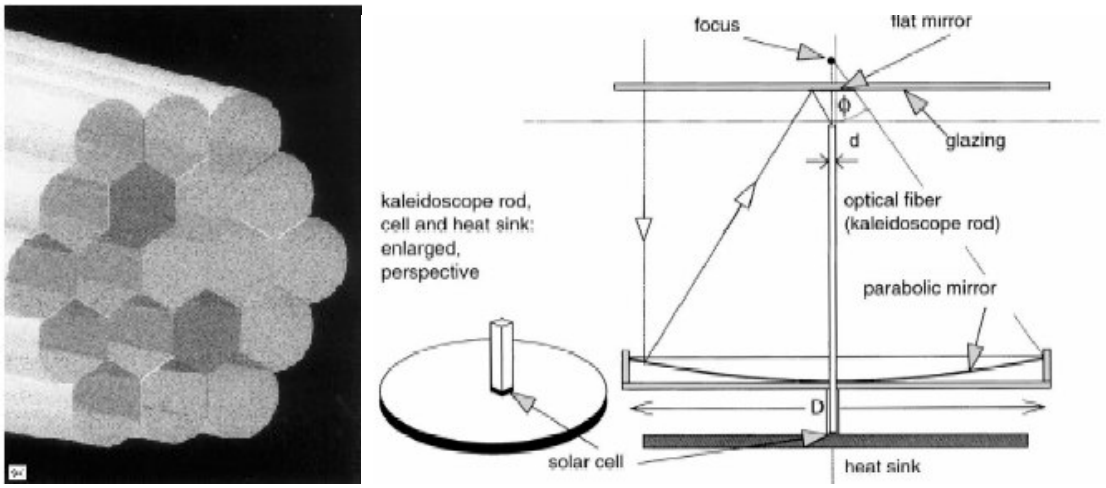

(a) **(b)**

Figure 2.12: (a) Polished fibre bundle, Liang
(b) Solar fibre-optic mini-dish, Gordon [29, 30]

Gordon [30] has investigated numerous applications of fibre optics for transmission of solar radiation. These include solar surgery, solar generation of nanomaterials, and solar electric power. Featuring in several of Gordon's publications is the solar fibre-optic mini-dish, see figure (2.12b), which effectively couples light from the dish to the optical fibre. Using a mini-dish of 20-cm diameter Gordon transmitted 8W of power over a 20m long fibre optic, demonstrating a transmission efficiency of 64%. Gordon predicts a maximum realizable system efficiency of 80% for fibre optic transmission, and identifies the importance of selecting an appropriate concentrator

[4] A fused silica core fibre optic with a doped silica cladding.

rim angle[5], which is dependant on the numerical aperture (*NA*) of the fibre optic, related to the sine of the fibre's acceptance half-angle ψ_a.

$$NA = n_e \sin \psi_a = \sqrt{n_{core}^2 - n_{clad}^2} \quad \ldots\ldots(2.7)$$

Where n_e is the external refractive index and n_{core} and n_{clad} are the refractive indices of the fibre core and fibre cladding. The numerical aperture of the fibre should be matched with the rim angle of the concentrator such that all light from the concentrator is able to pass through the fibre. Also the focal spot size attainable with the concentrator should be matched with the fibre bundle's diameter for efficient coupling between the two. In order to achieve the 80% efficiency previously mentioned Gordon stresses the importance of accurate alignment of the fibre tip with the focal spot and the use of a highly accurate sun pointing mechanism. Feuermann estimates absorption of 7% over a 100m length of fibre [31].

2.2.2 Optical Fibres for Space Based Applications

Nakamura has contributed greatly to the concepts involving fibre optics for space applications. In 2002 Nakamura [32] reports on the development of an Optical Waveguide Solar Plant (OWSP) system. Light collected by solar concentrators and transmitted through fibre optic cables is utilised for materials processing, plant lighting and solar heating on board spacecraft, as shown in figure (2.13a).

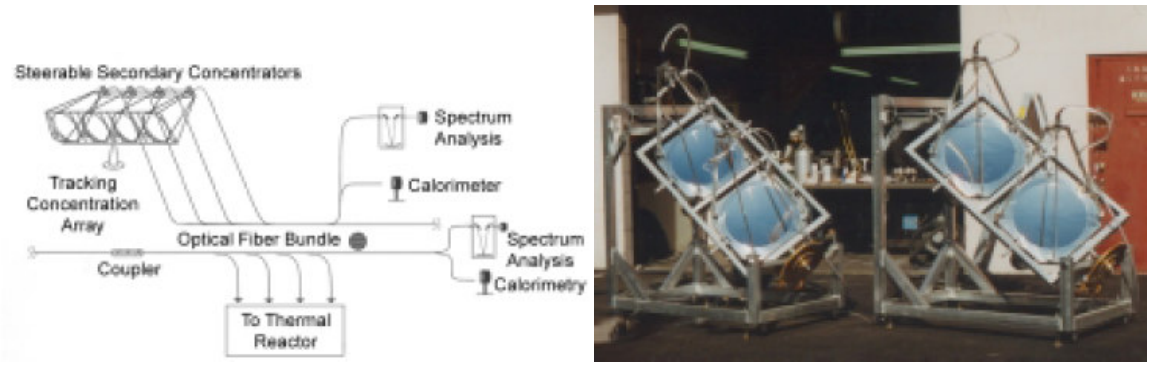

(a) **(b)**

Figure 2.13: (a) OWSP system architecture. (b) Prototype OWSP system

A rigorous component testing strategy was devised and undertaken for the OWSP system through the manufacture of a prototype, figure (2.13b). Four concentrators with rim angles matched with a fibre optic *NA* of 0.44 were coupled to a hexagonal shaped bundle of 37 fused silica core fibres. The concentration ratio achievable by these concentrators was limited to 7,500 by the fibre *NA*. A special vacuum chamber constructed for the fibre bundle was employed to determine the expected bundle tip temperature when operating in the space environment. When ground tested, the fibre

[5] This is the angle between the focal axis and the line between the focal point and the mirror rim.

bundle vacuum temperature reported was ~450°C. Given this result Nakamura estimates a maximum tip temperature of 725°C during space operation. This figure falls below the continuous service temperature of fused silica fibre optics.

In 2004 Kennedy [33] and Nakamura [34] suggest the use of fibre optics to augment a solar thermal propulsion system. Both concepts exploit the ability to use multiple concentrators to heat a single or multiple cavity receivers. Testing conducted by Nakamura has demonstrated fibre optic heating of a solar receiver with the solar receiver reaching temperatures as high as 1,600°C.

2.3 Summary

This section has provided a history of the concepts of solar thermal propulsion and fibre optic transmission of solar radiation. These technologies have recently found a common ground in the form of a solar thermal propulsion system augmented by fibre optics.

STP has been under development for over 40 years. The research originally undertaken was commonly a costly venture due to the requirement to attain a high system performance on the order of 1000s Isp. This invariably required the use of very large inflatable/deployable solar concentrators that could collect a massive amount of solar power. This power was delivered to a heat exchanger designed to operate at temperatures as high as 3000 K. The propellant selected was hydrogen, which at such high temperatures would deliver the required performance. Subsequently this demanded the design of large-scale spacecraft, dominated by their propulsion systems. The designs of these systems harboured many technological unknowns. Specifically: inflatable structures, high temperature ceramics and the storage of cryogenic hydrogen. Rockwell, AFRL and other agencies devoted resources to the development of these technologies and specific hardware, such as inflatable concentrators and solar cavity receiver heat exchangers, were manufactured. However, despite substantial research and development a solar thermal propulsion system is yet to be flown.

More recently the development of fibre optics for solar energy transmission has received a great deal of attention. Typically light collected by a parabolic mini-dish is focused onto the tip of a fused silica fibre optic bundle. Transmission efficiencies as high as 70% have been demonstrated practically for reasonably large distances, on the order of tens of meters. Vacuum heating tests also demonstrated the survivability of fused silica fibres in a space environment.

Section 3

3 Mission Analysis

In this section the difference between *thermal-storage* and *direct-gain* STP propulsion systems is discussed in more detail and missions applicable to each system are identified and reviewed. The benefits of augmenting both types of STP systems with fibre optics are also discussed. A case study is performed to demonstrate the feasibility of employing an STP system on a microsatellite. Finally a number of missions suitable for a fibre augmented STP technology demonstration are identified.

3.1 Preliminary Mission Analysis

In this analysis the advantages and disadvantages of *thermal-storage* and *direct-gain* STP systems are considered. Several missions for which STP is applicable are identified and categorised into either thermal-storage or direct-gain. For each mission STP systems are traded against competing conventional systems. Satellite platforms are categorised in to mass categories as follows:

Table 3.1: Satellite mass categories [35]

Category Name	Mass Range (kg)
Macrosatellite	>500
Minisatellite	500-100
Microsatellite	100-10
Nanosatellite	10-1

3.1.1 STP Options

In section 2 the two general types of STP were identified, namely direct-gain and thermal-storage. To reiterate what these terms mean:

- Direct-gain: This term refers to the direct heating of the propellant via a heat exchanger. Thus the power available to heat the propellant is limited to that collectable by the solar concentrators. The solar concentrators must be orientated at the Sun for the duration of the burn.

- Thermal-storage: This term refers to the storage of solar energy in a high heat capacity cavity receiver. The concentrators heat the receiver to high temperatures whilst pointing on-Sun. Thus the power available is only limited to that storable within the receiver. Then the spacecraft orientates itself such that the receiver can thrust in the desired direction.

Each of these types of STP system has advantages and disadvantages, which are now discussed; some of the disadvantages of each system can be alleviated with the application of fibre optics.

Direct-gain STP, is power limited by the size of the concentrator array. This limits the thrust deliverable by the system for a given performance. For STP systems employing large concentrator arrays such as in figure (2.3b) this is not a major issue. However for microsatellites, which are restricted in size and mass, large mechanically complex deployable systems are not viable. So for a microsatellite its physical size limits the area of the concentrator used. A typical microsatellite facet area is approximately 0.5 m^2; a circular concentrator of this size will collect approximately 260W of solar energy (solar intensity = 1370 Wm^{-2}). For this level of power (P) a thrust can be estimated by using the standard formula for electrothermal propulsion [7]:

$$\eta P = \frac{1}{2} T u_e \ldots\ldots (3.1)$$

Where η is a conversion factor of electric energy to thermal energy. Equating η to the efficiency at which an STP system collects light and delivers it to the cavity receiver we can see that a direct-gain system on a microsatellite is restricted to a thrust of 90mN for a specific impulse of 350s and an efficiency of 0.6. Direct-gain is usually suited to low/continuous thrust applications. A direct-gain STP system that has a concentrator array that is static with respect to the satellite has a very limited range of applications. This is because a direct-gain STP system conducts a burn while pointing at the Sun, thus the thrust vector is restricted to be towards the Sun. The only real application of this is for orbit raising in a 12 O'clock Sun synchronous orbit. Therefore it is necessary for a direct-gain system to have articulating concentrators, which can track the Sun independently of the orientation of the satellite. This is not necessarily true for a fibre optic augmented direct-gain STP system as fibre optics offer the possibility to mechanically decouple the concentrator from the cavity receiver and place them as desired on the spacecraft. This brings back the option of a static concentrator that can perform orbit raising and circularisation manoeuvres in any circular orbit as long as prior knowledge of the orbit is known. Typically direct-gain systems have complicated optical/mechanical devices for solar tracking and collection but simple and light cavity receivers [13].

Thermal-storage STP is not limited in power the same way as a direct-gain STP system is. The ability to store energy allows much more power to be deliverable to the propellant for a single

burn. However the size of the concentrator array does ultimately limit the final temperature to which the thermal-storage cavity receiver can approach. For microsatellites thermal-storage can extend the range of microsatellite applications with the ability to provide high thrust with competitive performance. Manoeuvres such as Geo synchronous orbit insertion and Near Earth Escape become viable for a microsatellite and could be completed within a reasonable time [13]. Consider a 0.5kg high heat capacity receiver with a specific heat (C_p) of 1,000 J/kg-K, heated to a temperature of 3000K. The Power available to heat the propellant can be estimated for a 500s burn time (Δt) through the following relation:

$$P = M_r C_p \frac{\Delta T_r}{\Delta t} \quad \ldots\ldots(3.2)$$

Where M_r is the mass of the receiver. This simple relation indicates a power of 3000W available to heat the propellant. This equates to an achievable thrust of 1.75N, by the application of equation (3.1) assuming a specific impulse of 350s and an efficiency of 1.0 (ideal)[6]. To thermally charge the thermal-storage cavity receiver the concentrator must be pointed on-Sun for a long period of time (>6000s), to attain a high receiver temperature. Once this is achieved the spacecraft can slew to the orientation required to thrust. Thus for a thermal-storage system there is no requirement to have an articulating concentrator array however during the slew manoeuvre the receiver will cool down, reducing available power. Typically thermal-storage systems have complex and heavy cavity receivers but simpler optical/mechanical devices for solar tracking and collection.

Both thermal-storage and direct-gain systems can benefit from augmentation by fibre optics. In addition to the system flexibility granted by fibre optics a mass advantage can also be attained through the use of multiple small concentrators. This will be discussed further in section 4.

3.1.2 Candidate Missions

We now consider missions for which STP could enable microsatellites to perform. The following analysis is restricted to the consideration of mini/microsatellite platforms only as platform restrictions allow for a fair trade between other propulsion systems and the applicability of STP to microsatellites is the main feature of this research. Kennedy [13] identifies three general classes of missions applicable to a microsatellite STP system, these are summarised in table 3.2:

[6] This ideal efficiency is due to the concentrator system not taking part in the propellant heating during the burn.

Table 3.2: Microsatellite candidate mission classes[13]

Mission Class	Typical ΔV Requirement (m/s)	Candidate Missions
Near-Escape	700 - 1,200	L2 orbiter & Near Earth Object (NEO) missions
Geosynchronous Earth Orbit (GEO)	~1,500	Microsatellite GEO missions
Other Body Capture	1,500 – 4,000	Lunar and interplanetary missions

From table 3.2 we see that a relatively large ΔV is required for all mission classes when compared to conventional microsatellite ΔV requirements, which are on the order of ~50m/s [3]. Current microsatellite mission concepts are evolving to consider multiple satellite configurations such as Earth observation constellations and synthetic aperture formations. An STP formation flying propulsion system would be impractical as formation maintenance requires continuous propulsion response and STP requires a heat up period and cannot function in eclipse. However an STP system for a microsatellite constellation shows promise. Two high ΔV mission concepts involving microsatellite constellations are now discussed:

Microsatellite Inspector (MI): This mission concept is based on the Disaster Monitoring Constellation, a product of Surrey Satellite Technology Limited (SSTL) (figure (3.1a)). The current DMC constellation consists of 5 microsatellites in a 10am sun-synchronous orbit at an altitude of 700km. The DMC constellation is designed to achieve daily imaging of any part of the world for the purposes of global disaster monitoring [3]. The proposed mission takes the form of a microsatellite inspector that regularly visits each member of the DMC microsatellite for the purposes of inspection and maintenance. The inspector microsatellite has a lifetime equal to the lifetime of the DMC constellation, this being 5 years. The microsatellite inspector mission involves a two week transfer period, in which the inspector travels between the members of the constellation and a two week inspection period during which the inspector will take high resolution imagery of the constellation satellite and provide support if necessary. A ΔV requirement is estimated at 1,250 m/s for a 5 year mission.

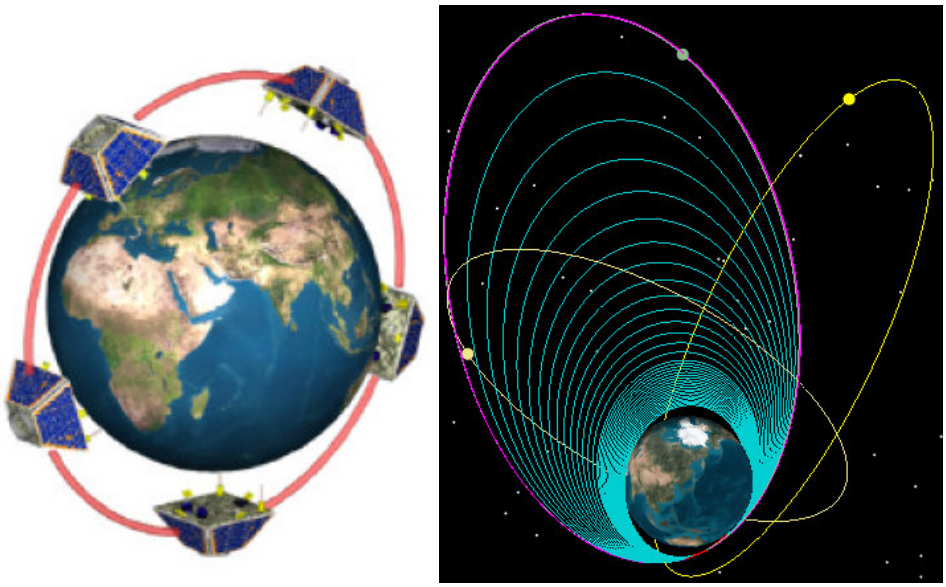

(a) **(b)**

Figure 3.1: (a) DMC constellation design. (b) VPGS constellation [3]

High Latitude Earth Observation (HLEO) Minisatellite Constellation: This mission concept is based on the Virtual Polar Geostationary Satellite (VPGS) a concept studied at the NASA Jet Propulsion Laboratory [36] (figure (3.1b)). The concept consists of a constellation of 3 satellites in separate Molniya orbits spaced 120° apart longitudinally. A Molniya orbit is a highly elliptical orbit inclined at 63.43° and has an apogee at near 40,000km altitude. These satellites are configured such that at least one satellite is functioning above the polar region at any one time. These satellites offer a large range of potential applications including:

- Monitoring of stratospheric ozone at high spatial resolution.
- Monitoring of polar tropospheric cloud systems.
- Prompt detection of high-latitude volcanic eruptions, with particular attention to airline safety.

For this mission concept it is assumed that each satellite begins in a low earth orbit at the correct inclination and must transfer into the Molniya orbit under it's own propulsion. A ΔV requirement is estimated at 2,300 m/s for insertion into a Molniya orbit.

3.1.3 First Order Propulsion System Trade

A first order comparison is now performed to establish the relative performance of STP systems with other competing systems. This analysis does not consider electric propulsion systems for the candidate missions proposed. This is due to the low amount of power available on mini/micro satellite platforms, (typically <100W) and the subsequent long duration transfer times incurred for low power electric propulsion systems. Low molecular weight monopropellants were also not

selected for consideration. Monopropellants such as hydrogen involve complex storage issues and require large storage vessels. The first order comparison considers ideal performance only, for all propulsions systems and does not take into account nozzle expansion and thermochemistry inefficiencies. System specific complexities have also not been considered. Table 3.3 lists candidate propulsion systems performance, as identified by Kennedy [13], and the required propellant mass to complete the DMC Inspector and HLEO Constellation missions:

Table 3.3 Candidate propulsion system propellant mass requirement

Propulsion System	Ideal Specific Impulse (s)	DMC Inspector: Prop Mass Satellite mass = 100kg ΔV = 1,250 m/s (kg)	HLEO Constellation: Prop Mass Satellite mass = 250kg ΔV = 2,300 m/s (kg)
Ammonia-STP	407	26.8	194.8
Hydrazine-STP	407	26.8	194.8
Water-STP	333	31.8	255.0
N_2O_4/MMH	319	33.0	271.4
H_2O_2/kerosene	298	34.8	299.0

As can be seen from table 2.3 there is a substantial difference in required propellant mass between STP and non-STP options. The mass saved for both missions could be utilised for mission enabling payloads, such as high-resolution cameras and high power antennas. Also effecting the overall mass of the propulsion system is the required storage volume for each propellant, this is summarised in table 3.4:

Table 3.4 Candidate propulsion systems propellant storage volume requirement[7]

Propulsion System	Storage Density (kg/m^3)	DMC Inspector: Propellant storage volume (Litres)	HLEO Constellation: Propellant storage volume (Litres)
Ammonia-STP	600	44.6	324.6
Hydrazine-STP	1,004.5	26.7	194.0
Water-STP	1,000	31.8	255.0
N_2O_4/MMH	1200	27.5	226.2
H_2O_2/kerosene	1310	26.56	228.2

[7] For bi-propellant options the storage density represents the average density of the oxidiser and fuel combination and thus the storage volume also represent an average value.

Each propellant is now considered:

- Ammonia-STP, although providing an ideal performance suffers from a low storage density and in the case of the HLEO constellation mission requires an unreasonable amount of storage volume. However for the DMC inspector mission the storage volume is within limits. Ammonia propulsion systems benefit from simple storage and feed systems as no pressurant is required to move the propellant from tank to thruster when stored at it's own vapour pressure of 8 bar [37].
- A monopropellant hydrazine STP system seems to offer a competitive choice in terms of storage and performance. Although technically more complex than an ammonia system (requires pressurant) it benefits from substantial space heritage. A further advantage is the additional heat gained from hydrazine decomposition [7].
- A water STP system offers relatively good performance at a low cost due to the propellants availability and ease of handling. However, water thrusters often experience complexities in propellant freezing, two-phase flow issues and thruster corrosion [13].
- The bi-propellant combination Nitrogen tetroxide (oxidiser, N_2O_4) and Monomethylhydrazine (fuel, MMH) are a hypergolic mix and has significant space heritage [35].
- The bi-propellant combination Hydrogen Peroxide (oxidiser, H_2O_2) and kerosene (fuel) are not a hypergolic mix and although it has a reasonable storage volume it requires the highest propellant mass to achieve the required ΔV [35].

In the following section a first order system design of a fibre augmented STP demonstration system is considered for flight on the UK-DMC microsatellite. The propellant chosen for this system is ammonia owing to the benefits of its simple storage and feed system.

3.2 Analysis of an STP system for the UK-DMC spacecraft

In order to study the performance and potential configuration of a Fibre augmented STP demonstration system, a conceptual system was designed for a microsatellite subject to the requirements of its conventional propulsion system. The figures stated in the following analysis are estimates based on model data and literature research. The microsatellite chosen for this study is the UK-DMC, a product of SSTL for the DMC international space consortium. Details of the UK-DMC propulsion system are given in table (3.5).

Table 3.5: DMC propulsion system details [3]

Propellant	**Butane (2.3 kg)**
Specific impulse	77s – 85s
Thrust	20 mN (minimum)
Velocity capability	20 m/s
System wet mass	7.8 kg

The STP system is required to meet thrusting requirements and remain within the system mass restriction of the UK-DMC propulsion system. UK-DMC is in a 10.00am, sun-synchronous orbit at an altitude of 700km, and is a 3 axis stabilized nadir pointed platform. An STP system cannot rely on the spacecraft to perform any sun-pointing manoeuvres, and should make use of a pointing mechanism with a large range of movement. To avoid shadowing and fibre stress issues, and to maintain a compact pointing system design, a base line is set for a 90° elevation and a ± 5° azimuth range of movement of the pointing mechanism. Figure (3.2a) shows concept drawings of a single/multi concentrator fibre augmented STP demonstration system on the UK-DMC.

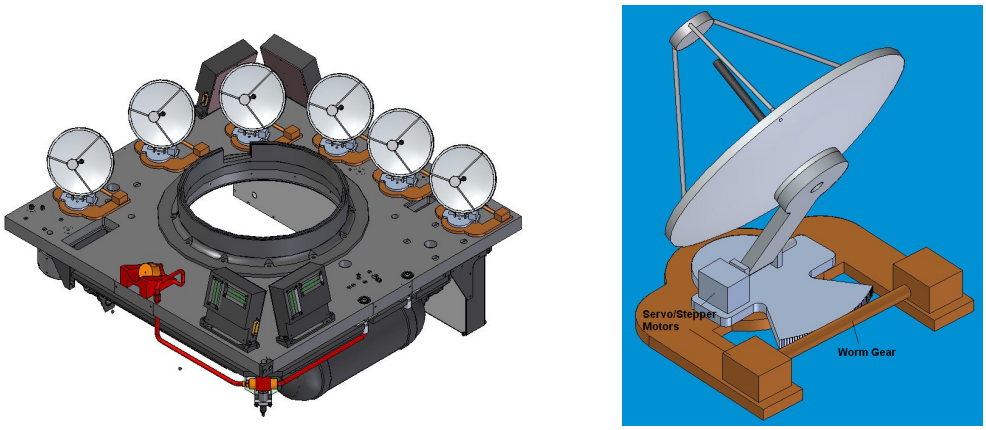

(a) (b)

Figure 3.2: (a) Multi concentrator arrangement on the UK-DMC space-facing facet. (b) Concentrator and pointing system unit concept

An ammonia direct-gain propulsion system is selected due to its simplicity in design and its reliability. Fused silica fibre-optics are employed to channel energy from the concentrator units to the direct-gain cavity receiver. The concentrating units (figure (3.2b)) are considered modular and independent of each other, having built in control electronics. They are constructed completely from silicon carbide and the concentrating mirror has an aluminised highly reflective surface. Table (3.6) details the properties of the designed fibre augmented STP demonstration system for the UK-DMC microsatellite.

Table 3.6: Fibre augmented STP system details for the UK-DMC

Parameter	Value	Comments
Specific impulse (s)	240	Average over long duration burn.
Thrust (mN)	20	Average over long duration burn. (Minimum)
Optical system mass (kg)	3.6	6 concentrator units.
Fiber optics mass (kg)	0.5	6 silica fibre bundles.
Receiver system mass (kg)	0.3	Molybdenum receiver, graphite insulation, support structure, and propellant feed system.
Structure mass (kg)	0.75	Tank support structure.
Propellant	Ammonia	Incorporates a simple storage/feed system.
Propellant tank volume (L)	2	Based on the propellant tanks of UK-DMC, which has two to store 2.3 kg of butane.
Propellant tank mass (kg)	1.5	
Propellant storage density (kg/m3)	600	
Propellant mass kg	1.2	
Propellant storage pressure (bar)	8	Ammonia vapour pressure.
ΔV capability (m/s)	31.5	Based on highest average Isp.
Total system mass (kg)	7.85	

The results reported in table (3.6) suggest that an fibre augmented STP demonstration system is capable of functioning within the design requirements of a microsatellite and can even provide performance competitive with conventional propulsion systems, for example hydrazine monopropellant thrusters. The STP propulsion system parameters in table (3.6) indicate an increased ΔV capability to 31.5 m/s compared to the UK-DMC butane resistojet propulsion system specifications, which could be used to extend the life of the satellite.

This approach of using modular concentrator units provides system flexibility for potential flight opportunities. The limiting factor for potential flight opportunities is the available spacecraft area and power. Therefore the concentrating units will be required to be as compact and light as possible, which is reflected in the above analysis. The system properties indicated in table (3.6) form the baseline concept for a fibre augmented STP demonstration system.

3.3 Candidate Microsatellite Missions for Technology Demonstration

For the purposes of a technology demonstration of a STP system a number of future microsatellite missions are now discussed and basic system requirements of a test demonstration are proposed. Future microsatellite missions are listed in table (3.7):

Table 3.7 Candidate missions for technology demonstration of STP system [38,39,40]

Programme	Status	Launch	Propulsion	Comments
PICARD	In Development	2008	Hydrazine	Solar observing satellite
MICROSCOPE	In Development	2008	FEEP	Equivalence Principle experiment
GEMINI	Concept Study	N/A	Hydrazine	Small satellite geo-stationary platform

The PICARD and MICROSCOPE missions identified in table (3.7) are particularly suitable for an STP demonstration mission. Both these satellites are members of the CNES MYRIADE series. They are both proposed to be in 6am-6pm polar sun-synchronous orbits and therefore, do not go into eclipse around the orbit. The GEMINI concept is under study at SSTL. GIOVE-A launched December 2005, demonstrated GEMINI core technologies.

(a) **(b)**

Figure 3.3: (a) PICARD illustration (b) MICROSCOPE illustration [38,39]

PICARD: This platform is designed for solar observation and subsequently requires deployable solar panels and a high pointing accuracy of 36 arcseconds. The spacecraft weighs 150kg, consumes 0.62 m^3 of volume and can provide 42W to the payload. This satellite would be an ideal platform for a STP demonstration. Deployable solar panels negate any shadowing issues that would otherwise occur for body-mounted panels. A reasonably large surface area would allow room for two mini concentrators to provide concentrated solar energy to a small ammonia direct gain thruster. This not only would demonstrate STP augmented with fibre optics but also the use

of multiple concentrators. The high pointing accuracy of the platform will assist a concentrator pointing system to acquire the Sun [38].

MICROSCOPE: This platform is designed primarily for an equivalence test experiment. This spacecraft weighs 200kg, consumes $1m^3$ of volume, and can provide 200W of power from its solar arrays. Like the PICARD platform deployable solar panels negate any shadowing issues. This platform having a much larger surface area than the PICARD platform offers the possibility of more concentrators to further demonstrate the multi mirror ganged principle of a fibre augmented STP system [39].

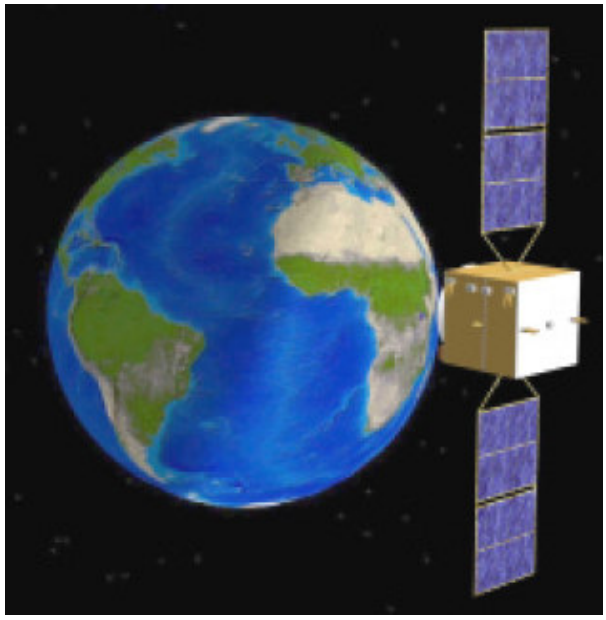

Figure 3.4: The GEMINI satellite platform [40]

GEMINI: This platform is designed as a small satellite geo-stationary platform and again offers the advantages of a relatively large volume ($1m^3$) and deployable solar panels providing 800W of power to the payload. As this satellite will be in a geo-stationary orbit, it will be in eclipse for certain periods of time. However, it is believed that through employing a direct gain ammonia system, rapid heat up of the thruster would resolve this issue [40].

A fibre augmented STP system suitable for a technology demonstration mission aboard any of the above satellites would require at least two small concentrators coupled to a single thruster. The size of these small concentrators is dependant on the spacecraft area available. For example these concentrators could have a diameter of 110mm. A suitable pointing mechanism would take up an area of $0.01m^2$, slightly larger than the area consumed by each concentrator. Thus the concentrators would take up a total area of 0.02 m^2. Such a mechanism would require approximately 0.5W of power. The thruster would be located towards the edge of the spacecraft

facet and would be coupled to the concentrators by fibre optic cables running through supported cables on the facet surface. The thruster, potentially reaching high temperatures, would be required to be thermally isolated from the structure to avoid compromising any sensitive instruments on the host satellite. The maximum temperature experienced by the thruster is dependant of the number of concentrators available.

3.4 Summary

Solar thermal propulsion is an enabling technology for microsatellites to perform a greater variety of missions, which have large ΔV requirements (~2,000 m/s). In this section the benefits of fibre optic augmentation of a solar thermal propulsion system have been discussed. Candidate missions enabled for microsatellites through solar thermal propulsion are identified. A case study of a fibre augmented solar thermal propulsion technology demonstration missions is performed for the UK-DMC microsatellite. Finally candidate host satellites are identified that would be suitable for a solar thermal propulsion demonstrator mission.

Section 4

4 System Design

This section discusses the design approach necessary to integrate fibre optics into a solar thermal propulsion system. To facilitate this discussion, the mission requirements in the previous section are used to develop system components. Through consideration of individual components, design trades and analyses are identified and essential theory is discussed.

4.1 System Configuration Design

We now consider the configuration of an STP system suitable for a microsatellite. The constraints imposed by a microsatellite platform demand a suitable STP system to be lightweight, volume efficient and reliable. Through consideration of other propulsion systems, such an STP system is also required to provide a high performance at a low cost. Simplicity is also generally desired although not a requirement. In the previous section, both types of solar energy manipulation were found to be applicable in specific microsatellite missions. For an STP demonstration mission, however, a direct-gain ammonia system was identified to be most appropriate. Thus, the main configuration design choice is a concentrator type using a concentrator pointing method. Table (4.1) lists the available options for concentrator type and table (4.2) lists concentrating pointing methods.

Table 4.1: Concentrator options

Concentrator Options	Comments
Rigid Fixed	Simple, cheap, reliable, highest areal density
Rigid Deployable	Complex, expensive, reliable, light weight
Inflatable	Complex, unreliable, lowest areal density

Table 4.2: Concentrator pointing methods

Concentrator Pointing Method	Comments
Non Articulated	Relies on satellite attitude control system, simple, limits performance and flexibility.
Articulating Mechanism	Complex, enhances performance and flexibility.

The concentrator options presented in table (4.1) outline general characteristics for the types of concentrator available. In light of these properties, a 'Rigid Fixed" concentrator is selected for the microsatellite fibre augmented STP system. The reason for this choice is not only due to the simplicity and low cost of the concentrator, but also because a rigid, fixed concentrator stands to benefit the most from augmentation via fibre optics. Fibre optics will allow multiple, smaller concentrators to take the place of a single, larger concentrator of the same collection area. This capability has the potential of lowering the overall mass of the concentrating system. This mass reduction will be discussed further in section (4.2).

The concentrator pointing options presented in table (4.2) indicate a choice must be made between the use of the satellite's attitude control system and the use of a mechanism. Relying on a satellite's attitude control system to point the concentrator at the Sun is the simplest, most reliable option, but this competes with the satellites requirement to point its photovoltaic arrays at the Sun. For a thermal-storage STP system, which can potentially require Sun exposure for several hours, this is a significant problem. Solutions include deployable photovoltaic arrays, canted body panels and additional/larger batteries. In addition, a satellite's attitude control system will have a very limited capability to compensate for spacecraft vibrations leading to pointing errors. Employing an articulating mechanism, although complex, allows the concentrator to track the Sun independently of the satellite's attitude. The satellites attitude system, however, would be required to compensate for the motion of the concentrating mechanism, which could potentially weigh up to 15kg. This is especially the case for a single concentrator, which would require a large mechanism to orientate it and compensate for other spacecraft vibrations. The use of multiple smaller concentrators could reduce or even nullify attitude control system compensation. In addition the mechanism for each small concentrator could light weight, compact, and compensate for a higher level of spacecraft vibration thus making the pointing system more accurate. A multiple concentrator system also has inherent redundancy, for example a single component failure may result in a single concentrator malfunctioning, but the system could still operate with the other concentrators available. This approach is selected for the fibre augmented STP demonstration system.

4.2 Concentrator Design

A number of optical components are available for the concentration of light. To avoid an over complicated concentrating optical system the number of concentrating components is limited to a single primary concentrator. Table (4.3) lists the available concentrating optical components.

Table 4.3: Rigid, fixed concentrator options [9]

Concentrator	Ideal Concentration Ratio	Comments
Parabolic mirror	~13,000	Highest concentration, light weight, simple, expensive
Spherical mirror	~150	Lowest concentration, light weight, simple, cheap
Fresnel lenses or mirrors	~1,000	Heavy (lenses only), complex, expensive

From table (4.3) we can see the relative performance of the candidates for the primary concentrating component. Spherical mirrors are relatively simple to manufacture, and therefore, cheap, however, their concentration ratio is unacceptably low for this application. Fresnel lenses and mirrors although granting higher concentration with respect to spherical concentrators, does not outperform parabolic concentrators, which were chosen for this application.

4.2.1 Parabolic Concentrator Optics

A parabola is a curve that is defined as being the locus of points which are equidistant from a fixed line (the directrix) and a fixed point (the focus). This geometry is shown in figure (4.1). Thus, the distance DR is always the same as VR [41]. If the origin of the parabola is taken to lie on the vertex (V), then the equation of the parabola becomes:

$$y = 4fx^2 \ldots\ldots\ldots(4.1)$$

Where f is the focal length, the distance between the vertex (V) and the focus (F). When ray tracing an incident light ray parallel to the optical axis, as in figure (4.1a), twice the reflection angle (2ρ) is always equal to the angle ψ through the laws of geometry. Light rays that are incident at any point on the mirror, therefore, will always be reflected towards the focal point, assuming they are incident parallel to the optical axis. For this reason, parabolas are ideal for the concentration of solar energy. For real parabolic surfaces of finite extent, the extremity of the mirror is defined by the rim angle (ψ_r) which is equal to twice the reflection angle at the mirror's edge.

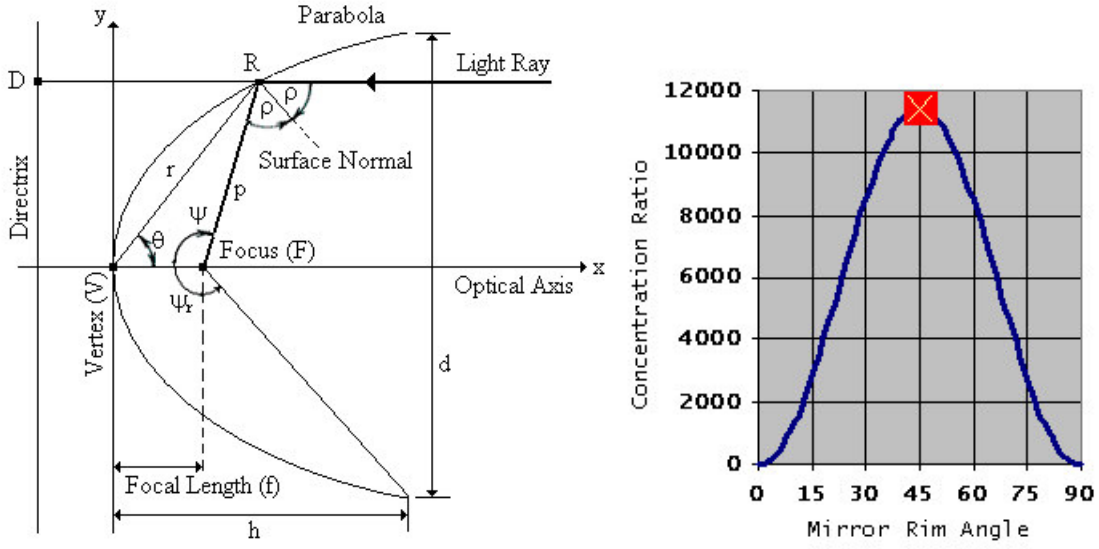

(a) **(b)**

Figure 4.1: (a) Parabolic geometry (b) Concentration ratio vs. rim angle for a parabolic concentrator

In order to compute the dimensions and physical characteristics of a parabolic concentrator, the initial inputs required are the concentrator diameter (d_c) and the rim angle. The concentrator height (h) and focal length (f) are then determined via the following relations [41]

$$h = \frac{d_c^{\,2}}{16f} \quad \text{.....(4.2)} \qquad \tan(\psi_r / 2) = \frac{1}{4(f / d_c)} \quad \text{.....(4.3)}$$

Parabolic concentrators are, therefore, characterised by specifying a rim angle, a diameter and choosing a section of the paraboloid, whether it is on or off-axis. Thus, a parabolic mirror has the unique property that all incident light rays parallel to the optical axis will be reflected to the same point on the optical axis. In practice, for sources of finite size at a finite distance, light rays will not be parallel to the optical axis and will form an image of the source at the focal point. The geometric concentration ratio is the ratio of concentrator area to image area and is subsequently related to the mirror rim angle, source angular size and mirror angular form error, a result of imperfect machining. Equation (4.4) relates the geometric concentration ratio to concentrator rim angle:

$$CR_g = \frac{A_c}{A_f} = \frac{\sin^2(\psi_r)\cos^2(\psi_r + \theta_s + \theta_f)}{\sin^2(\theta_s + \theta_f)} \quad \text{.....(4.4)}$$

Where θ_s is the solar half angle and θ_f is a measure of the mirrors angular form error. Plotting equation (4.4) we can see that the maximum concentration ratio is achieved for a rim angle of 45°, (see figure (4.1b)).

4.2.2 Fibre Optic Coupling

For a parabolic concentrator to direct light into a fibre optic, the fibre must lie along the optical axis with the fibre tip at the focal point as shown in figure (4.2).

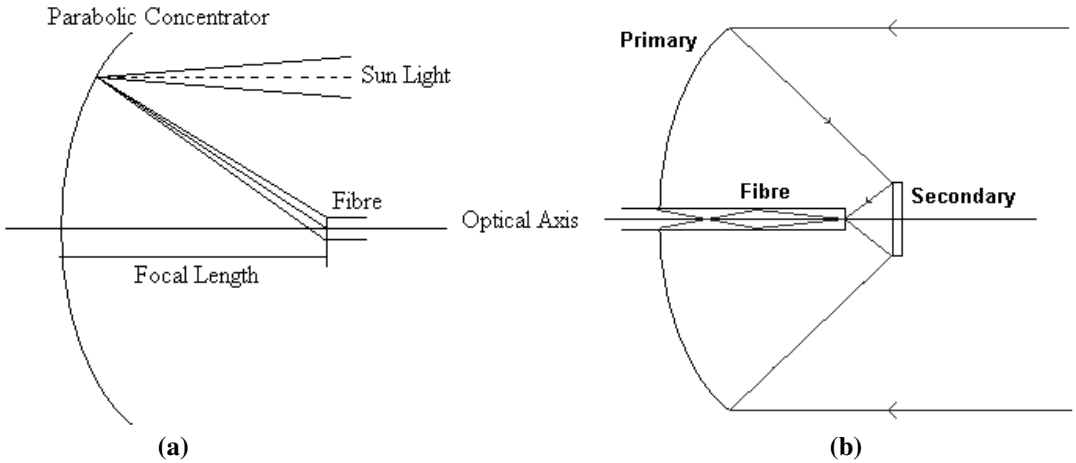

Figure 4.2: (a) Direct concentrator to fibre coupling. (b) Cassegrain concentrator to fibre coupling

From equation (4.4) the size of the image can be determined and a concentrator can be designed for a given image size.

$$d_f = \frac{d_c \sin(\theta_s + \theta_f)}{\sin(\psi_r)\cos(\theta_s + \psi_r + \theta_f)} \quad \ldots\ldots(4.5)$$

Thus, the concentrator diameter is restricted by the fibre's diameter. To couple a single fibre optic to a concentrator such that all light rays incident from the mirror propagate along the fibre optic requires that:

- The mirror is accurately pointed at the source
- The image size is the same as the fibre tip size, thus constraining the mirror size (Equation 4.5).[8]
- The light rays are incident at an angle less than the maximum acceptance angle of the fibre (NA), thus constraining the mirror rim angle.

This means the design of a concentrator is heavily dependant upon the fibre optic selected. The data presented in figure (4.3a) is from a study conducted at the Department of Solar Energy and Environment Physics of the Ben-Gurion University of the Negev. The study was designed to determine the performance of a solar concentrator focusing light into a fibre optic. The data shows the transmission of light through a fibre optic for various angles of incidence [42].

[8] The requirement would not be applicable to a bundle of fibres which can be made to any diameter.

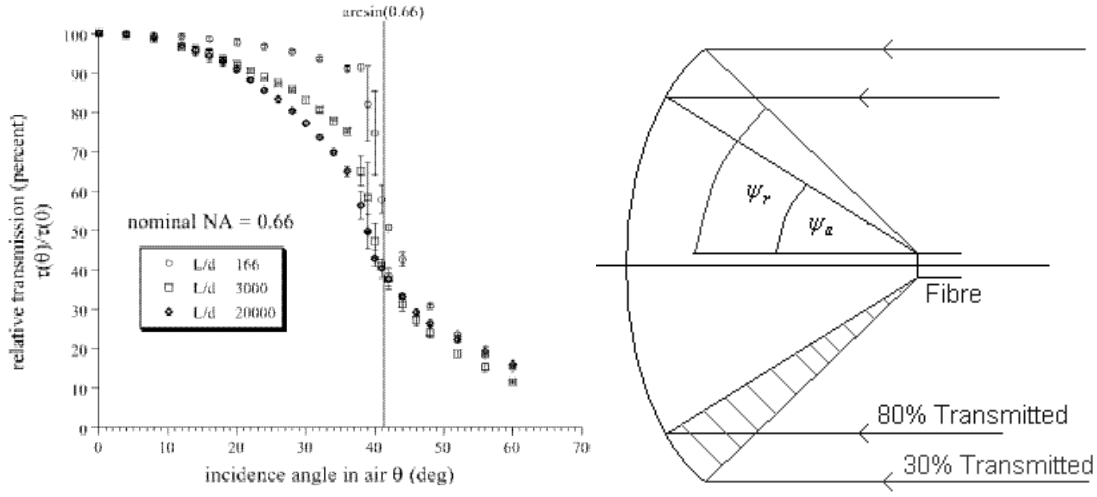

(a) **(b)**

Figure 4.3: (a) Transmission vs. incidence angle for a fused silica fibre optic [48]
(b) Restriction of rim angle due to fibre acceptance angle

The transmission through the fibre is good (100%-80%) up to the acceptance angle of the fibre (ψ_a = 41.3°). A huge decrease in transmission is then observed with increasing incidence angle. Figure (4.3b) demonstrates that a concentrator with a rim angle larger than the acceptance angle of the fibre optic will lead to light from the periphery of the mirror being significantly impeded upon transmission through the fibre optic. Implying the periphery of the mirror is somewhat redundant. In the context of spacecraft, for which weight is a precious commodity, this would be unacceptable. By reducing the rim angle of the concentrator mirror to the acceptance angle of the fibre optic, the mirror is optimised.

4.2.3 Practical Considerations

The limitation in concentrator diameter imposed by the fibre optic (single or bundle) further enforces the concept of multiple mirrors ganged together to produce a given power level. A consequence of this use of multiple parabolic concentrating mirrors is a significant reduction in optical system mass when compared to that of a single mirror system for a given collective power output. Figure (4.4a) demonstrates this trend for a number of suitable materials. It incorporates a simple structural support model that grows in mass and complexity with the addition of concentrators to the system. Figure (4.4a) suggests that there is an optimum number of concentrators that will result in the minimum system mass. At this optimum, the difference in total system mass between various mirror materials is much less than when comparing system masses for a single mirror design. This allows for the use of cheaper materials without a large mass trade-off. The equation relating mirrors mass (M) to mirror diameter (d) is given as:

$$M = \left(\frac{3g}{4\delta}\right)^{1/2} \pi \left(\frac{d}{2}\right)^4 \left(\frac{den^3}{E}\right) \ldots\ldots(4.6)$$

Where g is acceleration due to gravity, *den* is the material density, E is the materials Young's modulus and δ is maximum tolerated deflection of the mirror surface due to sag under it's own weight [43]. For this analysis, a value of 1×10^{-7} m was assumed for the maximum tolerated deflection. In this analysis, mirror light weighting techniques were neglected[9].

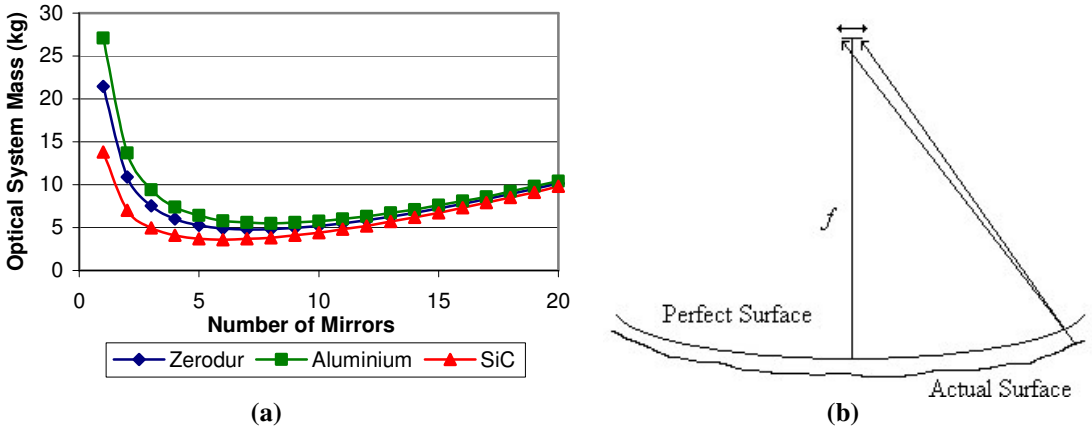

(a) **(b)**

Figure 4.4: (a) Optical system mass vs. number of concentrators for SiC, Zerodur and Aluminum. (b) Effect of non-perfect mirror surface

There are a number of practical concerns regarding optical surface manufacture that should be addressed when considering the concentrator mirror. Several terms refer to the quality of an optical component:

- Peak-to-Valley: This value refers to the sum of the largest negative deviation to the largest positive deviation of the actual surface from the ideal surface.
- Root-Mean-Square (RMS) Wave Front Error: This value refers to the deviation of the actual surface from the perfect surface (or wave front) averaged over the actual surface. For example, for optical quality mirrors, the RMS wave front error should have a value of no greater than λ/10 [44].
- Strehl Ratio: This is a measure of the mirrors ability to focus light within its ideal image size and is a direct measure of the reduction in intensity due to surface quality.

To achieve a good quality surface, a suitable machining method is required such as diamond turning. Common materials for space-based mirrors are fused silica, single or polycrystalline silicon and silicon carbide (SiC). In the 1980s, most mirrors were metals (aluminium and

[9] Light weighting techniques refer to the removal of material from the mirror blank while still maintaining the mirror's surface quality. this is done for the purpose of reducing the final mass of the mirror.

beryllium) and glasses (ULE and Zerodur). In some cases, it is appropriate to include a silver coating to increase reflection and reduce the amount of energy absorbed by the mirror. Thermal expansion and contraction of a parabolic concentrator mirror would result in the focal point shifting back and forth around the optical axis which could cause a misalignment with a fibre optic. To account for thermal expansion of the concentrator, the supporting structure would ideally be athermal with the concentrator. SiC is noteworthy at this point due to its low thermal expansion and specific stiffness properties (3.4×10^{-6}m/m·°K for reaction bonded SiC) [45]. Even the vacuum heating of less advanced materials can be somewhat negligible. For example, a 300g aluminium mirror 105mm in diameter would absorb 0.5 W (assuming 0.95 reflectivity from a diamond turned surface) resulting in an 8K rise in temperature over an hour heating period in vacuum. What is of more concern thermally is when a flat secondary (relay) mirror is employed to create a Cassegrain style concentrating system as shown in figure (4.5a)[10]. The benefit of such a system is evident in that the fibre can be easily supported and aligned along the focal axis. The smaller secondary mirror, however, is subject to a much higher intensity of light and could consequently reach a much higher temperature. Figure (4.5b) shows the vacuum heating curve for an 18mm diameter, silver coated, BK7 substrate, secondary mirror subject to heating from a 105mm diameter aluminium concentrator, optimised for a 1mm diameter fibre.

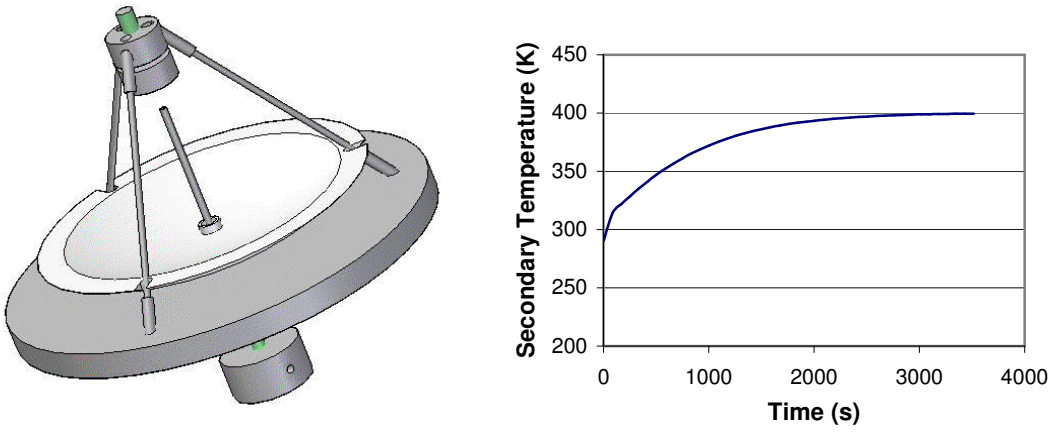

(a) **(b)**

Figure 4.5: (a) Compact cassegrain concentrator assembly.
(b) Heat up of a silver coated, BK7 substrate, secondary relay mirror.

Figure (4.5b) shows the secondary mirror approaching 400K after an hour of vacuum heating. At this temperature, the mirror would have expanded by 0.1mm in diameter and 0.02mm in depth. The most critical of these expansions is the latter as this is along the focal axis and would cause a growth of the solar image on the fibre tip, resulting in a loss of power. In this case, however, the alignment tolerance could afford to be much greater than this expansion. For example, if a power tolerance of ± 0.2 W were acceptable, the alignment tolerance would be ± 0.5mm along the

[10] Cassegrain system designed and constructed at the University of Surrey for ground testing purposes.

optical axis. Thus, provided that at this temperature, the optical properties of the silver surface were not compromised, this type of secondary mirror would offer a suitable solution.

4.2.4 Detailed Concentrator Analysis

For the purposes of a solar thermal propulsion demonstration mission, a fibre with a 1mm core sized is considered to be the smallest practical target at the focal point of the concentrator. Using equation (4.5) we can see that the smallest practical parabolic concentrator will have a diameter of 105mm. Furthermore the largest commercially available acceptance angle for a fibre optic cable is 41.3°. These values define the requirements of a parabolic concentrator designed for this research. A series of ray-trace programs were created to analyse the optical behaviour of such a concentrator in terms of image size, intensity distribution across the image and coma effects due to miss-alignment of the focal axis with the sun vector.

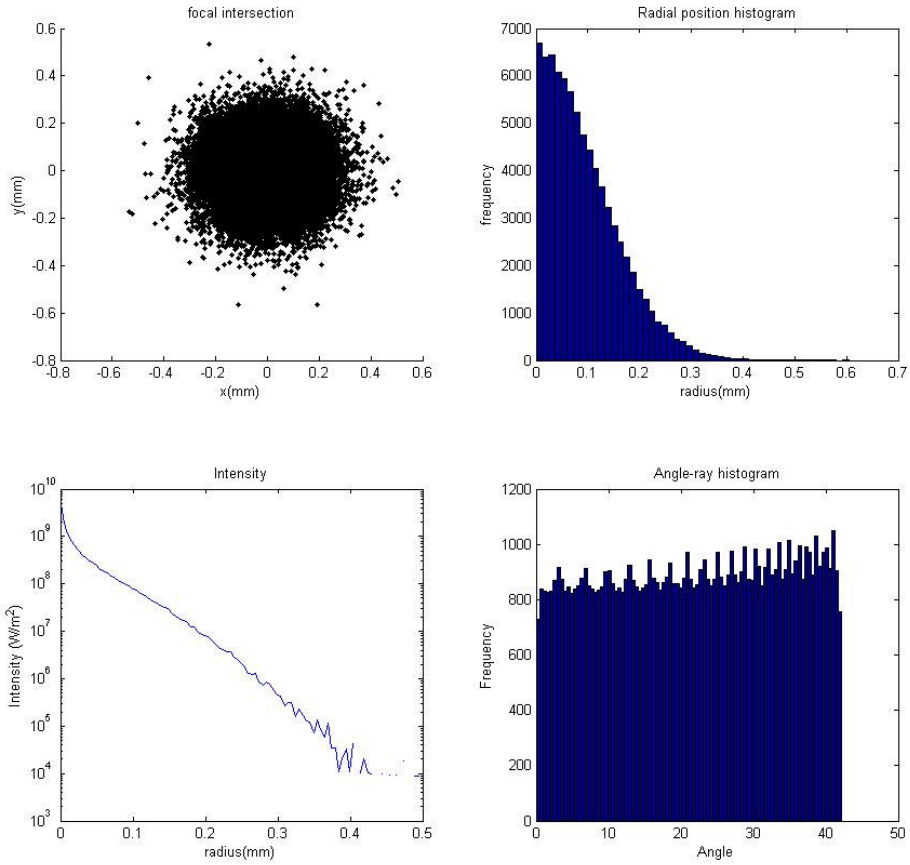

Figure 4.6: Ray trace analysis of parabolic concentrator. Upper left: Ray trace of focal spot size. Upper right: Histogram of ray radial intersections on focal plane. Lower left: Radial intensity distribution of focal spot. Lower right. Histogram of ray incidence angles

Figure (4.6) depicts the results of a ray-trace program designed for the study of spot size and intensity distribution across the image. In figure (4.6), we can see that the spot size (upper left plot) is the same size as indicated by equation (4.5) (~1mm diameter), however, the majority of rays are concentrated within a radius of 0.3mm. Moreover the intensity variation across the spot is seen to vary and peaks toward the lower right hand side plot with intensities approaching $10^9 W/m^2$. This demonstrates that a 1mm fibre optic would theoretically be sufficient to capture all the power deliverable from this concentrator design, provided the fibre was correctly aligned with the focal point. Due to the nature of the intensity distribution, it is clear that an alignment tolerance of the fibre with the focal point is required to be on the order of ± 0.1mm. The effect of coma is seen as an enlargement of the image at the focal point in the direction of misalignment.

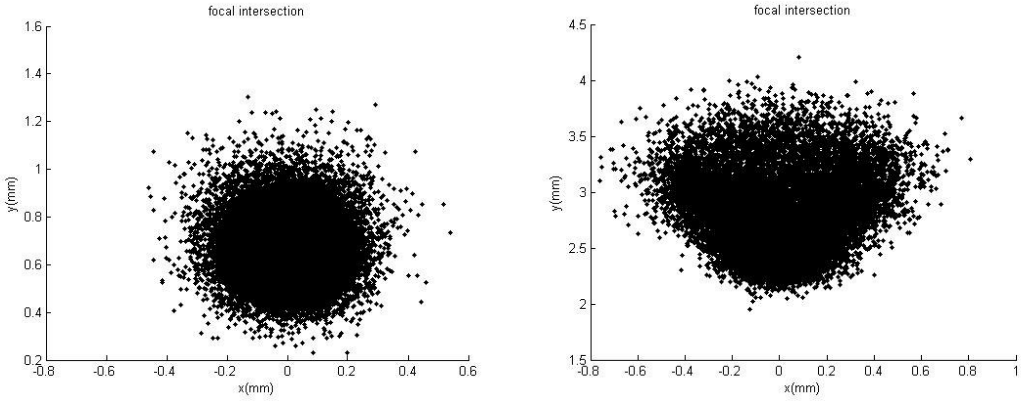

(a) **(b)**

Figure 4.7: (a) Spot size for 1/2° misalignment
(b) Spot size for 2° misalignment

In figure (4.7a), we see the effect of coma for a 0.5° misalignment and in figure (4.7b), for a 2° misalignment. Not only can it be seen that the spot is larger, but also displaced from the focal point in the optical plane. For a 0.5° misalignment, the fibre could capture a portion of the spot's energy, but in the 2° case, the fibre would accept almost no energy. This indicates a required pointing accuracy of ±0.05° to allow efficient energy transmission. Further analysis reveals the relationship between concentration and surface error.

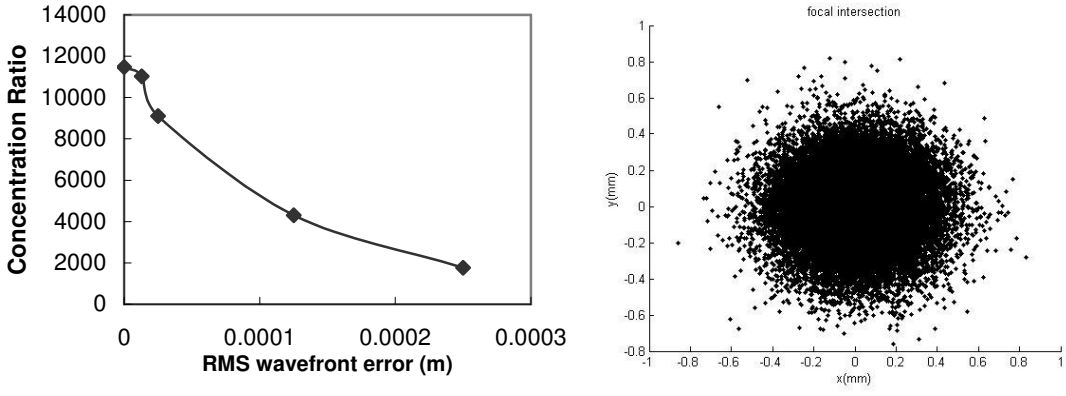

(a) **(b)**

Figure 4.8: (a) Concetration ration vs. RMS wave front error.
(b) Spot size for RMS surface error of 1.25×10^{-4}m

Figure (4.8b) demonstrates the enlargement of the image size for an RMS surface error of 1.25×10^{-4}m, resulting in an estimated concentration ratio of ~4000. Figure (4.8a) shows the general trend in the decrease of concentration ratio with increasing RMS surface error. This demonstrates that an RMS surface error of less that 10μm is required for concentration ratios approaching 11,000.

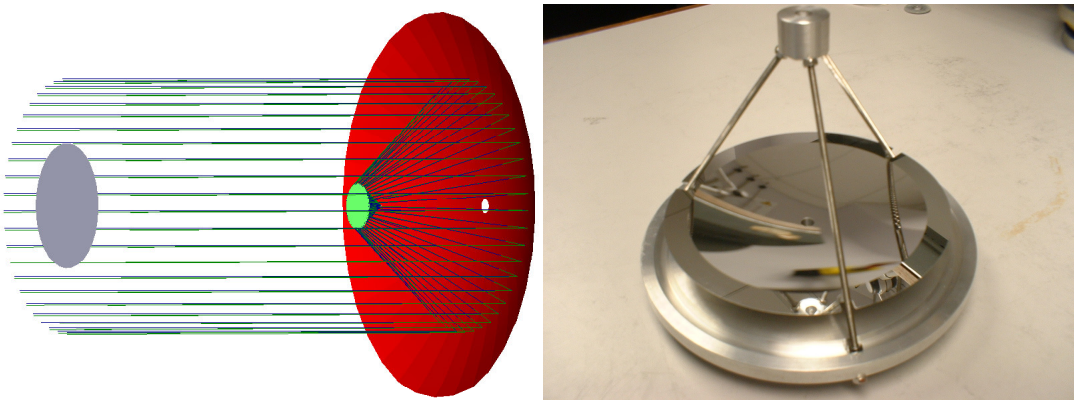

(a) **(b)**

Figure 4.9: (a) ZMAX design of prototype Cassegrain concentrator.
(b) Manufactured prototype Cassegrain concentrator.

A Cassegrain parabolic concentrator assembly was designed using ZMAX, a commercial optical design software, and was subsequently manufactured by Precision-Optical Engineering, a company based in Hitchin (UK). Figure (4.9a) depicts the ZMAX model and figure (4.9b) shows the manufactured assembly. Results from the analysis of the parabolic concentrator assembly are discussed in section 5.

4.3 Solar Receiver Design

In section 3 the two types of STP cavity receiver were identified, namely, *direct-gain* and *thermal-storage.* In this section we consider the sizing and basic design of a direct-gain cavity receiver based on the system design requirements of the STP demonstration system discussed in section 3.

4.3.1 Receiver materials

Candidate materials for a direct-gain receiver are dependant on its target temperature and the creep tolerance at that temperature. For the purpose of achieving performances in the range of 240 to 300s specific impulse, the target temperature range for the cavity receiver is set at 1,400-1,800 K**.** Ideally, the receiver material should also have high thermal conductivity, a moderately low heat capacity, be chemically stable with the propellant at receiver temperature and be non-brittle over the range of operating temperatures. These properties allow the receiver to achieve temperature quickly and efficiently transfer heat to the propellant. Suitable materials are typically

high temperature metals, which are generally referred to as refractory metals. Table 4.4 suggests some candidate direct-gain receiver materials.

Table 4.4: Candidate Direct-gain receiver materials [37]

Candidate Material	Haynes Stainless Steel	Chromium	Molybdenum	Rhenium
Melting temperature (°C)	1300	1860	2617	3180
Thermal conductivity (W/m-°C)	8.9	69.1	138	39.6
Specific heat capacity (J/g-°C)	0.397	0.461	0.255	0.138
Density (kg/m^3)	8,030	7,200	10,220	21,040

From table 4.4 we can see that both Molybdenum and Rhenium would be suitable for the target temperature range. Molybdenum stands out with its exceptionally high thermal conductivity.

4.3.2 Receiver Sizing

The size of a direct gain thruster is directly dependant on the input power and the mass flow rate through the thruster. Estimating the size of a direct gain cavity receiver is a complex matter as the heat transfer coefficient (h_c) between the receiver and propellant is required for the calculation. Equation (4.7) is used to calculate the heat transfer rate ($\dot{Q}$) to the propellant from the receiver [7]:

$$\dot{Q} = h_c A \Delta T \quad \text{.....(4.7)}$$

Where A is the transfer area and ΔT is the difference in temperature between propellant and receiver. The values of $\dot{Q}$ and ΔT can be estimated from the direct gain thruster requirements of section 3, however, the heat transfer coefficient is dependent on the mechanism of heat transfer from receiver to propellant. There are two approaches to heat transfer that are well suited to a microsatellite STP receiver [46]:

- Single/Multi Pass Channels: Channels spiral around a central receiver. Flow typically experiences a low-pressure drop and moderate heat transfer efficiency.
- Particle Beds: Central receiver, surrounded by a packed bed of heat transfer material particles. Flow typically experiences a high-pressure drop and high heat transfer, however, flow instabilities and channeling are a likely consequence of low flow rates and an unsuitable choice of bed material.

Particle bed receivers are more complex than single/multi channel receivers because of the need to contain the particle bed within the receiver volume. Thus, particle bed receivers tend to be more massive. Also, fine mesh, which is tolerant to high temperatures, is required to keep the particle bed material in place during thrusting, and there is the risk of the bed material clogging the mesh or throat of the thruster nozzle. Kennedy examined receiver heat transfer options in detail and opted for the simpler solution as more appropriate for rapid testing of STP on a microsatellite. To maintain simplicity a single pass channel heat transfer scheme is selected for the direct-gain thruster. We now consider forced convection flow within a circular tube. The quantities describing such heat transfer are the Reynolds number (Re), the Prandtl number (Pr) and the Nusselt number (Nu) [7]:

$$\mathrm{Re} = \frac{\dot{m}D}{\mu A} \qquad \mathrm{Pr} = \frac{\mu C_p}{k} \qquad Nu = \frac{h_c D}{k} \quad \text{.....(4.8)}$$

Here $\dot{m}$ is the mass flow rate, D is the tube diameter, μ is the propellant viscosity, A is the flow cross-section area and k is the propellant thermal conductivity. In order to calculate the heat transfer coefficient, the correct heat transfer correlation must be selected for the given flow conditions. For a channel flow heat exchanger, Petukhov provides a suitable correlation [47]:

$$Nu = \frac{f_f}{8} \frac{\mathrm{Re}\,\mathrm{Pr}}{\left[1.07 + 12.7\sqrt{\frac{f_f}{8}}(\mathrm{Pr}^{2/3} - 1)\right]} \quad \text{.....(4.9)}$$

Where the Darcy-Weisbach friction factor f_f is estimated via the equation:

$$f_f = \frac{1}{1.82\log_{10}(\mathrm{Re}) - 1.64} \quad \text{.....(4.10)}$$

For ammonia flowing through 1mm bore channels of a hot receiver (1,800 K), the heat transfer coefficient is estimated to be ~1000 W/m^2-K. Using equation (4.7), the required heat transfer area is estimated to be ~1cm^2, assuming a 50W power input from six 105mm diameter concentrators. This value represents the area of the channel wall required to heat the propellant and allows an estimation of the channel length to be 3.2cm. Wrapping this channel around the receiver provides an estimate of the receiver length to be 2cm.

4.3.3 Cavity Receiver Modeling

An STP integrated analysis tool was employed to determine suitable receiver dimensions, model receiver heating characteristics and to simulate a receiver burn. This analysis tool was created by Kennedy [Fred] for the purpose of designing a thermal-storage STP system and consists of a

series of Microsoft Excel spreadsheets linked via visual basic code. A modified version of this analysis tool was created to assess a direct-gain receiver using fibre optics and ammonia.

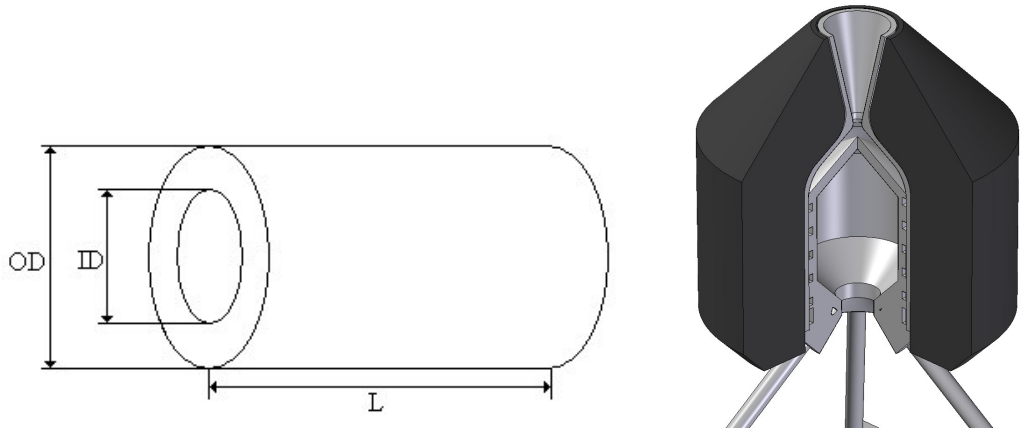

(a) **(b)**

Figure 4.10: (a) Characteristic receiver dimensions. (b) Receiver design

The design of the thruster is depicted in figure (4.10b), consisting of a molybdenum receiver surrounded by a graphite insulation package. The characteristic dimensions for the receiver are the inner diameter (ID), outer diameter (OD) and receiver length (L). Table (4.6) summarises the basic properties of the receiver.

Table 4.6: Basic receiver properties

Receiver Type	Receiver Material	Receiver Mass (kg)	ID (mm)	OD (mm)	L (mm)	Target Thrust (N)	Target Isp (s)	Burn Time (s)
Direct gain	Molybdenum	0.02	10	15	20	0.02	240-300	900

In table 4.6 the value for the ID has been kept small (10mm) to ensure that high intensity radiation from the fibre bundle is incident on the inner receiver cavity. The required heat transfer area for the direct gain thruster is accommodated for with these dimensions. Parameters remaining to be estimated for the receiver are the throat area (A^*) and nozzle area (A_e). Given the dimensions of the receiver, the nozzle diameter is restricted to 10mm. The throat area can be calculated from the following relationships [7]:

$$T = \dot{m}u_e + (P_e - P_a)A_e \quad \ldots\ldots(4.11)$$

$$\dot{m} = \frac{A^* P_c}{\sqrt{\bar{R}T_c}} \sqrt{\gamma \left(\frac{2}{\gamma+1}\right)^{(\gamma+1)/(\gamma-1)}} \quad \ldots\ldots(4.12)$$

Where P_a is the ambient pressure. These relationships assume that the propellant is a perfect gas of constant composition and the expansion process is steady, one dimensional and isentropic.

Thus, for a thrust of 20mN at a specific impulse of 300s, the throat diameter is estimated to be 1mm. With these first-order parameters a model of the thruster can be built in the direct-gain analysis tool. This analysis tool takes into account ammonia decomposition, heat transfer along the channel of the receiver and graphite insulation sizing, providing a more accurate analysis of the thruster. The power delivered to the receiver cavity (50W) is provided by 6 fibre optics, each coupled to a 105mm diameter parabolic concentrator as in the UK-DMC case study in section 3. The concentrators are assumed to be 90% efficient and the fibre optics 80% efficient. In figure (4.11), we see the performance data for the direct-gain thruster. The receiver takes approximately 400s to heat to a temperature of 1534K with a graphite insulation thickness of 30mm. During a modeled burn the propellant temperature approaches a steady state value of 1050K after ~600s. The average thrust is 19.8mN and the average specific impulse is 285s over the 1000s modeled burn time. It was necessary to increase the channel length to 40mm to ensure that the propellant had reached the steady state receiver temperature after traversing the channel length. This receiver design fulfills the requirements stated in section 3. A means of coupling the fibre optics to the receiver is discussed later in this section.

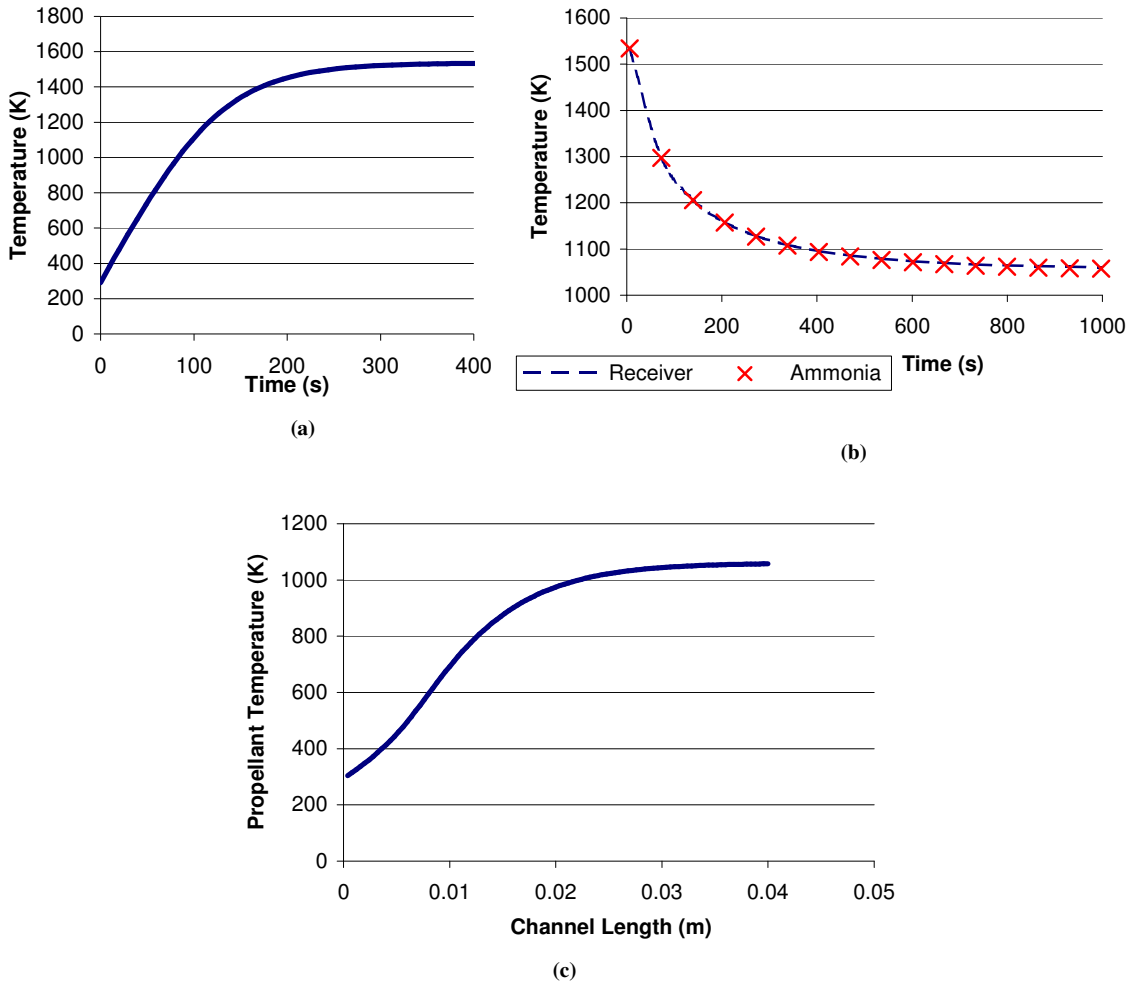

Figure 4.11 (a) Molybdenum cavity receiver heating, (b) Molybdenum receiver and ammonia propellant temperature during thrusting, (c) Ammonia propellant temperature while traversing the receiver channel length, end of burn.

4.4 Fibre Optic Cable

In this section the optical and physical properties of fibre optics are discussed in terms of STP and candidate fibre optics are identified. Various fibre-to-receiver coupling configurations are investigated in terms of receiver wall intensity distributions and fibre optic temperature.

4.4.1 Fibre Optic Properties and Selection

A fibre optic suitable for a STP application should have the following properties:

1. Multimode step index fibre
2. Large numerical aperture (NA)
3. Low attenuation over the solar spectrum
4. Extreme temperature resilience
5. Radiation and solarization resilience

A multimode step index is necessary to provide a large number of propagation paths (modes) along the fibre. Light from a parabolic mirror will be incident at angles up to the rim angle of the concentrator (ψ_r), so it is important for the fibre optic to be able to support many light propagation paths. The acceptance angle (ψ_a) of a fibre optic is defined by its numerical aperture (NA) which is related directly to the refractive indices of the core and cladding (n_{core} and n_{clad} respectively, equation (4.11)) [48].

$$NA = \sin(\psi_a) = \sqrt{n_{core}^2 - n_{clad}^2} \quad \ldots\ldots(4.13)$$

The successful transmission of light from a parabolic mirror through a fibre optic requires that $\psi_r \geq \psi_a$. For a fibre optic to operate efficiently in a STP system it should have a low attenuation over the solar spectrum. Solar radiance is greatest, at >0.2 $Wm^{-2}nm^{-1}$ in a spectral range of 300nm to 2200nm, corresponding to the UV and NIR regions of the EM spectrum. A fibre optic is required that is transparent in this wave band. Pure fused silica fiber optic cables are commonplace within the optical communications industry due to their very low attenuation over the optical waveband. A typical use of fused silica optical fiber is for single mode long distance data cables. For STP, fused silica fiber optics offer an excellent compromise between available NA, spectral coverage, attenuation and intrinsic resilience to radiation and temperature. Therefore these fibers are considered in detail for this application.

Table 4.7. Candidate fibre materials [49,50]

Material	Category	Wave Band[11]
Silica (Low OH^-)	Glass	UV – Vis (180nm – 2000nm)
Sapphire	Crystal	Vis – MidIR (500nm – 3100nm)
Zirconium Fluoride	Glass	Vis – MidIR (450nm – 5000nm)

The materials in table (4.7) are, to an extent, free of molecular rotation and vibration energy states within the visible region of the spectrum. These states tend to occur further into the IR. The electron transition energy states for these materials occur approaching UV photon energies. These facts mean these materials have a good transmission window between the UV and IR absorption bands. A very problematic contaminant of fused silica fibre optics in the visible waveband is the hydroxyl ion (OH^-). OH^- gives rise to a fundamental vibrational absorption at 2.73µm and 4.2µm, and more importantly, harmonics at 1.38, 1.24, 0.95 and 0.72µm. The presence of OH^- is usually attributed to an abundance of water vapour during the fibre manufacture. Transition metal impurities also give rise to unwanted absorption mechanisms. The concentration of these contaminants can be minimized via fine control of the manufacturing environment, although these processes tend to be expensive. The attenuation spectrum of a low OH^- pure fused silica fibre optic is shown in figure (4.12) superimposed upon the solar spectrum [51].

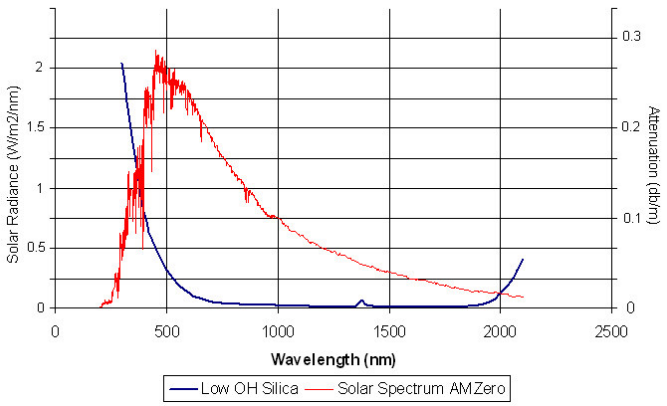

Figure 4.12: Solar spectrum and attenuation spectrum for a low OH^- pure fused silica fiber optic [55].

Figure (4.12) indicates that most absorption occurs within the UV portion of the solar spectrum.

Another form of intrinsic attenuation is via Rayleigh scattering. This is caused by microirregularities within the core glass. These irregularities tend to arise from density and composition fluctuations within the glass itself. Equations (4.14) and (4.15) give the level of scattering due to each of these effects respectively [48].

[11] UV=Ultra Violet, Vis = Visual, NIR = Near Infrared, MidIR = Medium Infrared

$$\alpha_{scat,\rho} = \frac{8\pi^3}{3\lambda^4}(n^8 p^2)(k_b T_f)\beta_T \quad \text{.....(4.14)}$$

$$\alpha_{scat,c} = \frac{32\pi^3 n^2}{3\lambda^4 \rho N_A}\sum_{j=1}^{m}\left[\left(\frac{\partial n}{\partial x_j}\right)_{T_f, x_i \neq x_j} + \left(\frac{\partial n}{\partial \rho}\right)_{T_f, x_i}\left(\frac{\partial \rho}{\partial x_j}\right)_{P, T_f, x_i \neq x_j}\right]^2 M_j x_j \quad \text{.....(4.15)}$$

Equation (4.14), reveals the scattering due to density fluctuations has a dependence on fictive temperature (the temperature at which the core material can achieve thermal equilibrium). This suggests that fibers formed at higher temperatures will suffer larger scattering losses. Another source of light loss is photoluminescence which is a result of high intensity light exciting the core material electrons to higher energy states. Attenuation of light transmitted along a fiber optic can also be increased by external influences. These are outlined in table (4.8).

Table (4.8): Attenuation in fiber optics due to external influences.

External Influence	Attenuation
Macro bend	Physical bend in the fibre. Has the effect of reducing the number of higher order propagation modes available.
Micro bend	Fibre subjected to physical stresses, leading to unrecoverable distortions along the core material.
Core/Cladding scratches	Damage to either core or cladding can result in fibre breakage and a breakdown in the local total internal reflection. A suitable buffer and jacket typically protect a fibre optic.
Elevated temperatures	Exposure to temperature exceeding the operational range of the fibre can lead to a breakdown in the fibres optical properties.
Radiation exposure	Exposure to radiation results in the formation of defects (color centers) in the fibre. These, in turn, absorb light.
Solarization	This effect is caused by exposure to very intense UV light, thus forming centers of excited electron energy states.

To ensure the minimum amount of non-intrinsic attenuation, the fibre should be protected from these influences.

Ideally, a fibre operating in a STP system should be as flexible as possible without adding to its intrinsic attenuation. The fracture bend radius of a fibre optic is often proportional to a fibre's core diameter and quoted by the manufacturer. For silica fibre, this is typically 300 times the core radius. Smaller bends are achievable with smaller core sizes, however, the desire for a flexible fibre conflicts with that for a large fibre optic core diameter to reduce concentrator tolerances. A

compromise can be met by using a fibre optic bundle of suitably flexible fibres, constructed for a given concentrator. This, however, will result in packing loses due to gaps between neighbouring fibres. Liang [29] was successful in constructing fibre optic bundles of 7 and 19 fibres that were tightly packed via polishing the fibre tips into closely-fitting hexagonal shapes. This minimized bundle-packing losses and on transmission of concentrated solar light, 60% efficiency was observed.

To avoid micro bends, the fibre optic would be sheathed in Kevlar fibres within the fibre jacket for support. The fibre optic cable would not be allowed to have very sharp bends along its length. A suitable buffer would protect the fibre from surface scratches and wear. As the fibre is likely to experience heating and transverse temperature gradients a buffer able to withstand high temperatures would be appropriate. For silica fibres, silicone is an appropriate choice with an operating temperature up to 400°C [51]. A fibre optic transmitting concentrated solar energy will experience heating through absorption of light energy and also through any conductive contact the fibre optic has with the solar thermal receiver. In 1998, Jaramillo [52] demonstrated that a silica fibre optic operating terrestrially could function for up to six hours and remain within its working temperature limits. Jaramillo demonstrated this numerically, employing an attenuation spectrum substantially more absorbing than that shown in figure (4.12). A one-dimensional finite difference thermal analysis of a fibre operating in a vacuum was performed to ascertain the likely thermal environment of the silica (low OH^-) fibre selected for use with the STP system. The attenuation spectrum of figure (4.12) was used for this analysis, and radiative power loss was included. Figure (4.13) shows the heating profile of the fibre tip.

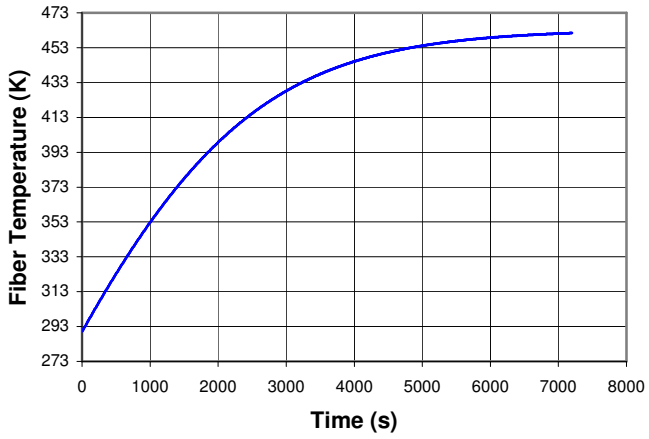

Figure 4.13: Fiber tip heating profile for a single 1mm ∅ core size; low OH^- silica fiber

Pure fused silica can operate at temperatures as high as 1000°C. What limits the operational temperature range is the cladding, buffer and jacket employed. Table (4.9) presents a number of silica fibre optic that are currently available commercially.

Table 4.9. Candidate commercially available fibre optic cables[12].

Product	Manufacturer	Cladding	Buffer	NA	Temperature Range (°C)
FLU	Polymicro	Teflon	Silicone	0.66	-10 to +160
Optran Ultra	CeramOptec	Silica	Polymide	0.37	-190 to +400
Optran UVNS	CeramOptec	Fluorine doped silica	Silicone	0.30	-190 to +400

Table (4.9) suggests that there is a trade-off between fibre temperature range and NA. This trade – off will affect operation and heating periods in that a higher NA fibre cannot be operated for long periods at high temperature. Silica's fictive temperature, similar to its melting temperature, is approximately the same as the desired operating temperature of the solar receiver, 1600°C. This implies that in coupling the fibre optic to a solar receiver, the fibre should not come into direct thermal contact with the receiver. An STP subsystem analysis tool, written by Kennedy [13], is used to determine the variation in outer insulation temperature for varying graphite insulation thickness. Figure (4.14a) shows the trend in outer insulation temperature with increasing insulation thickness for a constant receiver temperature of 1600°C.

Figure (4.14a) implies that a fibre optic can be mechanically supported by suitably thick insulation and remain within its working temperature range during heating of the receiver. The fibre would protrude into the receiver without physical contact with the receiver as depicted in figure (4.14b). The fibre protrudes from an alumina ceramic tube which maintains the fibres rigidity and decreases the amount of heat absorbed. As the cladding of a silica fibre cannot withstand the high temperatures as well as silica can, the cladding is stripped away from the portion of the fibre emerging from the ceramic tube.

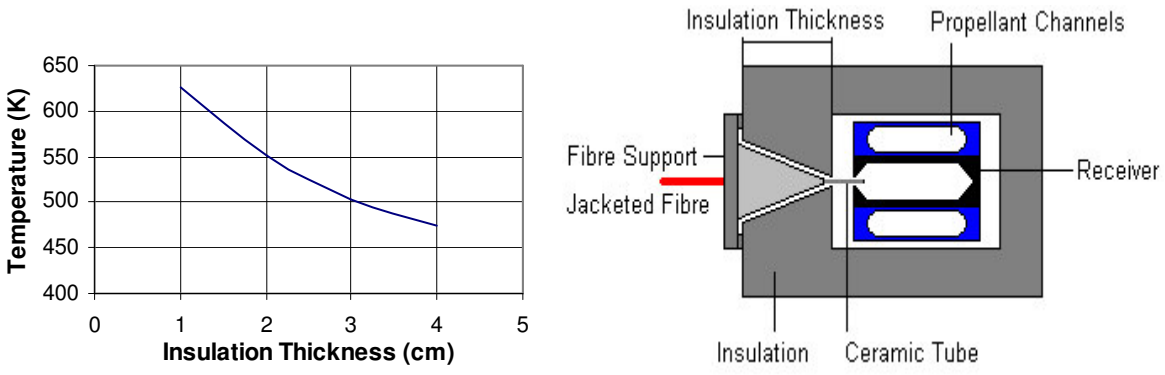

(a) (b)

Figure 4.14: (a) Outer insulation temperature for increasing insulation thickness, receiver temperature 1600K (b) Fiber-receiver coupling concept.

[12] Fiber data obtained from manufactures websites: http://www.polymicro.com/, http://www.ceramoptec.com/.

In recent years, a major effort has been devoted to the study of ionising radiation upon silicon dioxide glass. The purpose of this study was to develop radiation-resistant glass for fusion plasmas diagnostic. Brichard [53,54] observed the growth of the first overtone of the OH^- absorption peaks in polymer coated silica fibre and also reports that in aluminium jacketed silica fibre this growth did not occur. Brichard [55] discusses a method for developing radiation hardened fibres via a hydrogen treatment of the glass core. A fibre optic operating in space will be subjected to radiation exposure, and hence, its optical performance will degrade over time. A typical dose rate of radiation in low earth orbit is 5-10 krads/year, increasing for higher inclinations and increased solar activity. Brichard observes a 12 db/m increase in attenuation at 1380 nm in silica for a dose rate of 590 Mrads/hr. A survey conducted by the NASA Goddard Space Flight Centre [56] complied data on gamma ray induced attenuation for a number of commercial fibre optics. From this survey, it was discovered that low-OH^- fused silica fibres would suffer induced attenuations at 750 and 850 nm on the order of 0.6 db/m for doses of on order of 250 krads. This suggests that in a low earth orbit environment, the radiation-induced absorption in silica fibre would not be substantial enough to prevent its use. Data of radiation-induced absorptions in silica fibres covering the entire solar spectrum have not been found.

Solarization in fibre optics causes the formation of colour centres in the core silica glass. Impurities within the core interact with UV radiation to form colour centres causing massive absorptions between 215-254nm and further into the UV region. This effect is outside the waveband of interest, and attenuation recovers at approximately 300nm. Nevertheless solarization resistant fibres are preferable to minimize the formation of colour centres [57].

4.4.2 Fibre-to-Receiver Coupling

In considering fibre-to-receiver coupling two things are of interest, namely the intensity profile on the cavity wall of the receiver and the temperature gradient experienced by the fibre optic bundle exposed to a hot receiver. To investigate these parameters, a series of ray-trace programs and thermal models have been created using Matlab and Thermxl.

4.4.2.1 Cavity Intensity

Studying the intensity distribution of radiation upon the cavity wall of the receiver is important for direct-gain receivers to ensure effective power transfer from incoming radiation through the cavity walls to the propellant. To determine the intensity distribution on the cavity wall, it is necessary to create a ray trace model of the fibre coupled to the receiver. Figure (4.15) shows a ray-trace model of a bundle of six fibre optics inserted into a small cavity receiver of 20mm length, representative of a direct gain cavity receiver:

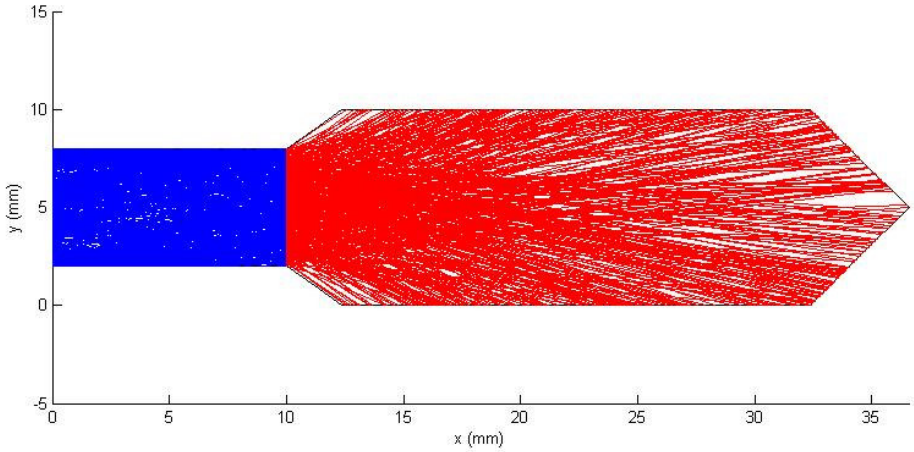

Figure 4.15: Cavity receiver ray trace model

The ray-trace shown in figure (4.15) is designed such that the rays traversing the fibre optics are traveling at angles in agreement with the ray-trace models of the concentrator (see section 4.2). Throughout the ray-trace, 100% total internal reflection is assumed and the rays are monochromatic. Each ray has an associated power calculated by the total power (300W) divided by the number of rays (5000). The intensity distribution is calculated by determining how many rays fall within a certain area and then dividing the accumulated power by that area. Figure (4.16) shows the monochromatic intensity distribution over the cavity wall.

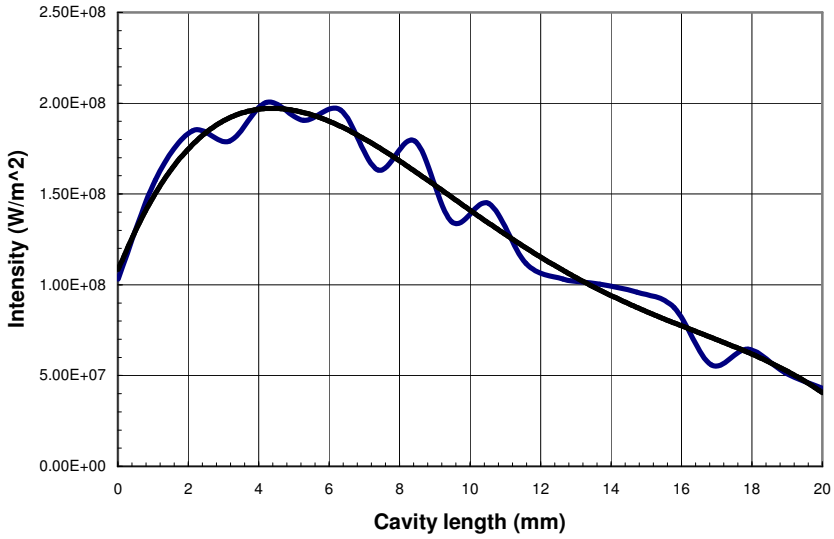

Figure 4.16: Monochromatic cavity wall intensity distribution

The monochromatic cavity wall intensity distribution shown in figure (4.16) indicates that the highest intensity will occur around 5mm along the cavity wall. Over this region, the heat transfer to the propellant will be greatest as this section of the wall will be hottest. Thus, it would be necessary to design the spiraling channel around the cavity to be longer over this region than the less intense regions to maintain a constant temperature along the receiver wall. This would minimize inefficiencies due to hotter sections of the cavity wall being closer to the cavity aperture, as sections closer to the aperture will have a larger view factor than those further away.

A similar result was obtained form a study into refractive secondary concentrators for a solar thermal propulsion system (NASA shooting star project [63]). It was determined that the intensity distribution on the cavity wall could be tailored to provide a more even distribution that peaked further into the cavity reducing inefficiencies. The secondary refractive concentrator was made of zirconium or sapphire which are capable of withstanding the high temperature.

4.4.2.2 Fibre Temperature Profile

The fibre will be exposed to high temperatures when coupled to the cavity receiver. It is important to design the coupling method such that the fibre core temperature is maintained within working limits. A two-dimensional thermal model was created in Thermxl of the fibre-receiver coupling technique depicted in figure (4.14b). The receiver is assumed to be at a constant peak temperature of 2227°C. It is surrounded by a graphite insulation package of various thicknesses. The fused silica fibre is supported by an alumina tube which is attached to the outside of the graphite insulation package. The fibre is inserted into the receiver, but does not come into contact with it. The model takes into account conductive and radiative heat flow and computes the steady-state result. Figure (4.17) shows model temperature profiles for various insulation thicknesses.

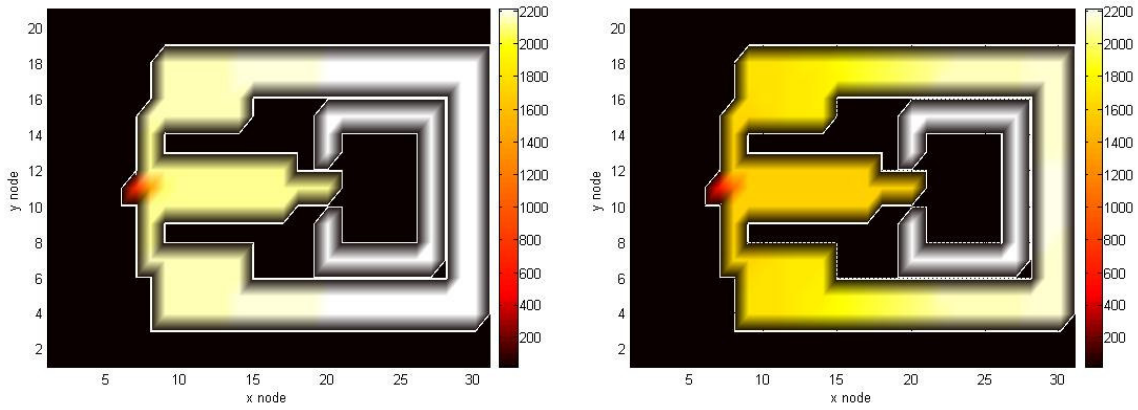

(a) 1cm insulation **(b) 5cm insulation**

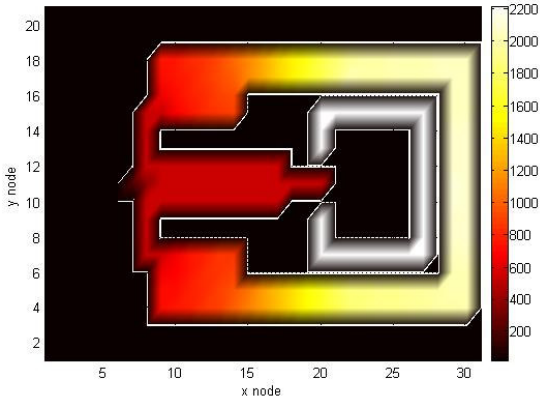

(c) 10 cm insulation

Figure 4.17: Thermxl models of fibre-to-cavity coupling concept

In figures (4.17a) to (4.17c) the insulation thickness is increased from 1cm through to 10cm. By increasing the conductive path between receiver and fibre, the steady state temperature of the fibre decreases. The fibre is assigned an absorbtivity value of 0.001, accounting for its low attenuation and approaches temperatures ranging from 2100°C, for thin insulation, to 700°C for thick insulation. The minimum fibre temperature modeled is much less than the melting point of fused silica, but is much higher than the manufacturer specified working temperature limit and the melting point of the Teflon cladding. In section 5 fibre temperature limits are investigated further.

A complication of this fibre to receiver coupling arrangement is that at such high temperatures receiver material could deposit on the tip of the fibre, blocking light from entering the receiver and possibly melting the fibre. This problem could be minimized by baking a receiver prior to launch. A possible solution to this would be a high-temperature zirconium or sapphire receiver insert, which would be coupled to the fibre bundle. This arrangement is depicted in figure (4.18a):

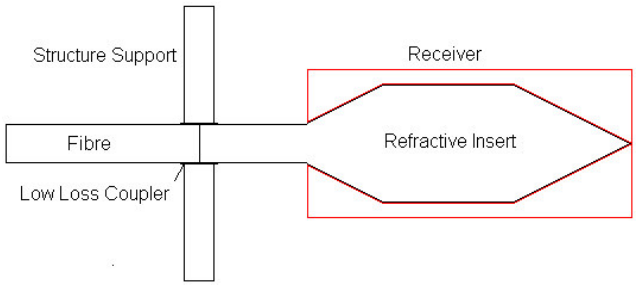

(a)

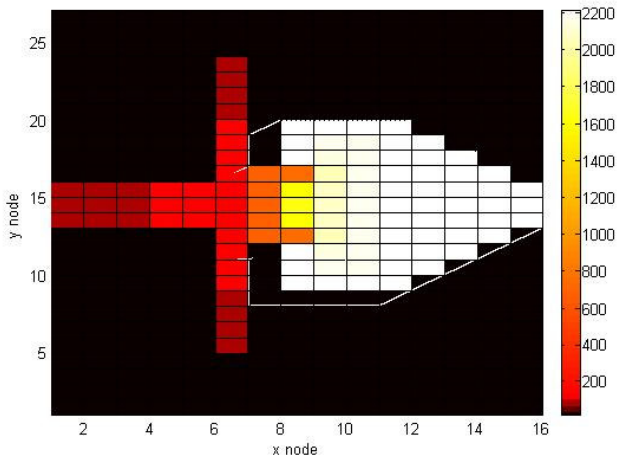

(b)

Figure 4.18: (a) Refractive insert for fibre coupling to receiver (b) Thermxl model of refractive insert

Figure (4.19b) is a Thermxl model created for this arrangement of fibre and refractive insert. It indicates that the fibre would have to be coupled to the refractive insert ~5cm from the receiver aperture. However, this would increase the cost of the receiver.

4.5 Pointing System Design

Pointing the concentrator system to align accurately with the sun-vector is critical to the success of the system. The pointing requirement is directly related to the fiber optic (or bundle) diameter and the concentrator image size. From analysing concentrator optics, the pointing accuracy requirement is set at 0.05° for a single 1mm core diameter fibre optic. It would be challenging for a small satellite attitude control system to provide this accuracy. Normal attitude system pointing accuracies are on the order of 0.5° [58]. In terms of mass and size, a fibre augmented STP system inherently favors the multiple mirror approach. Because of the need for fine pointing accuracy, each of the mirrors would need to be separately pointed. Thus, each mirror would need a pointing mechanism, a sun sensor, and a closed loop control system. This would result in increased system complexity and a decrease in the mass advantage over a single concentrator.

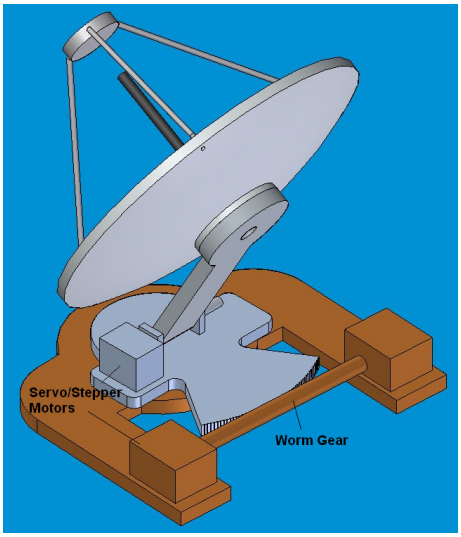

Figure 4.19: Pointing system concept

The pointing mechanism should have very fine angular resolution be capable of both slow and fast slewing for sun tracking and sun acquisition respectively. A large portion of a microsatellite's orbit can be in shadow, thus a fast slew rate is required to minimize sun acquisition time. A maximum slew rate of $6°s^{-1}$ would be appropriate, allowing the mirror to rotate relatively quickly without creating to much of a disturbance torque. The mechanism would be a two axis 'alt-azimuth', assembly employing two geared motors. An example of such a mechanism is show in figure (4.19). Hybrid stepper motors are simple, robust candidates for the geared mechanism motors. Hybrid stepper motors are available that can operate at 200 steps/revolution, requiring a gear ratio of 54 to achieve a one arc minute angular step size. DC servomotors can also be employed and can offer improved performance in speed and precision when incorporating a PID (proportional integral differential) compensator [59,60].

The angular range of the pointing mechanism should maximize the portion of the orbit over which the STP system can operate, and at the same time, prevent shadowing and excessive fiber stress. Moreover, to minimize and compensate for satellite induced disturbance torques the pointing and optical systems should be lightweight, compact and suitably damped. A lower concentrator mass will result in faster sun acquisition times and lower concentrator induced disturbance torques on the spacecraft when compared to a larger single concentrator. A further demand of the pointing mechanism and control system will be to attenuate local spacecraft vibrations. Suhonen discusses the pointing requirements for a scanning micromechanical mirror for intersatellite communication links and identifies a control bandwidth of 200 Hz for angular spacecraft vibrations of < 1mrad [61]. For angular vibrations of 0.05°, a control bandwidth of 100Hz would be required.

The spacecraft's sun sensors if available would provide the mechanism pointing determination system with an estimate of the sun-vector. Sun sensors, however, are unable to track the solar image on the focal plane. This is desirable for accurate alignment of the fiber with the solar image. A concept that can solve this problem is currently being studied at the University of Surrey. The concept is shown in figure (4.20a) and consists of a bundle of seven fibre optics. Each fibre has a photodiode attached on their side a certain distance from the concentrator end of the bundle. The photodiodes measure the photoluminescence emitted by each fibre resulting from the high intensity light traversing the fibre. The outputs from the photodiodes allow the mechanism pointing determination system to estimate the position of the sun image on the focal plane.

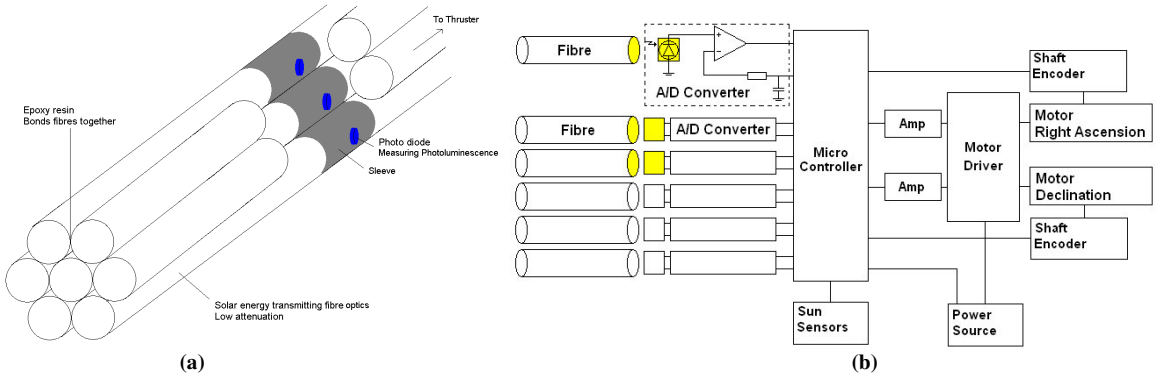

Figure 4.20: (a) Fibre bundle with attached photodiodes (b) Pointing control system.

Figure (4.20b) depicts the control system for this concept. The angular range of the fibre bundle is limited; such that a search algorithm is required for Sun acquisition after a coarse acquisition is made based on the initial estimate of the Sun vector. However this concept should enable the pointing mechanism to track the Sun and compensate for vibrations and disturbances.

4.5.1 Pointing Mechanism Design and Modeling

For the purposes of ground testing and concept proving, a pointing mechanism was designed and constructed. The pointing mechanism was designed to be an elevation-azimuth style pointing system that was of the correct size to steer the Cassegrain concentrator unit described in section 4.2. Two 24V DC brushed motors drive each axis of revolution. Each motor has a gearbox such that the overall gear ratio for each motor is 50:1, providing an axel no load speed of 108rpm. The pointing mechanism is estimated to have a bandwidth of 20Hz. The design of the mechanism structure was modeled in Solid Edge, a computer aided design analysis tool, to determine the moments of inertia about each axis of revolution (figure 4.21a). Thus allows modeling of the motor speed which aided motor selection. In figure (4.21b) the constructed mechanism is shown:

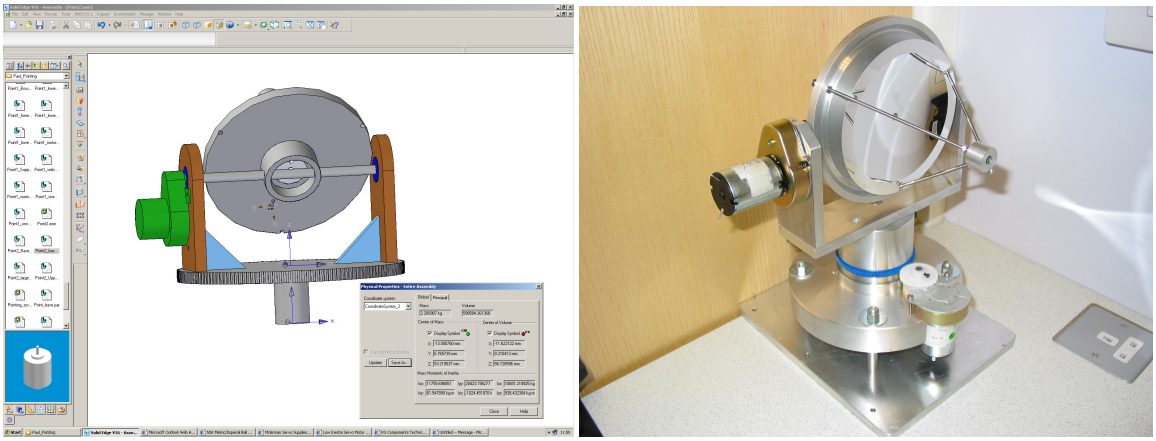

(a) **(b)**

Figure 4.21: (a) Solid edge analysis of pointing mechanism. (b) Constructed pointing system

To model a DC motor, we must consider the electric circuit in which the motor is placed and the motion of the rotor, as seen in figure (4.22).

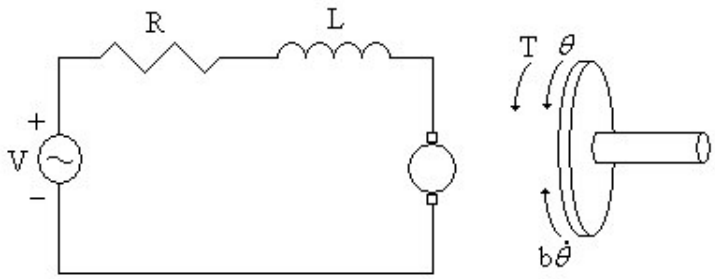

Figure 4.22: Motor speed model

Here, R is the circuit resistance, L is the circuit inductance, V is the source voltage, T is the motor torque, θ is the angular position of the rotor and b is the damping ratio of the mechanism [62]. The motor torque is considered to be proportional to the armature current (I), such that:

$$T = k_t I \text{ ……(4.16)}$$

Where k_t is the armature constant. Similarly, the back emf (e)[13] is related to the rotational angular velocity by:

$$e = k_t \dot{\theta} \text{ ……(4.17)}$$

Employing Kirchhoff's and Newton's laws [62] along with equations (4.16) and (4.17) allows us to write the transfer function for the motor as:

$$\frac{\dot{\theta}}{V} = \frac{k_t}{(Js+b)(Ls+R)+k_t^2} \text{ ……(4.18)}$$

Where J is the rotor inertia and s is the complex frequency. The transfer function describes the response of the system to a given input. In this case, for a given applied voltage, the motor transfer function predicts the motor angular velocity, taking into account friction and angular momentum. Using the motor transfer function, the theoretical open loop time and frequency response of the motor can be assessed [62].

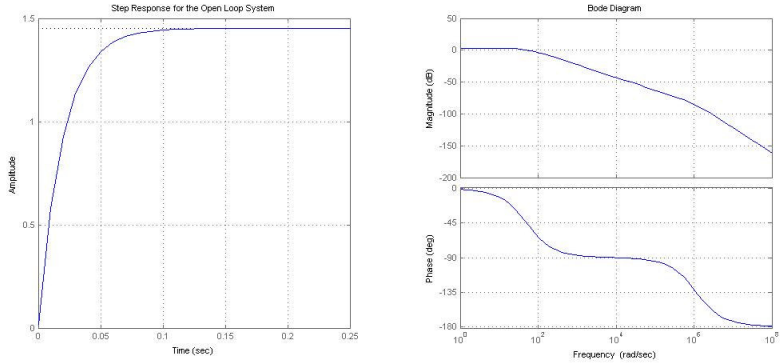

(a) **(b)**

Figure 4.23: (a) Open loop response of DC motor to 12V step input. (b) Bode diagram of DC motor

Figure (4.23a) is the predicted open loop response of the motors and pointing mechanism, shown in figure (4.23b). It estimates a top speed of 1.5 rads/s for an applied voltage of 12V when under load. Figure (4.43b) is the Bode diagram of the motor, which describes its frequency response. At the desired bandwidth frequency of 100Hz, we can see that the motor output will be lagging by 60°. The Bode diagram for a motor suitable for a space based mechanism is shown in figure (4.24b). Here, the desired bandwidth of 100Hz is within range of the motor bandwidth and lagging is reduced to ~10°.

[13] Back emf is a voltage which opposes the applied voltage to the motor and is produced by the inductance of the motor.

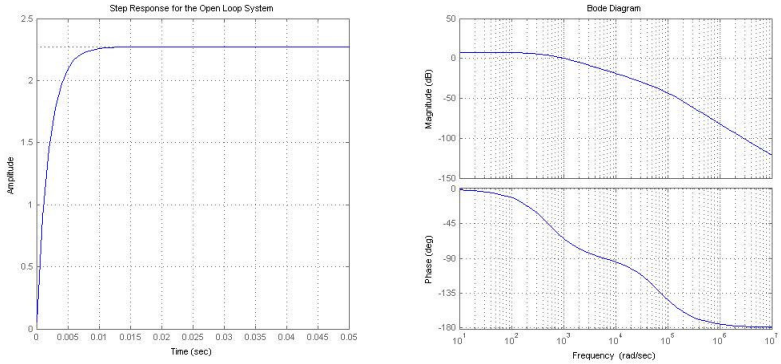

(a) **(b)**

Figure 4.24: (a) Open loop response of DC motor to 12V step input. (b) Bode diagram of DC motor

4.5.2 Pointing System Tracking Algorithm

There are several approaches for developing a tracking algorithm for the pointing mechanism. The simplest approach involves the comparison of the calibrated photoluminescence of opposite fibers in the bundle and driving the motors such that the value for each fibre is within a given tolerance. This will provide a fast system, but degeneracy in results limits the range over which this tracking algorithm can operate.

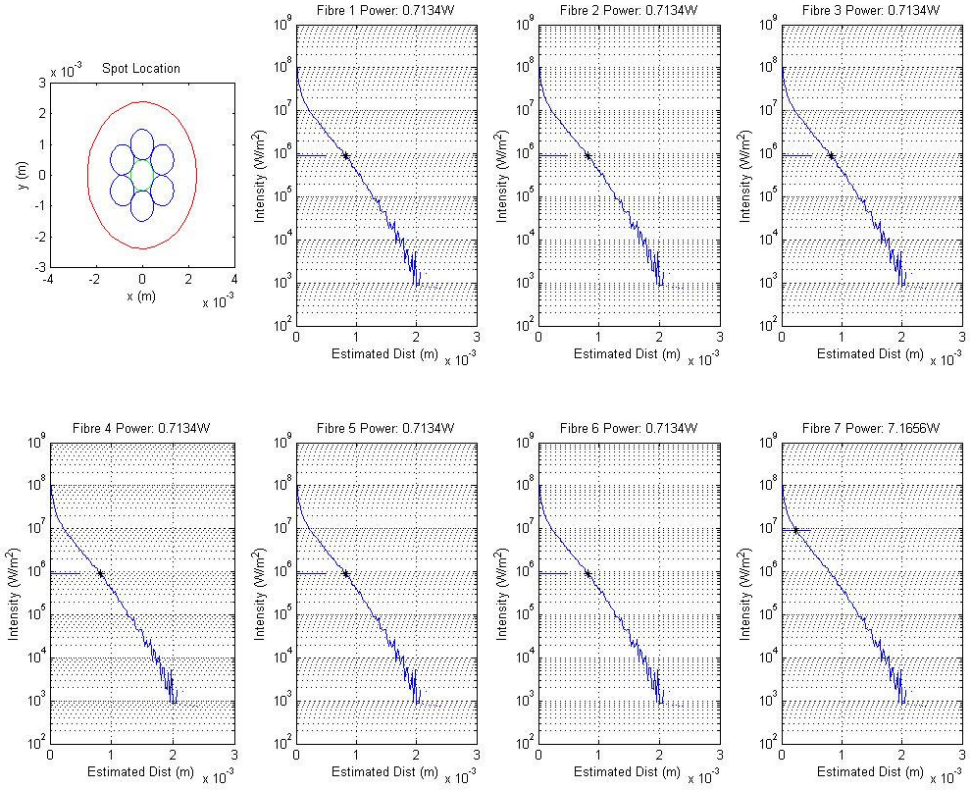

Figure 4.25 Pointing software correlation comparison

A more complex approach involves calculating the power traveling through each fibre from the photoluminescence measurements and then calculating an average value for the intensity on each fibre tip. This is then compared to the concentrator spot intensity distribution in section 4.2 to estimate the likely radial distance from the center of the spot. Through a locus technique the location of the spot center can then be estimated. This approach, although computationally demanding, allows tracking to be accomplished with any size of focal spot provided the intensity distribution is known. A model of this method was created in Matlab to assess its accuracy. Figure (4.25) shows the correlation graphs for each fibre in the model. The locus technique estimates the position of the spot by calculating the intersection of circles which are centred on each fibre and have radii corresponding to the estimated distance of each fibre from the spot. Averaging the coordinates of these intersections estimates the spot location. Figure (4.26) depicts this locus technique in practice for two spot displacements:

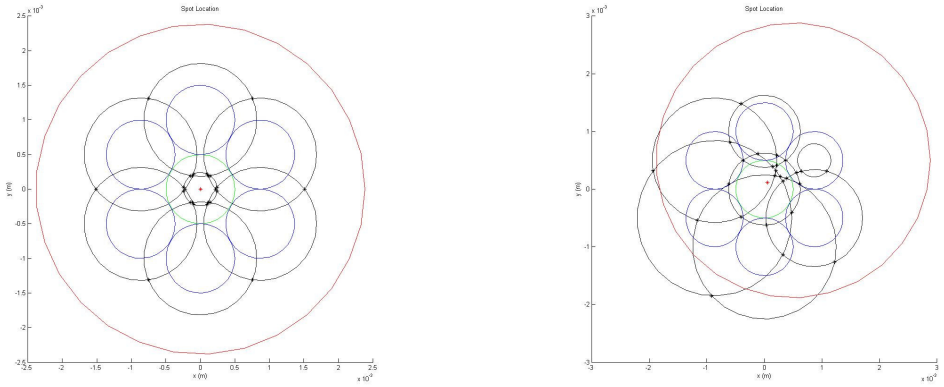

(a) **(b)**

Figure 4.26: (a) Position estimation for 0mm offset. (b) Position estimation for 0.5mm offset.

In figure (4.26) the red spot is the estimated position of the spot centre and the red circle is the actual spot. Position error increase with increased distance from the centre, however the vector of motion is always correct. Figure (4.27) depicts the increase in estimate position error with increasing radial distance of the bundle from the centre of the spot.

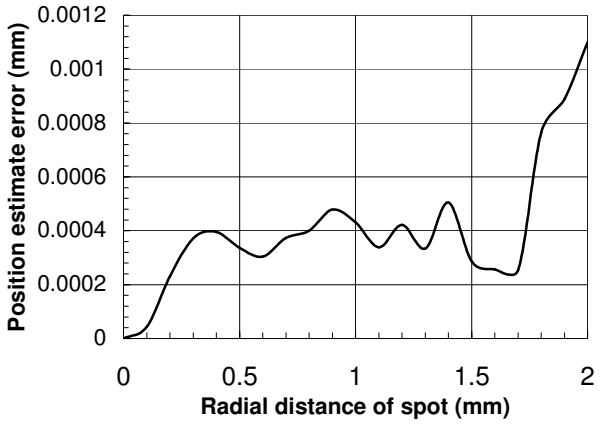

Figure 4.27: Position estimation error vs. radial distance of spot centre from central fibre

4.6 Summary

In this section the design considerations for a fibre optic augmented system have been discussed and requirements have been identified for specific components.

A concentrator design has been optimised for coupling to a 1mm core size fibre optic. Pointing accuracy of the concentrator and required concentrator RMS wavefront error have been specified. A direct-gain receiver has been scaled and designed from requirements outlined in section 3. A direct-gain receiver model is used to predict expected performance of the thruster. The consequences of using fibre optics for transmission of concentrated solar energy are discussed in depth and suitable fibre optic candidates are identified. A pointing system is formulated, including a proposal for a novel feedback mechanism/system.

Section 5

5 Component Test Campaign

The main technology focus of this research is the delivery of solar power to the solar cavity receiver via a fibre optic cable. In this section the testing conducted for three separate system components is discussed, namely:

- Cassegrain Concentrating Unit: Optimised for a 1mm core diameter FLU fibre optic.
- Fibre Optic Cable: FLU fibre optic cable 1mm core size, NA of 0.66.
- Pointing System: Designed for accurate pointing of the Cassegrain concentrating unit.

The design of each component is discussed in section 4.

5.1 Cassegrain Concentrating Unit Testing

A Cassegrain concentrating unit shown in figure (5.1) consists of two optical components, a primary parabolic concentrator and a flat secondary relay mirror which functions to make the whole assembly more compact and allows the fibre optics to be accurately aligned with the focal point of the primary. The concentrator was designed to couple concentrated light into a 1mm core size fibre optic with a NA of 0.66, thus it has a rim angle of ~42° providing near ideal concentration.

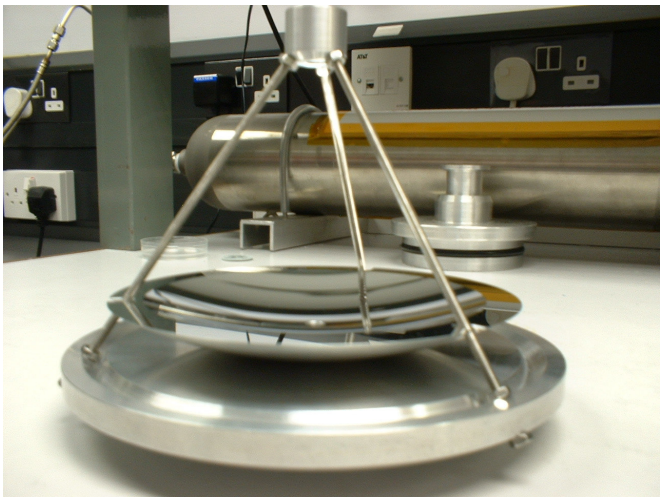

Figure 5.1: Prototype Cassegrain concentrating unit

Precision Optical Engineering (POE), a company based in Hertfordshire, UK, manufactured the primary concentrating parabolic mirror at their diamond turning facility. Testing of the primary concentrating unit at POE provides the following details of the concentrator quality:

- Peak-to-Valley: 0.34µm (Addition of largest peak and valley)
- Strehl ratio: 0.8 (80% of energy within ideal spot size)
- F number: 0.687 (ratio of focal length to concentrator aperture)

The aluminium primary was probed at POE after completing the diamond turning process to produce the form error graph shown in figure (5.2)

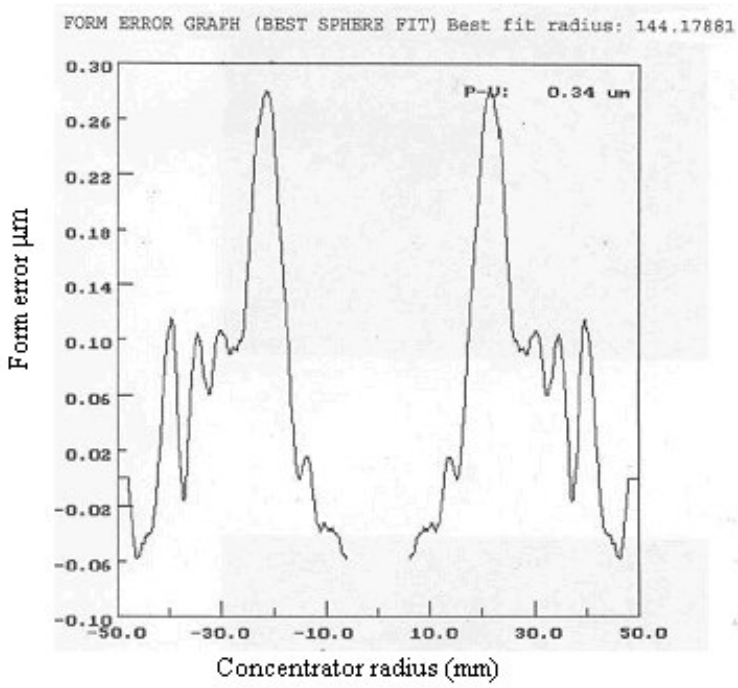

Figure 5.2: Form error graph for prototype Cassegrain concentrating unit

Figure (5.2) indicates the variation of the mirror surface from the ideal surface. The largest peak occurs quite close to the centre of the mirror, which is fortunate as peaks closer to the mirror centre have less impact of the resulting image because they take up less area on the mirror. From figure (5.2) we can estimate a value for the RMS form error of the mirror as 0.08µm. From this value of the RMS form error we can estimate that the primary has a concentration ratio close to the ideal value of ~12,000 and should easily be able to produce a spot size suitable for coupling to a 1mm core size fibre optic cable. POE quotes the focal length of the primary as 72.1mm ±0.1mm.

On-Sun experiments conducted during the summer of 2005 tested the cassegrain optical units overall efficiency and identified a suitable secondary relay mirror. In these experiments the

concentrating unit was employed to heat up a small (1g) graphite sample. The initial temperature gradient of the graphite sample upon heating provides an estimate of the power directed at the graphite sample, figure (5.3). A pyroheliometer is used to determine the intensity of the incident solar radiation and a thermocouple is used to measure the graphite temperature.

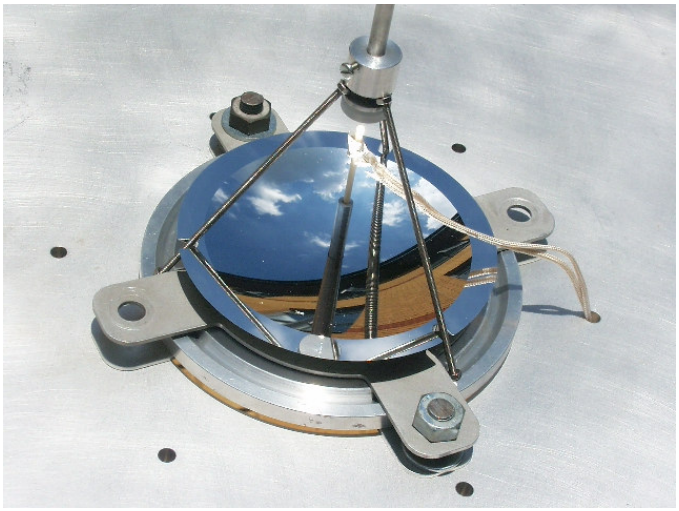

Figure 5.3: Summer test 2005, prototype Cassegrain concentrating unit

The primary, rated at 90% efficiency, directed 6.3W of power at the graphite sample with a local intensity of 800W/m^2. The graphite sample obtained a temperature of 450K over 60s period.

A number of candidate secondary relay mirrors were selected for use with the Cassegrain concentrating unit. Each secondary had a different surface material and surface quality; these are listed in table (5.1):

Table 5.1: Candidate secondary relay mirrors (λ=450nm)

LINOS Part No	Surface Quality	Surface Material	Efficiency of Secondary
340342	1/2λ	Aluminium	80%
340334	1/10λ	Aluminium	92%
340621	1/4λ	Silver	83%
340618	1/2λ	Silver	75%

Each secondary relay mirror was tested in a similar manner to the primary, by heating a graphite sample. The graphite sample and secondary were placed along the focal axis of the primary such that the graphite sample always received the same amount of radiant power from the primary. Then by measuring the initial temperature gradient of the graphite sample an efficiency is calculated for each secondary, as seen in table (5.1). The importance of secondary surface quality

is highlighted by these results, with the most efficient secondary having a surface quality of $1/10^{th}$ λ. With this secondary the Cassegrain optical unit will have an overall efficiency of 83%.

5.2 Fibre Optic Cable Testing

The fibre optic cable selected for this research is Polymicro's FLU Teflon clad silica core fibre optic cable. This fibre was chosen due to its unusually large NA. Gordon [63] indicates that this particular fibre exhibits high non-perfect total internal reflection in comparison to other fibre optic cables; he attributed this to inconsistencies in the Teflon cladding. However given the short distances over which an STP technology demonstration system will operate (<1m) the ability to have near ideal concentration ratio was favoured. Polymicro supplied a 50m order of the FLU cable sectioned into ten 2m lengths, one 10m length and one 20m length. The tips of each fibre were machine polished to ensure optimal coupling between concentrator and fibre.

5.2.1 Fibre Transmission Tests

In the winter of 2004 initial tests were conducted at SSTL's solar simulator facility to determine the transmission efficiency of the FLU fibre optic cable. The experimental set up is shown in figure (5.4)

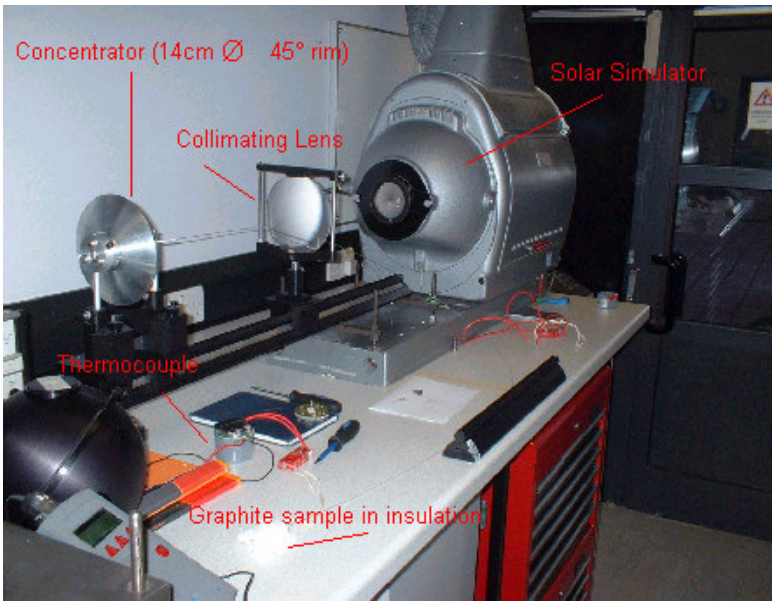

Figure 5.4: Solar simulator fibre transmission experiments, December 2004.

The fibre optic cable is coupled to a 14cm diameter parabolic concentrator on an optical rail aligned with the aperture of a xenon arc lamp solar simulator. The solar simulator itself is cable of producing AM0 intensity and higher over a 14cm diameter beam. A Collimating lens is used to

reduce divergence of the solar simulator beam. The other end of the fibre optic cable is inserted into a small graphite sample wrapped in insulation, in order to reduce convective effects. The temperature of the graphite sample is monitored by a thermocouple. The beam from the solar simulator is concentrated by the parabolic mirror into the FLU fibre optic cable. This energy traverses the fibre optic and is delivered to heat the graphite sample. To determine the transmission efficiency the graphite sample was also heated directly by the parabolic mirror. The temperature time graphs for both direct heating and fibre heating are shown in figure (5.5), with corresponding polynomial fits to aid visualisation:

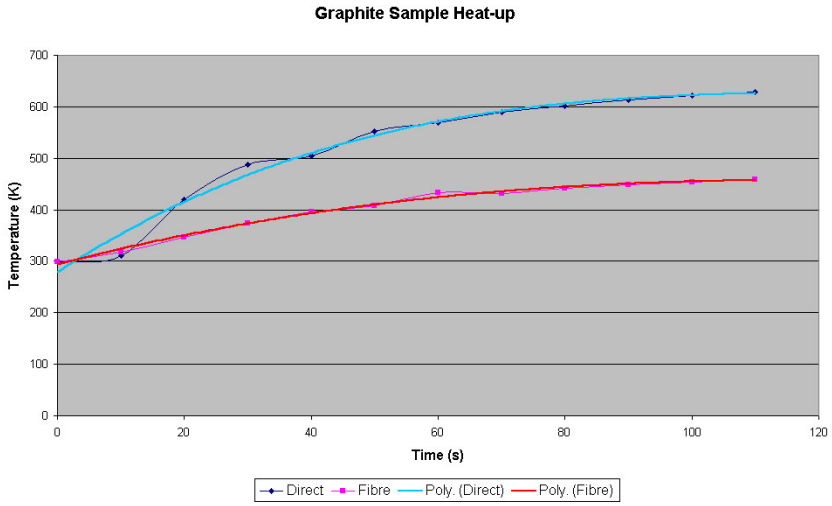

Figure 5.5: Graphite sample heating tests, December 2004.

The power used to heat the graphite sample is estimated from the initial gradient of the best-fit lines shown in figure (5.5). The power estimated for direct heating by the parabolic concentrator was 10W and the power estimated for fibre heating was 4.9W. Thus demonstrating ~50% transmission efficiency. However, it was observed that the spot size produced by the concentrator was significantly larger than the fibre tip area. This is due to divergence of the solar simultor beam and results in a reduced intensity at the graphite sample. The spot diameter was measured to be ~3mm. As discussed in section 4 the intensity distribution of the concentrator spot is most intense at its centre, explaining how the 1mm fibre was able to capture the 4.9W of power. However a large portion of the power delivered by the concentrator will not enter the fibre, indicating the potential for greater transmission efficiencies.

Further transmission testing was conducted during the summer of 2005. The purpose of this testing was to study the effect of fibre length on transmission efficiency and to confirm the linearity of the addition of power from multiple fibres. Although the FLU fibre has a very low attenuation spectrum, transmission of high intensities can increase loss mechanisms such as photoluminescence and non-perfect total internal reflection. The tests were conducted outside using the Sun as a power source. A Losmandy solar tracking tripod mount was used to orientate a

14 cm diameter concentrator to point at the Sun. A two-axis micrometer stage was employed to locate the fibre tip at the concentrator's focal point. Delivered fibre power was measured using a LOT-Oriel thermopile sensor, having a response over a broad range of wavelengths. A pyroheliometer is used to measure local solar intensity. The equipment set up is depicted in figure (5.6):

Figure 5.6: Fibre transmission tests, summer 2005.

Fibre lengths of 2m, 10m and 20m were used to analyse the effects of fibre length on transmission efficiency. These results are plotted in figure (5.7). On swapping over different lengths of fibre optic cable the focal position was maintained.

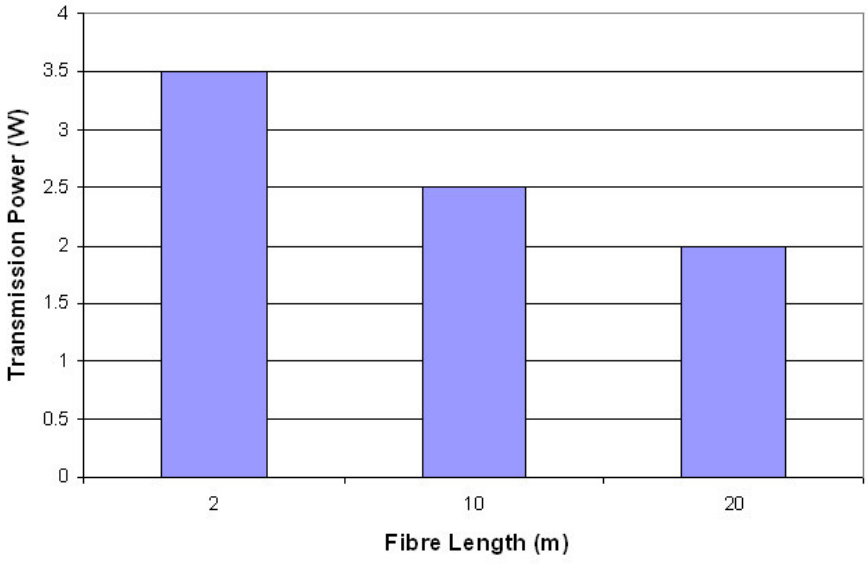

Figure 5.7: Transmission power vs. fibre length, summer 2005 transmission tests.

From figure (5.7) we can see that there is a significant decrease in transmitted power for a relatively small increase in length. This indicates an increase in loss mechanisms for higher intensity power transmission through the fibre optic cable. The linearity of power addition for multiple fibre optics was confirmed by employing two parabolic concentrators each coupled to a fibre optic cable. Their separate transmitted power added linearly to produce a total output power of 1.6W as measured by the thermopile detector.

A connector was manufactured for the fibre optic to allow it to be accurately positioned along the focal axis of the concentrator, see figure (5.8):

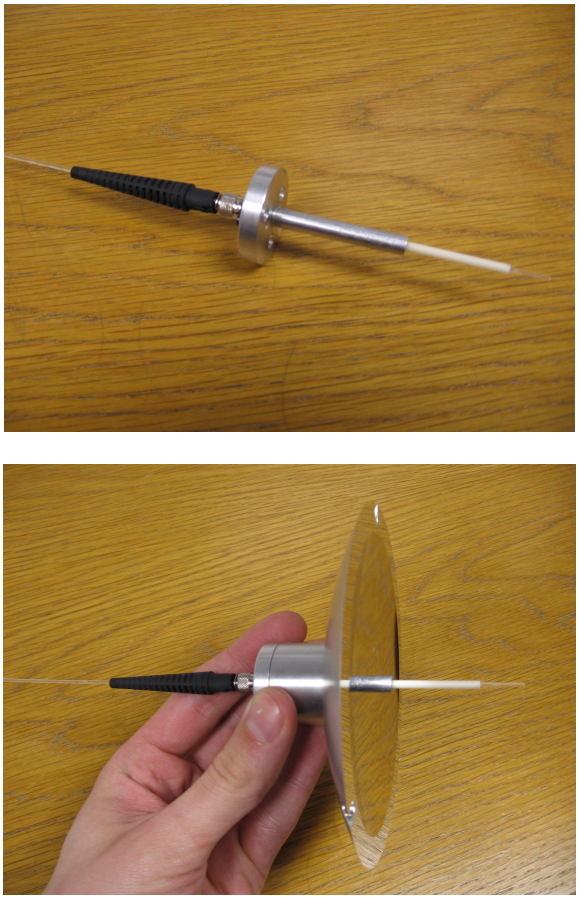

Figure 5.8: Fibre optic connector for prototype Cassegrain concentrator unit.

An alumina ceramic tube is fed through an aluminium outer support, which is accurately aligned with the focal axis. The fibre is bonded to the alumina tube with high temperature epoxy resin. The connector can be easily removed from the concentrator via threaded bearing. The alumina tube having a high stiffness supports the fibre to the focal spot with a tolerance of ± 0.1 mm. This connector was employed to position the fibre along the focal axis of the Cassegrain concentrating unit in the 2005 summer transmission tests. Difficulty was initially experienced in aligning the fibre tip with the focal point. This was due to error in the machining of the aluminium support for the alumina tube. A second aluminium support was fabricated that more accurately aligned the

fibre tip with the focal point. The Casegrain concentrating prototype was then used to concentrate solar energy into a 2 m long FLU fibre optic. A 3.2 W power transmission was observed demonstrating an end-to-end efficiency of 50%.

A further transmission test was conducted in December 2005, aimed a determining the effect of fibre optic cable bend radius on transmission. Using a solar simulator light was concentrated into the FLU fibre optic cable via a 14cm diameter parabolic mirror. No loss in transmitted power was observed at bend radii as small as 30mm, for a 180° bend. However significant elastic energy was observed in the fibre as this bend radius, indicating a need to mechanically support the fibre for such tight bends.

5.2.2 Fibre Optic Cable Attenuation Spectrum Analysis

In light of the fibre transmission experiments conducted in the summer of 2005 it was deemed necessary to independently measure the attenuation spectrum of the FLU fibre optic cable and compare it to the manufactures specification. To do this the fibre was taken to Surrey Universities Advanced Technology Institute (ATI), where an optical spectrum analyser (OSA) was used to measure the spectrum of a calibrated white light source, which was transmitted through the fibre optic, see figure (5.9).

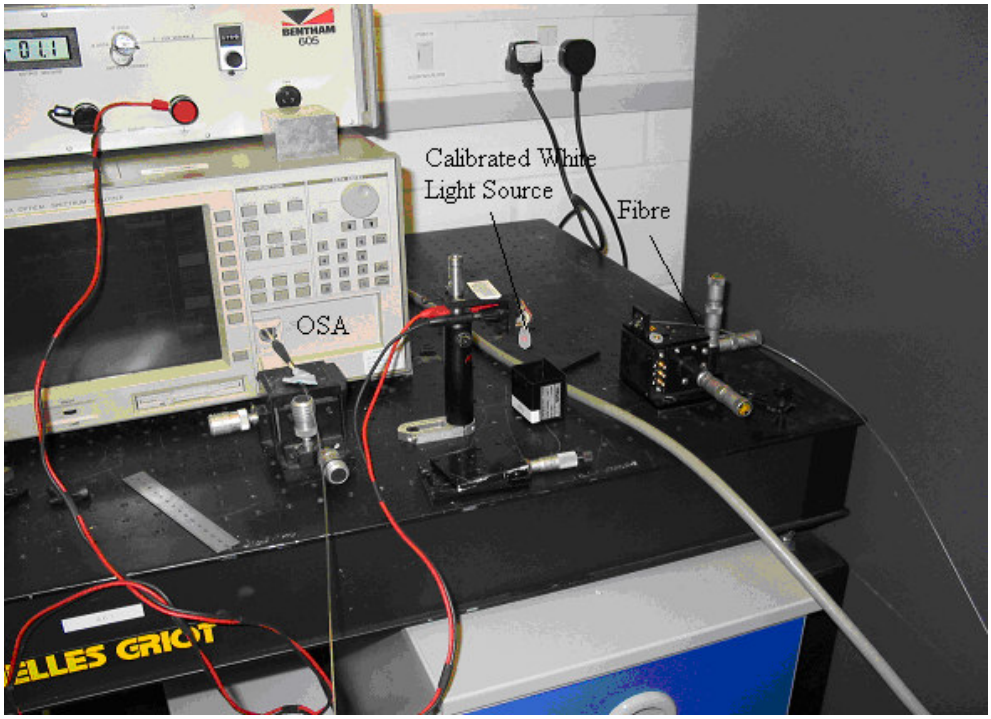

Figure 5.9: FLU fibre optic attenuation spectrum measurment experiment.

A technique known as the 'cut back method' was used to calculate the fibres attenuation spectrum. This involves measuring the transmitted spectrum of the calibrated white light source for two lengths of fibre optic cable. Comparing the two spectrums allows the calculation of the attenuation over the difference in distance between the two lengths of fibre. Two metre and twenty metre fibre optic lengths were used to maximise the difference in transmitted spectrum. The OSA has a wavelength range of 350nm to 1750nm allowing the analysis Ultraviolet (UV), Visible (V) and near Infra Red (IR) regions of the fibre attenuation spectrum. This is also the range over which the solar spectrum is most prominent. Figure (5.10) compares the manufacture attenuation spectrum and that calculated via the cut back method:

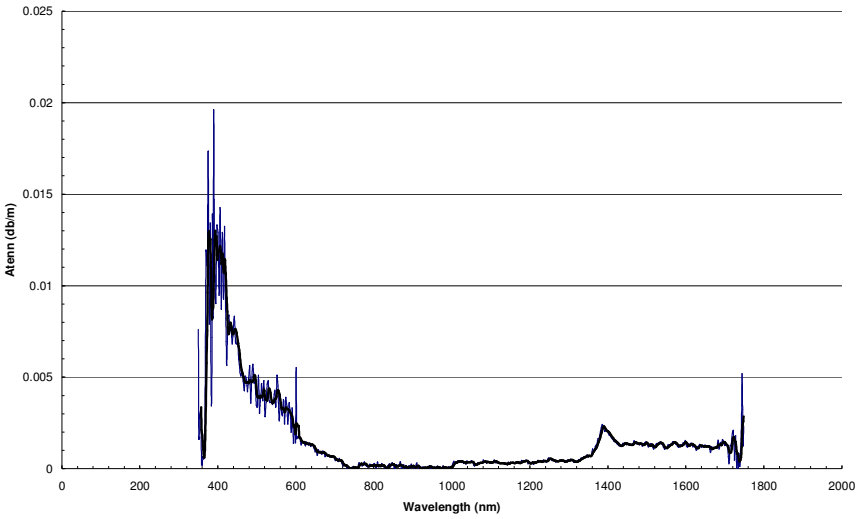

(a)

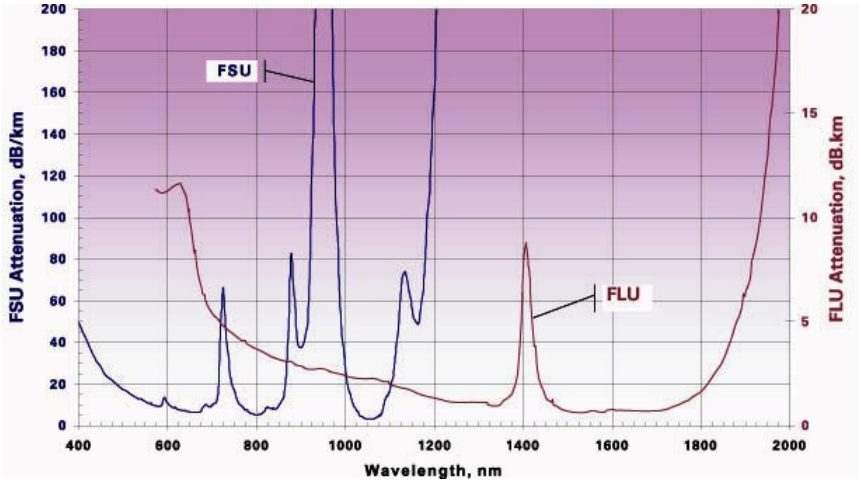

(b)

Figure 5.10 (a): Measure FLU fibre attenuation spectrum. (b) Manufacturer supplied spectrum

The two attenuation spectrums, shown in figure (5.10) agree strongly, taking into account the attenuation units (dm/km to db/m). This strong agreement confirms that the substantial decrease

in transmitted solar power observed in the summer 2005 tests for increasing fibre length is due to other loss mechanisms such as non-perfect total internal reflection and photoluminescence.

5.2.3 Fibre Optic Attenuation Spectrum Thermal Analysis

When the fibre optic is coupled to the receiver it will be exposed to very high temperatures. The FLU fibre optic is rated by the manufacturer to 160°C. However it was shown earlier that the fibre would be exposed to temperatures of at least 700°C when coupled to a hot receiver at 2,227°C. Thus it was deemed necessary to study the effects of high temperatures on the attenuation spectrum of the FLU fibre optic. A 20m length of the FLU fibre was again taken to the ATI were it was fed through a cylindrical furnace with one end coupled to a white light source and the other to an OSA, as shown in figure (5.11).

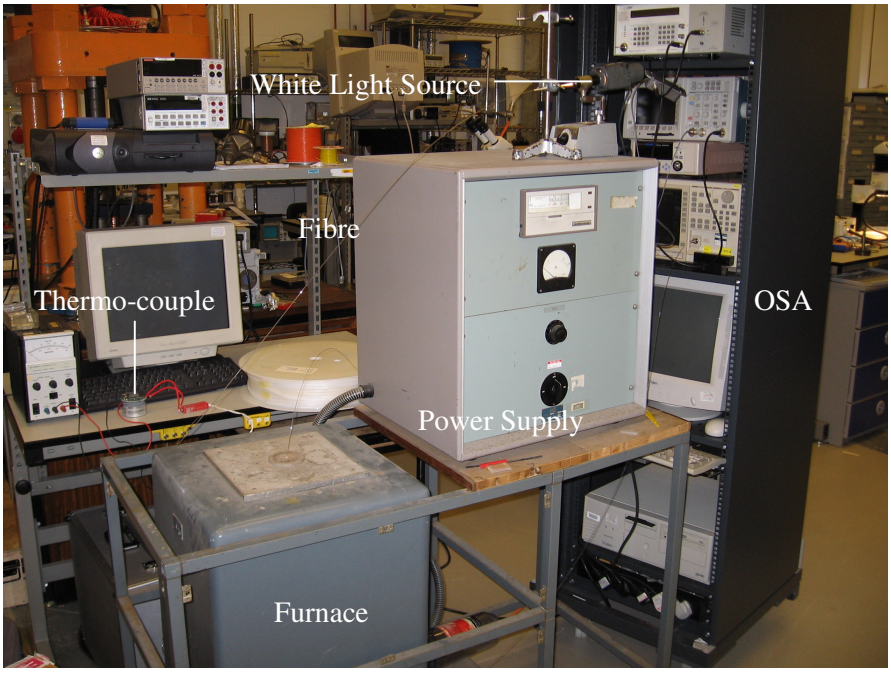

Figure 5.11: FLU fibre thermal attenuation spectrum experiment.

The fibre temperature was monitored by a thermocouple attached to the fibre surface with high temperature epoxy resin. The furnace has a 0.4m long cylindrical heating area through which the fibre was passed. The fibre was tensioned such that the fibre did not touch the sides of the furnace wall, ensuring an even heating along the fibre surface. The fibre was heated up to a temperature of 1,000°K and the white light source spectrum transmitted through the fibre optic cable was measures at 400°K, 550°K and 1,000°K. Intermediate fibre temperatures were difficult to obtain due to the rapid heat up of the furnace. The fibre was left at a temperature of 1,000°K for 40 minutes to ensure the fibre reached thermal equilibrium with the furnace, after which the fibre

was then allowed to cool. During cooling the white light source spectrum was again monitored at fibre temperatures of 800°K, 600°K, 550°K and 400°K. On analysing the spectrum data from the OSA it was found that the IR regions of the white light source were dominated by IR radiation from the furnace entering the fibre and being transmitted along its length. However this did not affect the UV and visible regions of the spectrum up to 900nm. Each spectrum (corresponding to a particular fibre temperature) was compared to a room temperature white light source spectrum taken before fibre heating. These results are plotted in figure (5.12):

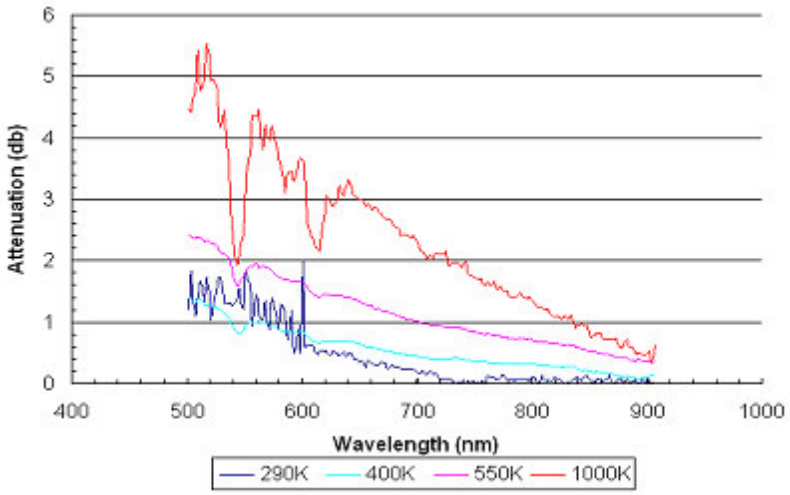

(a)

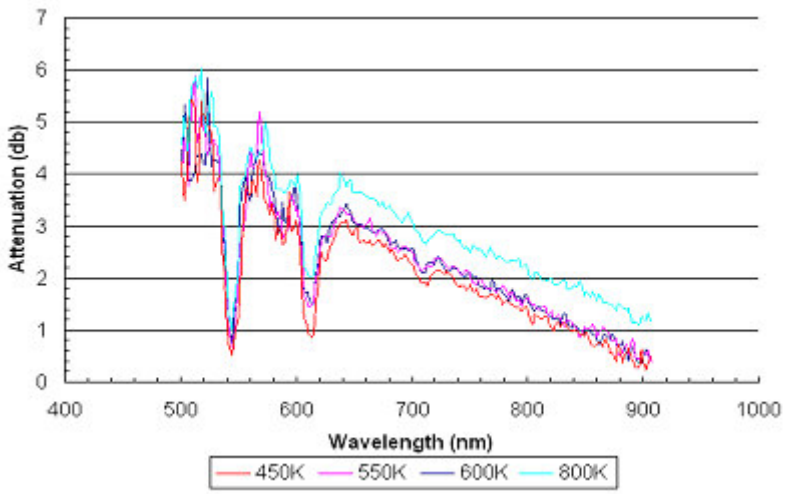

(b)

Figure 5.12 (a) Fibre attenuation increase during heat up.

(b) Fibre attenuation decrease during cool down.

From figure (5.12a) we can see that there is an increase in fibre attenuation for increasing fibre temperature. Upon cooling we can see that the attenuation recovers to an extent, in figure (5.12b). An explanation for this increase in attenuation is partly due to the loss of the fibre buffer and cladding during the fibre heating, even though the silica core did survive. This explains why the attenuation spectrum does not return to its original state. Interestingly there are troughs in each spectrum at 545nm and 613nm, indicating that transmission of these wavelengths is less affected by the increase in temperature and loss of cladding. After removal of the fibre from the furnace, the fibre cores physical properties appeared unaffected, however, the fibre buffer and cladding had become charred and crumbled easily away from the fibre core, as shown in figure (5.13).

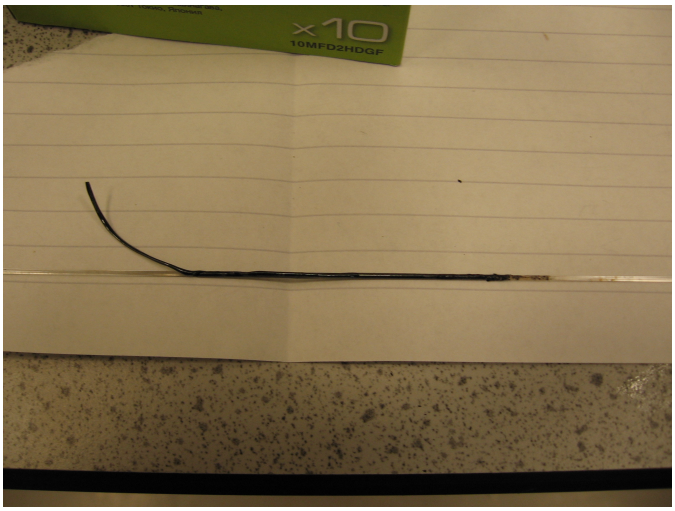

Figure 5.13: FLU fibre Teflon cladding after heating.

Taking into account the loss of the cladding for the transmission properties of the fibre we can see that the physical properties of the silica core begin to be significantly affected by temperatures above 1000°K. Comparing the attenuation spectrums of the fibre before and after heating, a 1.5db increase in attenuation is observed on average attributed to a 0.4m loss of cladding. Taking into account the loss of cladding there appears to be a non-linear relation of attenuation as a function of fibre temperature, which increases towards larger temperatures. This stresses the need to minimise the temperature to which the fibre is exposed. A silica core, silica clad fibre optic would perform better at these elevated temperatures, however this reduces the attainable concentration ratio of the system. Given that only small lengths of fibre optic will be exposed to high temperature, however, does not prevent the use of the FLU fibre to deliver energy to the receiver as long as its temperature can be maintained below 1000K.

5.3 Pointing System Testing

The pointing system proposed in section 4 consisted of a pointing mechanism supporting a Cassegrain concentrating unit, which focuses solar energy on to a bundle of 7 fibre optics. The photoluminescence exhibited by the fibres when transmitting high intensity energy is measured by photodiodes whose response is fedback to a controller which tracks the sun via the two DC motors of the pointing mechanism. The first step necessary to develop this system is to ascertain the ability of a photodiode to measure the photoluminescence of the FLU fibre optic. The photodiode selected for this application is the OPT101P photodiode, a product of Burr-Brown. This particular photodiode has an inbuilt transimpedance amplifier and a bandwidth of 14kHz. These photodiodes are commonly found within medical and laboratory instrumentation. A single OPT101P photodiode was integrated into the circuit shown in figure (5.14a). Light from a solar simulator was focused into a 2m FLU fibre optic cable that transmitted this light to a thermopile sensor. The OPT101P photodiode was used to measure the intensity of the photoluminescence of the fibre for different light intensities from the solar simulator. The results from this test are shown in figure (5.14b).

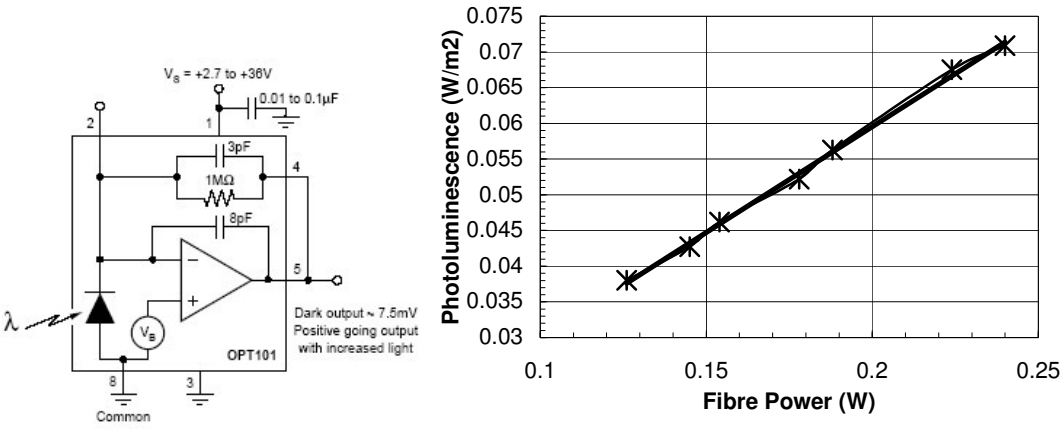

(a) **(b)**

Figure 5.14: (a) Photodiode amplifier circuit. (b) Photoluminescence vs. fibre power.

This test demonstrated the ability of the OPT101P photodiode to measure the photoluminescence of the FLU fibre optic cable, even for a transmitted power as low as 0.1W. In figure (5.14b) we see a linear relationship between transmitted fibre power and photoluminescence, resulting in a simple conversion from one to another within this power range. Upon demonstrating the feasibility of using a photodiode, a sensor array was constructed consisting of 7 OPT101P photodiodes, shown in figure (5.15a).

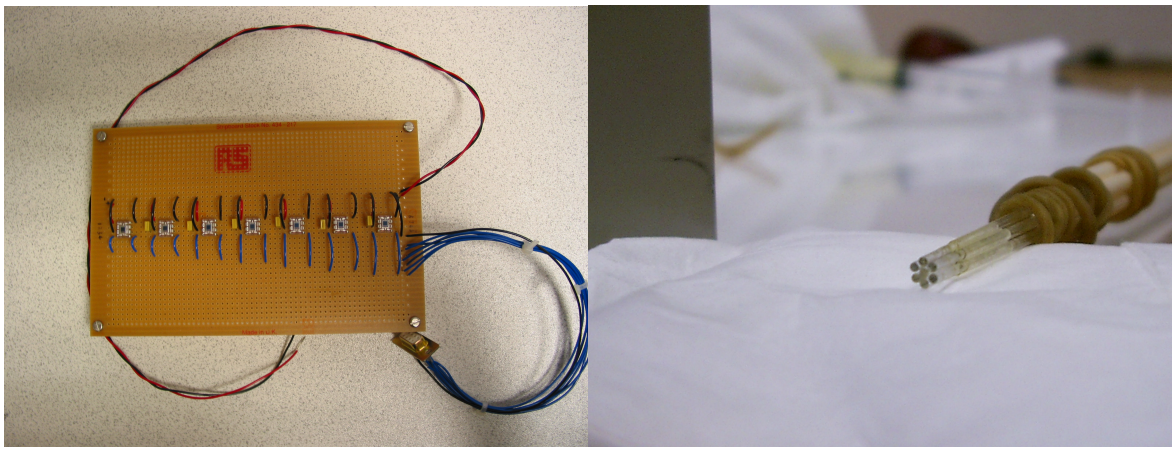

Figure 5.15: (a) Photodiode sensor array (b) FLU fibre bundle

The next step taken was to construct the fibre optic bundle. Seven, hand polished FLU fibre optic cables were glued together using RT153FC, a high temperature epoxy product of ResinTech (see figure (5.15b). Then an XPC-target system was constructed for the feedback and control of the photodiodes and DC motors respectively. XPC-target is a rapid prototype development package that enables realtime implementation and analysis of hardware through a Matlab/simulink interface. XPC-target employs a 'host' computer that creates the simulation code and downloads this to a 'target' computer, which interfaces with the hardware via a national instruments 6024E PCI card to implement the real-time code. The whole prototype system set-up is shown in figure (5.16).

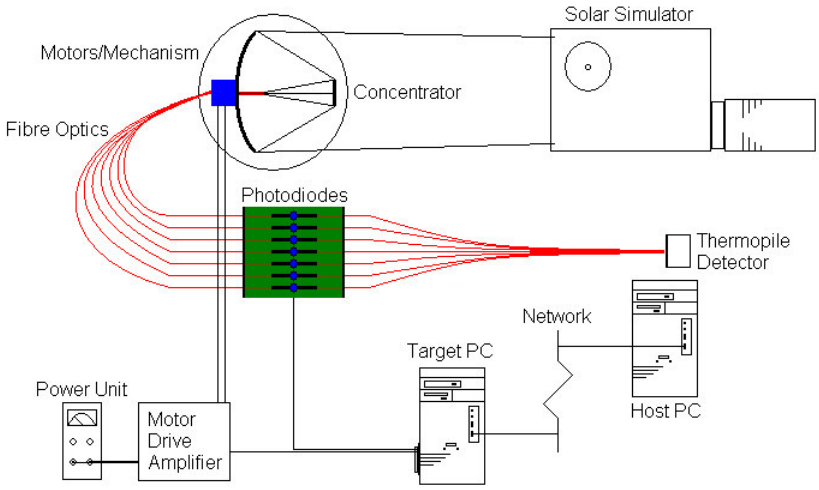

Figure 5.16: XPC-Target control system experiment set up.

The final system component required is the motor drive amplifier circuit. The motor drive circuit selected for this application was the MD22 Dual 5Amp H-Bridge switching motor drive circuit, a product of Devantech Ltd. The MD22 has the advantage that it can drive two DC motors

independently and has a switching frequency of 15kHz, thus making full use of the photodiode bandwidth. The input signals accepted by the MD22 must have a 2.5 V offset.

Initially, a simple control algorithm was employed to control the elevation of the concentrator mounted in the pointing mechanism. The algorithm compares the top fibre of the bundle with the bottom fibre to determine which way to drive the elevation motor. During the simulation with the solar simulator spot centred on the bundle the mechanism remained still. On disturbing the mechanism elevation by a small amount (<0.5°) the mechanism was observed to make a corrective motion. A greater disturbance (>0.5°) resulted in a correction that over compensated and resulted in erratic motion of the mechanism. The feedback of the photodiodes was recorded and is presented in figure (5.17):

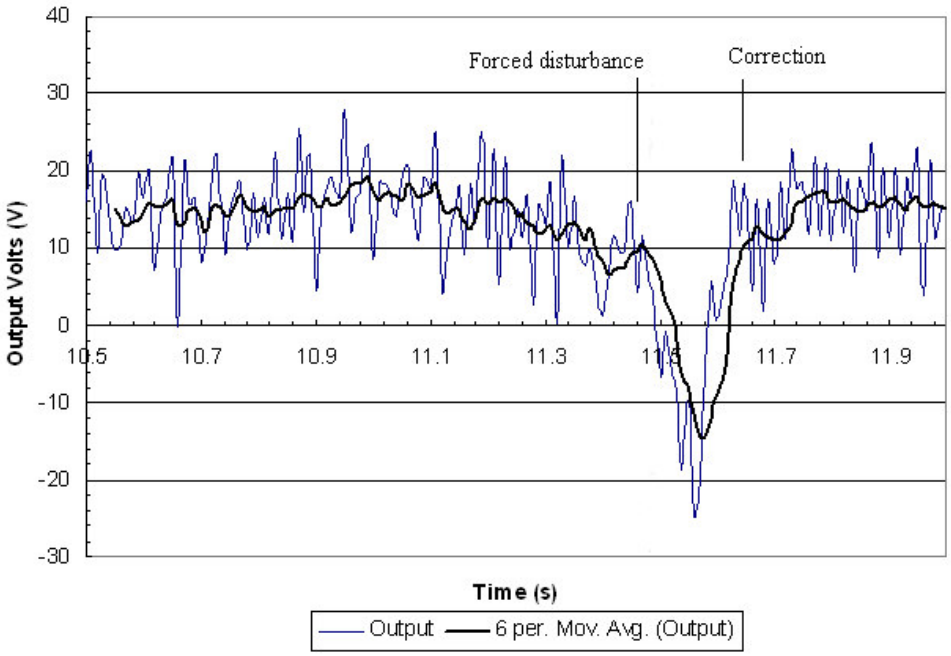

Figure 5.17: Photodiode feedback for off axis pointing.

In figure (5.17) the photodiode feedback is attempting to maintain the position feedback at an offset voltage. The offset voltage shown in figure (5.17) (~15V) is subject to a gain to bring it into range of the MD22 input. A moving average fit is plotted in figure (5.17) to aid visualisation. This preliminary test demonstrates that the motor will respond in a positive manner to feedback from the photodiode array. Further progression of this research has been slowed down by photodiode calibration difficulties. However, development of this technology is continuing at the University of Surrey to provide a robust control algorithm that will be used to track the Sun during the summer months of 2006.

5.4 Summary

In this section the technological unknowns associated with the transmission of high intensity radiation through fibre optic cables has been investigated.

A parabolic concentrator, optimised for a l mm core size fibre optic cable, is tested to determine surface form error and efficiency. Analysis of form error tests demonstrates the prototypes suitability for focusing light into a fibre optic. Various secondary relay mirrors were tested to ascertain desirable secondary properties, and an aluminium secondary was selected.

Fibre optic transmission tests demonstrate a 50% end-to-end concentrator and fibre efficiency. These tests were conducted using a solar simulator and also on-Sun with a Sun tracking mount.

Finally, preliminary tests have been conducted of a novel pointing control system demonstrating proof of concept.

Section 6

6 Summary and Conclusions

6.1 Overview

This report details the research conducted at the University of Surrey for the development of a technology demonstration solar thermal propulsion system incorporating fibre optics for the transmission of high intensity solar radiation to a blackbody cavity receiver.

6.2 Summary

For this research an in-depth literature review was conducted, which identified significant heritage in the areas of solar thermal receivers and solar concentrators, and indicated a need to investigate the technological unknowns of fibre optic transmission of high intensity radiation and the pointing control of the solar concentrators.

A series of missions for which solar thermal propulsion would be applicable as a main propulsion system are discussed to demonstrate the range of mission enabled by this technology for a microsatellite. Microsatellite missions suitable for a solar thermal propulsion technology demonstration in the near future are identified and provide design requirements for such a system.

System components are separately analysed given these requirements. Each component (concentrator, thruster, fibre, pointing mechanism) is designed and modelled to derive expected performance.

Practical component testing focused on the technological unknowns of the system. A concentrator manufactured for this research is analysed for quality and efficiency. Fibre optic transmission tests were conducted demonstrating 50% transmission efficiency over a 2m length of silica fibre optic. The attenuation of the fibre was measured subject to heating and stress conditions indicating the survivability of the fibre. Finally preliminary results from a novel concentrator pointing control system are presented.

The ultimate goal of this work is to provide a flight ready, prototype, solar thermal propulsion system, which can be rapidly incorporated on to an appropriate microsatellite platform. The research detailed in this report has achieved the following milestones towards this goal:

- Design, manufacture and testing of prototype Cassegrain concentrator assembly.
- Design and modelling of a direct-gain solar thermal cavity receiver.
- Extreme environment testing of a silica core fibre optic.
- Transmission testing of a silica core fibre optic.
- Demonstration of fibre optic heating of small graphite samples.
- Design and manufacture of fibre optic to concentrator connector.
- Design and modelling of fibre optic to receiver connector.
- Design, manufacture and testing of concentrator pointing control system.

To achieve the ultimate goal of this research the following is required:

- Manufacture and testing of direct-gain solar thermal cavity receiver.
- Manufacture and testing of fibre to receiver connector.
- Devise and implement a robust solar tracking algorithm for the concentrator pointing system.

Through this research significant heritage and facility for solar thermal propulsion has been developed at the University of Surrey. Current research at the University of Surrey is continuing towards this goal to fly the first solar thermal propulsion system in space.

7 References

[1] Grossman, G., Williams, G., "*Inflatable Concentrators for Solar Propulsion and Dynamic Space Power*," ASME International Solar Energy Conference, April, 1989.

[2] Jaworske, D.A., Skowronski, T.J., "*Optical Efficiency of a Refractive Secondary Concentrator*," AIAA-2000-2994.

[3] Stephens, P., Cooksley, J., Silva Curiel, A., Boland, L., Jason, S., Northham, J., Brewer, A., Anzalchi, J., Newell, H., Underwood, D., Machin, S., Sun, W., Sweeting, M., , "*Launch of the International Disaster Monitoring Constellation; the development of a novel international partnership in space*," IEEE, RAST, 2003.

[4] Feuermann, D., Gordon, J.M, "*Solar Fibre-Optic Mini-Dishes: A New Approach To The Efficient Collection Of Sunlight,*" Solar Energy, Vol. 65, No. 3, 1999.

[5] Shoji, J.M., Frye, P.E., McClanahan, J.A., "*Solar Thermal Propulsion Status and Future,*" Space Programs and Technologies Conference, Huntsville, 1992.

[6] Etheridge, F., "*Solar Rocket System Concept Analysis*," AFRPL-TR-79-79, Final Technical Report, Rockwell International, 1979.

[7] Hill, P., Peterson, C., "*Mechanics and Thermodynamics of Propulsion*," Second Edition, Addison-Wesley, 1992.

[8] Borell, G.J., Campbell, J.S., "*ISUS Solar Concentrator Array Development*," AIAA Joint Propulsion Conference, 1996.

[9] Meinel, A.B., Meinel, M.P., "Applied Solar Energy, An Introduction," Addison-Wesley, 1976.

[10] Stine, W.B., Geyer, M., "*Power from the Sun*," John Wiley and Sons, Inc. 1985.

[11] Schreiber, J.G., "*A Deep Space Power System Option Based on Synergistic Power Conversion Technologies*," 2000 Space Technology and Applications International Forum.

[12] Pearson, J.C., Gierow, P., Lester, D., "*Near term in-space demonstration of an inflatable concentrator*" AIAA-1999-1073, Aerospace Sciences Meeting and Exhibit, 1999.

[13] Kennedy, F.G., "*Solar Thermal Propulsion for Microsatellite Manoeuvring*," PhD Thesis, University of Surrey, 2004.

[14] Wong, W.A., Geng, S.M., "*Design, Fabrication and Test of a High Efficiency Refractive Secondary Concentrator for Solar Applications*," 35th Intersociety Energy Conversion Engineering Conference, 2000.

[15] Wong, W.A., Macosko, R.P., "*Refractive Secondary Concentrators for Solar Thermal Applications*," 34th Intersociety Energy Conversion Engineering Conference, 1999.

[16] Kessler, T.L., "*An Overview of a Solar Thermal Propulsion and Power System Demonstration Applicable to HEDS*," AIAA Space 2001 Conference.

[17] Shoji, J.M., Perry, F.J., Lim, D.P., Pard, A.G., "*Windowed Porous Material Absorption Concept – A New Solar Thermal Propulsion Concept*," JANNAF Propulsion Meeting, 1986.

[18] Rault, D., Hertzberg, A., "*Radiation Energy Receiver for Laser and Solar Propulsion Systems*," AIAA-83-1207, June 1983.

[19] Shoji, J.M., Kaith, I., Pard, A.G., "*Solar Thermal Rocket Design and Fabrication*," JANNAF Propulsion Meeting, 1985.

[20] Shimizu, M., Itoh, K., Sato, H., Sahara, H., Fujii, T., Okamoto, K., Takaoka, S., Nakamura, Y., "*Very Small Solar Thermal Thruster Made of single Crystal Tungsten for Micro/Nanosatellites*," AIAA-2000-3832.

[21] Partch, R., Frye, P., "*Solar Orbit Transfer Vehicle Space Experiment Conceptual Design*," 35th AIAA Joint Propulsion Conference, AIAA-99-2476, 1999.

[22] Frye, P.E., Kudija, C.T., "*Integrated Solar Upper Stage Engine Ground Demonstration Test Results And Data Analysis*," AIAA Joint Propulsion conference, AIAA98-3958, 1998.

[23] Kennedy, F.G., Palmer, P.L., "*Preliminary Design of a Micro-Scale Solar Thermal Propulsion System*," 38th AIAA Joint Propulsion Conference, AIAA-2002-3928, 2002.

[24] Cady, E.C., Olsen, A.D., "*Cryogenic Storage and Propellant Feed System For The Integrated Solar Upper Stage (ISUS) Program*," 32nd AIAA Joint Propulsion Conference, AIAA-96-3011, 1996.

[25] Chato, D.J., Van-Dyke, M., Batty, J., Schick, S., "*Status and Design Concepts for the Hydrogen On-Orbit Storge and Supply Experiment*," Space Technology and Applications International Forum, 1998.

[26] Kato, D., Nakamura, T., "*Application of optical fibres to the transmission of solar radiation*," Journal of Applied Physics, Vol. 47, No. 10, 1976.

[27] Polymicro Technologies, "*Silicon/Teflon AF Clad Optical Fiber*," 2004.

[28] Cariou, J., Dugas, J., Martin, L., "*Transport of Solar Energy with Optical Fibres*," Journal of Solar Energy, Vol. 5, 1982.

[29] Liang, D., Monteiro, L.F., Teixeira, M.R., Monteiro, M.L.F., Collares-Pereira, M., "*Fibre-optic solar energy transmission and concentration*," Solar Energy Materials and Solar Cells, 1998.

[30] Gordon, J.M., Feuermann, D., Huleihil, M., Katz, E.A., "*New optical systems for the generation of nanomaterials*," SPIE Syposium on Nonimaging Optics, 2003.

[31] Feuermann, D., Gordon, J.M., "*Solar Fiber-Optic Mini-Dishes: A New Approach To The Efficient Collection Of Sunlight*," Journal of Solar Energy, Vol.65, No.3, 1999.

[32] Nakamura, T., Comaskey, B., Bell, M., "*Development of Optical Components for Space-Based Solar Power System for ISRU and Regenerative Life Support*," 40th AIAA Aerospace Sciences Meeting and Exhibit, 2002.

[33] Kennedy, F.G., Henshall, P., Gibbon, D., "*Preparing for Flight: The Surrey Space Centre's Microscale Solar Thermal Propulsion Experiment*," 4th International Spacecraft Propulsion Conference, 2004.

[34] Nakamura, T., Krech, R.H., McClanahan, J.A., Shoji, J.M., Partch, R., Quinn, S., "*Solar Thermal Propulsion for Small Spacecraft – Engineering System Development and Evaluation*,"41st AIAA Joint Propulsion Conference, 2005.

[35] Wertz, J.R., Larson, W.J., "*Space Mission Analysis and Design – Third Edition*," Kluwer Academic, 1999.

[36] Pieri, D.C., "*Virtual Polar Geostationary Satellite (VPGS)*," Final Technical Report, Jet Propulsion Laboratory, 2000.

[37] Henshall, P.R., Palmer, P., Baker, A., "*Solar Thermal Propulsion Augmented with Fibre Optics: - A Design Proposal*," 41st AIAA Joint Propulsion Conference, 2005.

[38] Dame, L., Brun, J.F., Cugnet, D., Derrien, M., Leroy, C., Meftah, M., Meissonnier, M., Porteneuve, J., "*A Solar Diameter Metrology Measurement: The PICARD Microsatellite Program*," CNES Technical Report, 2000.

[39] CNES website: **http://smsc.cnes.fr/MICROSCOPE/index.htm**.

[40] SSTL web source: **http://centaur.sstl.co.uk/datasheets/Platform_GEMINI_HQ.pdf**

[41] Stine, W.B., Geyer, M., "*Power from the Sun*," John Wiley and Sons, Inc. 1985.

[42] Feuermann, D., Gordon, J.M., Huleihil, M., "*Solar Fibre-Optic Mini-Dish Concentrators: First Experimental Results and Field Experience,"* Solar Energy Vol. 72, April 2002.

[43] Ashby, M.F., Jones, D.R.H., "*Engineering Materials - An Introduction to their Properties and Applications*," International Series on Materials Sciences and Technology, Vol.34, 1980.

[44] Carlin, P.S., "*Lightweight Mirror Systems for Spacecraft – An Overview of Materials & Manufacturing Needs*," Proceedings of the IEEE Aerospace Conference, Vol. 4, pp. 169-182, March 2000.

[45] Zhang, Y., Zhang, J., Han, J., He, X., Yao, W., "*Large-Scale Fabrication of Lightweight Si/SiC Ceramic Composite Optical Mirror*," 14th International Conference on Composite Materials, 2003.

[46] Lawrence, J.T., "*Research into Resistojet Rockets for Small Satellite Applications*," Ph.D. Thesis, Surrey Space Centre, School of Electronics and Physical Sciences, University of Surrey, 1998.

[47] Lienhard, J., "*A Heat Transfer Textbook, 2nd Edition,*" Prentice-Hall, 1987.

[48] Midwinter, J.E., "*Optical Fibers for Transmission*," Wiley, 1979.

[49] Reisfeld, R., "*Industrial Applications of Rare Earths in Fiber Optics, Luminescent Solar Concentrators and Lasers*," *Inorganica Chimica Acta* Vol. 140, pp. 345-350, 1987

[50] Harrington, J.A., "*Infrared Fiber Optics*," Handbook of Optics, Vol. 4, Chapter 14, McGraw-Hill, New York, NY, 2001.

[51] Polymicro Technologies, "*Silicon/Teflon AF Clad Optical Fiber*," 2004.

[52] Jaramillo, O.A., Rio, J.A., Huelsz, G.. "*A Thermal Study of Optical Fibres Transmitting Concentrated Solar Energy*," *J. Phys. D: Appl. Phys.* Vol.32, pp.1000-1005, 1999.

[53] Brichard, B., Fernandez Fernandez, A., Berghmans, F., Decréton, M., "*Origin of the Radiation-Induced OH Vibrational Band in Polymer-Coated Optical Fibers Irradiated in a Nuclear Fission Reactor*," IEEE Transactions on Nuclear Science Vol.49, No.6, 2002.

[54] Brichard, B., Borgermans, P., Fernandez Fernandez, A., Lammens, K., Decréton, M., "*Radiation Effect in Silica Optical Fiber Exposed to Intense Mixed Neutron-Gamma Radiation Field*," IEEE Transactions on Nuclear Science Vol.48, No.6, 2001.

[55] Brichard, B., Fernandez Fernandez, A., Ooms, H., Berghmans, F., Decréton, M., Tomashuk, A., Klyamkin, S., Zabezhailov, M., Nikolin, V., Hodgson, E., Kakuta, T., Shikama, T., Nishitani, T., Costley, A., Vayakis, G., "*Radiation-Hardening techniques of dedicated optical fibres used in plasma diagnostics systems in ITER*," Journal of Nuclear Materials, 329-333, 1456-1460, 2004.

[56] Ott, M.N., "*Radiation Effects Data on Commercially Available Optical Fiber: Database Summary*," Nuclear Science and Radiation Effects Conference, Data Workshop Proceedings, pp. 24-31, 2002.

[57] Skutnik, B.J., Trebst, T., Harschack, A., "*Reliability of High Na, UV Non-Solarizing Optical Fibers*," CeramOptec Industries, Inc. 2004.

[58] SSTL web source: **http://centaur.sstl.co.uk/datasheets/Platform_rapid2micro_HQ.pdf**

[59] Roth, P., Georgiev, A., Boudinov, H., "*Cheap Two Axis Sun Following Device*" Energy Conservation and Management, 2005.

[60] Wang, D., Anapol, M., "*Ultra-Lightweight Telescopes and Precision Pointers as Enabling Technologies for Small, Low Cost Missions*," AIAA Space Programs and Technologies Conference, 1995.

[61] Suhonen, M., Graeffe, J., Sillanpaa, T., Sipola, H., Eiden, M., "*Scanning micromechanical mirror for fine-pointing units of intersatellite optical links*," Smart Materials and Structures, Institute of Physics, 2001.

[62] Nise, N.S., "*Control Systems Engineering, 3rd Edition*," John Wiley & Sons, 2000.

[63] Feuermann, D., Gordon, J.M., Huleihil, M., "*Light Leakage In Optical Fibers: Experimental Results Modelling And The Consequences For Solar Concentrators*," Journal of Solar Energy, Vol. 72, No. 3, 2002.